

MECHANICALLY ACTIVATED COMBUSTION SYNTHESIS OF NIOBIUM SILICIDE
BASED COMPOSITES

REINA TREVIÑO

Doctoral Program in Mechanical Engineering

APPROVED:

Evgeny Shafirovich, Ph.D., Chair

Arturo Bronson, Ph.D.

David Roberson, Ph.D.

Stephen L. Crites, Jr., Ph.D.
Dean of the Graduate School

Copyright ©

by

Reina Treviño

2020

Dedication

Dedicated to my loved ones, for pushing me from the start and supporting me until the end.

Look Mom, I'm a doctor.

MECHANICALLY ACTIVATED COMBUSTION SYNTHESIS OF NIOBIUM SILICIDE
BASED COMPOSITES

by

REINA TREVIÑO, B.S.M.E.

DISSERTATION

Presented to the Faculty of the Graduate School of

The University of Texas at El Paso

in Partial Fulfillment

of the Requirements

for the Degree of

DOCTOR OF PHILOSOPHY

Department of Mechanical Engineering

THE UNIVERSITY OF TEXAS AT EL PASO

August 2020

Acknowledgements

I would like to thank my loved ones for all the support that was given to me the past years. I would especially like to thank my advisor Dr. Shafirovich for presenting me with this opportunity and putting me in a team with my amazing peers Edgar Maguregui, Frank Perez, Sergio Cordova, Robert Ferguson and Alan Esparza. I could not have made it without the support of all those mentioned.

This research was supported by the U.S. Office of Naval Research (Award # N00014-17-1-2636).

Abstract

Niobium silicide-based composites are promising materials for high-temperature structural applications, such as gas turbines, but their implementation is hindered by the lack of effective processing methods. Self-propagating high-temperature synthesis (SHS) is an attractive method for fabrication of advanced materials. However, it is difficult to perform SHS of niobium silicides because the melting point of Nb is higher than the combustion temperature, which greatly inhibits Nb-Si reaction. To ignite an Nb/Si mixture and obtain Nb_5Si_3 , the desired phase in niobium silicides, either preheating or mechanical activation of the mixture is necessary. This problem becomes even more critical in the SHS of $\text{Nb}_5\text{Si}_3/\text{Nb}$ composites, where the combustion temperature is lower than in the stoichiometric Nb/Si mixture. Niobium silicide-based alloys also contain various additives, the most important of which is titanium.

The present work focused on the mechanically activated SHS of Nb_5Si_3 , $\text{Nb}_5\text{Si}_3/\text{Nb}$, and $\text{Nb}_5\text{Si}_3/\text{Ti}_5\text{Si}_3/\text{Nb}$ materials. Thermodynamic calculations helped design the experiments and understand the results. Milling of Nb/Si mixtures (23 – 37.5 at% Si) in a planetary ball mill enabled SHS. The effects of the milling time, pellet diameter, and mixture ratio on the process characteristics and product composition were investigated. Combustion of the stoichiometric Nb/Si mixture produced primarily α and γ phases of Nb_5Si_3 . With adding more Nb, the content of the γ phase, which has poor mechanical properties, dramatically decreased. The addition of Ti, which melts at a relatively low temperature and readily reacts with Si, enabled combustion of mixtures with Si concentration as low as 20 at%. Such mixtures reacted in the spin combustion mode, producing α - $\text{Nb}_5\text{Si}_3/\text{Ti}_5\text{Si}_3/\text{Nb}$ composites.

Table of Contents

Acknowledgements.....	v
Dedication.....	iii
Abstract.....	vi
Table of Contents.....	vii
List of Tables.....	ix
List of Figures.....	x
Chapter 1: Introduction.....	1
Chapter 2: Literature Review.....	4
2.1 Niobium Silicide Based Composites.....	4
2.2 Self-Propagating High-Temperature Synthesis (SHS).....	9
2.2.1 History of SHS.....	9
2.2.2 Combustion Wave in the SHS Process.....	11
2.2.3 SHS of Niobium Silicides.....	19
Chapter 3: Experimental Procedures and Facilities.....	27
3.1 MASHS Procedures.....	27
3.1.1 Mixing.....	27
3.1.2 Mechanical Activation.....	30
3.1.3 Compaction.....	34
3.1.4 SHS Procedures.....	35
3.2 Characterization of Materials.....	37
3.2.1 Laser Diffraction Particle Size Analysis.....	37
3.2.2 X-Ray Diffraction Analysis.....	38

3.2.3 Scanning Electron Microscopy	39
3.2.4 Compressive Strength Testing	40
Chapter 4: Results and Discussion.....	41
4.1 MASHS of Nb ₅ Si ₃	41
4.2 MASHS of Nb ₅ Si ₃ /Nb Composites.....	53
4.3 MASHS of Nb ₅ Si ₃ /Ti ₅ Si ₃ /Nb Composites	81
Chapter 5: Conclusions	89
References.....	92
Vita	103

List of Tables

Table 2.1: Effect of milling on product composition [58].	24
Table 3.1: Masses of powders used for making 6 g samples.	27
Table 3.2: Masses of powders used for making 18.5 g samples.	28
Table 3.3: The adiabatic flame temperature and pressure of Nb/Si mixtures calculated at constant volume (20 mL and 80 mL).	33
Table 3.4: The adiabatic flame temperature and pressure of Nb/Si/Ti mixtures calculated at constant volume (80 mL).	34
Table 4.1: Particle size distribution parameters.	47
Table 4.3: Combustion front velocities of samples with excess Nb.	55
Table 4.4: Comparison of calculated and measured temperatures for Nb/Si mixtures with mole ratios of 1.67, 2, and 3.	64
Table 4.5: The parameters used for determination of activation energy.	66
Table 4.5: Spin combustion parameters.	77
Table 4.6: XRD peak intensities for the products obtained from Nb/Si mixtures with 23–25 at% Si.	80
Table 4.7: The adiabatic flame temperatures and numbers of moles of products for Nb/Si mixtures with additives.	82
Table 4.8: The adiabatic flame temperatures and numbers of moles of products for Nb/Si/Ti, Nb/Si/B, and Nb/Si/Mo mixtures that exhibit complete conversion.	83

List of Figures

Figure 1.1: Specific core power vs. turbine inlet temperature for gas turbine power plants [2-4].	2
Figure 2.1: Phase diagram of the Nb-Si system [17].	5
Figure 2.2: A schematic concept of the historical discovery of SHS [33].	10
Figure 2.3: An industrial SHS reactor [38].	11
Figure 2.4: Large-scale ceramic-lined steel pipes produced using SHS [17].	11
Figure 2.5: Schematic of the SHS process.	12
Figure 2.6: Typical structure of combustion wave in the SHS process [41].	13
Figure 2.7: Types of temperature profiles [40].	14
Figure 2.8: Steady one-spot spinning wave: (a) wave front structure, spatial distribution of (b) θ and (c) η in the cross section of θ_{\max} , and (d) the distribution of θ in the form of isotherms [49].	16
Figure 2.9: Diagram of chemical oven technique.	19
Figure 2.10: Dependence of the free calcium oxide content (W_{CaO_f}) of fly ash on the time of mechanochemical treatment (τ_{MT}) in (1) AGO-2 and (2) Fritsch Pulverisette 5 classic line [66].	23
Figure 2.11: Temperature profiles for the composition Nb:Si = 5:3, for the milling times (min): (a) 80; (b) 120; (c) 240; and (d) 285 [58].	25
Figure 3.1: Mixer (Inversina 2L, Bioengineering) with (a) closed and (b) open protective shield.	29
Figure 3.2: Bowl with purging valves.	29
Figure 3.3: Glovebox (Terra Universal, Series 300).	30
Figure 3.4: Planetary ball mill (Fritsch Pulverisette 7 Premium Line).	31

Figure 3.5 Pressing equipment: (a) die set for 13 mm diameter and (b) uniaxial hydraulic press.	35
Figure 3.6: Hot-wire ignition setup.....	36
Figure 3.7: Particle size analyzer (Microtrac Bluewave).	37
Figure 3.8: (a) Bruker D8 Discover XRD and (b) Rigaku MiniFlex II Desktop XRD.	38
Figure 3.9: (a) TM - 1000 Tabletop Microscope and (b) Hitachi S-4800 Scanning Electron Microscope.....	39
Figure 3.10 (a) Instron 5969 Universal Test Machine and (b) compression testing plates.	40
Figure 4.1: Images of combustion propagation over Nb/Si mixture (5:3 mole ratio), mechanically activated for (top) 2 min and (bottom) 10 min. Time zero was selected arbitrarily.	42
Figure 4.2: XRD pattern of combustion products of Nb/Si mixture milled for 2 min.	43
Figure 4.3: XRD pattern of combustion products of Nb/Si mixture milled for 5 min.	44
Figure 4.4: XRD pattern of combustion products of Nb/Si mixture milled for 10 min (diameter 13 mm).	45
Figure 4.5: SEM images of (a) non-activated mixture and (b) mixture milled for 10 min.	48
Figure 4.6: XRD pattern of combustion products of Nb/Si mixture milled for 10 min (diameter 6 mm).	49
Figure 4.7: XRD pattern of combustion products of Nb/Si mixture milled for 10 min (diameter 25 mm).	50
Figure 4.8: The γ -to- α peak intensity ratio in the combustion products of Nb/Si mixture vs. the pellet diameter.....	50

Figure 4.9: XRD pattern of combustion products of Nb/Si mixture obtained using the chemical oven technique 52

Figure 4.10: The adiabatic flame temperature vs. the mole fraction of excess Nb in the initial mixture. 54

Figure 4.11: Short-circuiting of a coil during combustion of the mixture with Nb/Si mole ratio of 1.89 (40 mol% excess Nb). Time zero was selected arbitrarily..... 55

Figure 4.12: XRD pattern of combustion products; Nb/Si mole ratio: 1.70 (10 mol% excess Nb). 56

Figure 4.13: XRD pattern of combustion products; Nb/Si mole ratio: 1.75 (20 mol% excess Nb). 57

Figure 4.14: XRD pattern of combustion products; Nb/Si mole ratio: 1.81 (30 mol% excess Nb). 57

Figure 4.15: XRD pattern of combustion products; Nb/Si mole ratio: 1.89 (40 mol% excess Nb). 58

Figure 4.16: XRD pattern of combustion products; Nb/Si mole ratio: 2.00 (50 mol% excess Nb). 58

Figure 4.17: XRD pattern of combustion products; Nb/Si mole ratio: 2.17 (60 mol% excess Nb). 59

Figure 4.18: XRD pattern of combustion products of the mixture with Nb/Si mole ratio of 2.44 (70 mol% excess Nb). 59

Figure 4.19: Images of combustion propagation over Nb/Si mixture pellets (height: 25±2 mm) with Nb/Si mole ratios of (a) 1.67, (b) 2, and (c) 3. Time zero was selected arbitrarily. 61

Figure 4.20: Temperature records during combustion propagation over Nb/Si mixture pellets (height: 25 mm) with Nb/Si mole ratios of (a) 1.67, (b) 2, and (c) 3.....	62
Figure 4.21: The adiabatic flame temperature (line) and measured maximum temperatures (circles) vs. the mole fraction of excess Nb in the initial mixture; the two data points at a mole fraction of 0.5 (correlating to Nb/Si ratio of 2) overlap each other.	64
Figure 4.22: The Arrhenius-type plot for determination of activation energy of Nb-Si reaction.	66
Figure 4.23: Photographs of the product pellets obtained from mixtures with Nb/Si mole ratios of (a) 1.67, (b) 2, and (c) 3.....	67
Figure 4.24: XRD pattern of combustion products of the mixture with Nb/Si mole ratio of 1.67 (height of the pellet: 25 mm).	68
Figure 4.25: XRD pattern of combustion products of the mixture with Nb/Si mole ratio of 2 (height of the pellet: 25 mm).	69
Figure 4.26: XRD pattern of combustion products of the mixture with Nb/Si mole ratio of 3 (height of the pellet: 25 mm).	70
Figure 4.27: SEM images of products (crushed to powders) obtained from mixtures with Nb/Si mole ratios of (a, d) 1.67, (b, e) 2, and (c, f) 3.....	72
Figure 4.28: SEM images of products (polished samples) obtained from mixtures with Nb/Si mole ratios of (a) 1.67, (b) 2, and (c) 3.	73
Figure 4.29: Stress-strain dependences of products obtained from mixtures with Nb/Si mole ratios of 1.67, 2, and 3.....	74
Figure 4.30: Images of combustion propagation over Nb/Si mixture pellets (height: 25±2 mm) with (a) 23, (b) 24 and (c) 25 at% Si. Time zero was selected arbitrarily.	76
Figure 4.31: XRD pattern of combustion products of the Nb/Si mixture with 23 at% Si.	78

Figure 4.32: XRD pattern of combustion products of the Nb/Si mixture with 24 at% Si.	79
Figure 4.33: XRD pattern of combustion products of the Nb/Si mixture with 25 at% Si.	80
Figure 4.34: Measured maximum temperatures (open circles and error bars), adiabatic flame temperatures (T_{ad}), and mole fractions of the products (filled circles and lines) vs. Nb/Si mole ratio.	84
Figure 4.35: Thermal profile during combustion of Nb/Si/Ti mixture (1:1:1 mole ratio).....	85
Figure 4.36: XRD patterns of the products obtained from mixtures with Nb/Si mole ratios of 1, 2, and 3.....	87
Figure 4.37: SEM images of the products obtained from the mixtures with Nb/Si mole ratios of (a) 2 and (b) 3.....	88

Chapter 1: Introduction

Gas turbines are widely used for industrial applications, such as electric power generation and aircraft propulsion. Natural gas has become the leading source of energy for electricity generation in the United States, surpassing coal, oil, wind, and solar-generated power. According to the Energy Information Administration (EIA), power plants that burn natural gas in gas turbines have accounted for 42% of the electricity generated in the U.S., as of December 2016. [1] For this reason, even a small increase in the efficiency of gas turbines would have significant impact on the natural gas consumption and air quality.

The efficiency of a gas turbine depends on the maximum temperature of the working fluid (air mixed with combustion products). According to the Carnot theory, the higher the maximum temperature, the higher the thermal efficiency. Thus, in order to increase efficiency, operating temperatures must be increased. Gas-turbine components made of single crystal nickel-based superalloys can withstand temperatures of approximately 1100 °C. Gas temperatures within the turbines, which define the engine operating temperature, are much higher, reaching temperatures as high as 1600 °C. The turbine blades are protected by ceramic thermal barrier coatings and air cooling; however, cooling consumes energy and hence decreases the efficiency (Fig. 1.1) [2-4]. It is estimated that operation at 1300 °C without auxiliary cooling would increase the specific output power by almost 50 %. [2] In addition, this would simplify manufacturing and eliminate the weight and complexity of auxiliary cooling equipment.

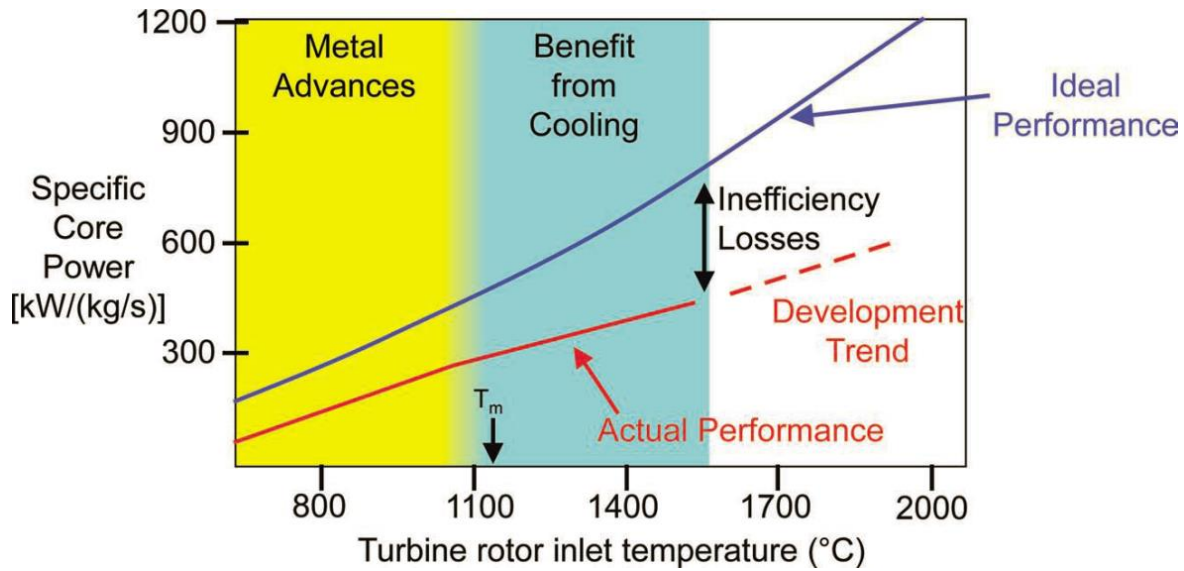


Figure 1.1: Specific core power vs. turbine inlet temperature for gas turbine power plants [2-4].

The overarching goal of this study is the development of inexpensive, low-energy consuming methods for the fabrication of refractory metal alloys that can replace the nickel-based superalloys and significantly increase the efficiency of gas turbines. Owing to melting points above 2000 °C and excellent mechanical properties at high temperatures, niobium silicide-based composites are considered among the main candidates for these applications. However, large-scale fabrication of these materials is a major hurdle. The development of a processing method that yields the desired final microstructure during initial alloy synthesis is crucial [2]. Innovative powder metallurgy processing is viewed as a practical approach to achieve a large-scale synthesis of uniform multiphase microstructures. Specifically, the present work focuses on self-propagating high-temperature synthesis (SHS), an attractive method for fabricating advanced materials from powders via exothermic reactions between the mixture constituents. SHS offers certain advantages, such as tailored microstructure and properties, low cost, low energy consumption, and high purity of the products [5].

However, SHS also has some drawbacks, such as difficult ignition of low-exothermic mixtures. Adding a mechanical activation step helps overcome this problem. This step is, in fact, ball milling of powders before the SHS process. The combined technique is called mechanically activated self-propagating high-temperature synthesis (MASHS) [6].

The first objective of the present work is to study MASHS of Nb_5Si_3 phase, which is one of three stable phases in the Nb-Si system. The high melting point, 2515 °C, and thermodynamical stability with other refractory metals make Nb_5Si_3 an attractive phase for formation of composite materials for high-temperature structural applications [7]. Specifically, the present work explores the feasibility of decreasing the milling time in the MASHS of Nb_5Si_3 by using a planetary ball mill for the mechanical activation step. Special attention is paid to the influence of the process parameters, such as the milling time and the sample size, on the formation of different phases of Nb_5Si_3 .

The second objective is to study MASHS of $\text{Nb}_5\text{Si}_3/\text{Nb}$ composites. Along with silicide phases, niobium silicide-based composites contain significant amounts of Nb phase. Since the excess niobium (with respect to Nb_5Si_3 stoichiometry) decreases the combustion temperature in the SHS process, it is important to investigate how an increase in Nb content affects the combustion characteristics and product composition.

The third objective is to explore MASHS of $\text{Nb}_5\text{Si}_3/\text{Ti}_5\text{Si}_3/\text{Nb}$ composites. To improve mechanical properties and oxidation resistance of niobium silicides, various additives are used, with titanium being the largest [7]. It is thus important to investigate how the addition of Ti affects the SHS process.

Chapter 2: Literature Review

2.1 Niobium Silicide Based Composites

Niobium silicide-based composites are promising for high-temperature structural applications due to their high melting points, low density (around 7 g/cm^3 , as compared with 9.2 g/cm^3 for Ni-based superalloys), high fracture toughness, and good fatigue behavior [8-10]. However, for use in applications such as gas turbines, their oxidation resistance and creep performance must be improved.

As a pure element, niobium (Nb) has poor oxidation resistance. The oxide layer that forms on Nb is non-protective against the penetration of oxygen and nitrogen upon exposure to air or combusive atmospheres. Oxygen and nitrogen diffuse into the alloy, creating a hard, brittle subsurface layer. For over 60 years, intensive research has been conducted to develop oxidation-resistant alloys of niobium that would be capable of forming protective oxide scales [11]. A promising and commonly used approach is based on making niobium silicides. They have better oxidation resistance compared to pure Nb because of protection by the silicates formed during oxidation [11, 12].

Among three stable silicides of niobium, Nb_5Si_3 , Nb_3Si , and NbSi_2 , the former has the highest melting point ($2515 \text{ }^\circ\text{C}$), and it is thermodynamically stable with Nb, molybdenum (Mo), and other refractory metals [8], making Nb_5Si_3 an attractive phase for forming the composite materials for high-temperature structural applications.

There exist two stable phases of Nb_5Si_3 (Fig. 2.1): a low-temperature α -phase and the high-temperature β -phase, both being tetragonal [8]. The eutectoid decomposition temperature of β - Nb_5Si_3 to α - Nb_5Si_3 and NbSi_2 is equal to $1650 \text{ }^\circ\text{C}$ (1923 K). In work by Schachner *et al.*, a metastable hexagonal γ -phase was reported for the first time [13]; later it was suggested that this

phase could be stabilized by interstitial impurities [14]. This phase could also be stabilized by Ti and Hf additives [15]. However, the metastability of the γ phase is controversial [13]. Computational thermodynamic studies of (α , β , γ)- Nb_5Si_3 phases have shown that all phases are stable, with α -phase possessing the highest structural stability [10]. The data on the elastic constants and elastic modulus, obtained in that work, indicate that α and β phases are brittle, while the γ phase is more ductile and has a lower hardness. The γ phase also exhibits poor creep performance [16]. In studies [9,16], additives have been implemented during the development of the material, with the goal of increasing ductility in the phases.

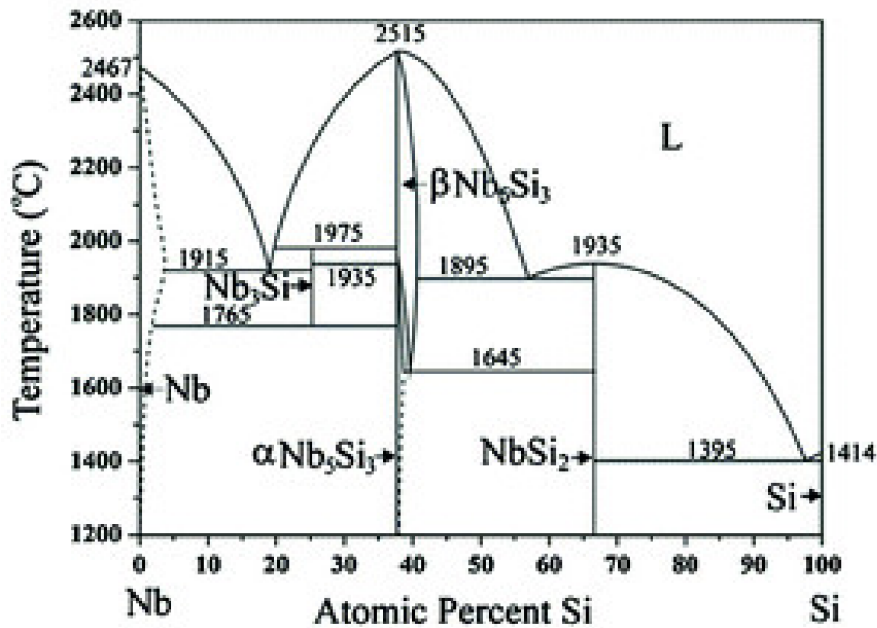


Figure 2.1: Phase diagram of the Nb-Si system [8].

Most intermetallics with high melting temperatures have complex, low symmetry crystal structures which possess strong directional atomic bonds. It is believed that the strong bonding is responsible for retention of mechanical properties, such as high strength, stiffness, and creep

resistance (due to low diffusivity) at high temperatures. The compiled data on these materials has shown that these properties directly scale with melting temperature. This same attribute often contributes to a lack of ductility and low fracture resistance at low temperatures. These compounds may be optimized for high-temperature use if their low-temperature fracture resistance can be improved without compromising their high-temperature resistant properties [18].

The phases of niobium silicides are very brittle at room temperature, preventing them from being used alone for practical applications [19]. Significant improvements in the fracture toughness of brittle intermetallic compounds have been achieved using a variety of extrinsic toughening approaches (ex. compositing) [20]. A promising method being utilized is the incorporation of ductile phases or reinforcements, producing toughened brittle solids. For niobium silicides, the inclusion of Nb particles was demonstrated to effectively improve the toughness of Nb₅Si₃ [19]. The fracture toughness of Nb₅Si₃ is 1-2 MPa $\sqrt{\text{m}}$, but it has been shown that including niobium particles in the Nb₅Si₃ matrix will bridge cracks and thus improve these values [21]. Extensive work with Nb₅Si₃/Nb laminates and arc-cast composites has been done to investigate ductile phase toughening in this system [21-25]. The work of Lewandowski's group on arc-melted composites used Nb with 10-16 at.% Si added as reactants: they reported fracture toughness improvements up to 21 MPa $\sqrt{\text{m}}$ [24].

The best balance of mechanical properties and oxidation resistance for niobium silicide-based materials is achieved by a combination of various additives to niobium silicide phases. Nb-Si in situ composites with Nb_{ss}, Nb₅Si₃ and/or Nb₃Si exhibit excellent creep strength, but poor oxidation resistance and fracture toughness [26]. To aid these problems additives such as, titanium (Ti), chromium (Cr), iron (Fe), aluminum (Al) and germanium (Ge) are used to improve oxidation resistance at high temperatures. Tin (Sn) can also be used for improved oxidation resistance at low

temperatures. The creep performance of Nb silicides can be improved by adding Ti, hafnium (Hf), and Ge [9]. The Cr and Al additions being used to improve oxidation resistance, however, were found to be detrimental for the fracture toughness of Nb_{ss}. The addition of Ti was found to improve the oxidation resistance of Nb_{ss} and Nb₅Si₃ silicides as well as the ductility of Nb_{ss}, and therefore the composite toughness [26].

Due to the issue of mechanical property deterioration, the application of a coating is considered an effective way to address the requirement of an enhanced resistance in high-strength Nb-based alloys [27]. Aluminide and silicide coatings have been investigated due to the oxidation protection by the Al₂O₃ and SiO₂ scales that form during the high temperature exposure. Hayashi *et al.* [28] developed an Al₂O₃ scale by a diffusion aluminizing process on an Nb-based alloy. Pure Nb alloys were produced, cut, ground, and finally cleaned in an ultrasonic bath. The samples were then embedded in Nb/NbO powder mixture and sealed in an evacuated quartz capsule. For the oxygen-diffusion process, they were heated to 1100 °C (1373 K) and held for 100 h in order to saturate the oxygen content in the alloys. The oxygen partial pressure in the quartz capsule was 2×10^{-22} atm in Nb/NbO equilibrium at 1100 °C. In the aluminum-diffusion process, samples were embedded in either an Al/Al₂O₃/NH₄Cl high Al-activity mixture, or Ni-50Al/ Al₂O₃/NH₄Cl low Al-activity mixture in an Al₂O₃ crucible and heat-treated at 1100 °C under a dynamic vacuum condition for 64 h. The outcome of the study showed that the Al₂O₃ scale was able to be formed using this two-step diffusion process successfully [28].

Another, more popular, method of coating is through pack cementation. In an example of this process, conducted by Wang *et al.* [29], components consisted of Ge, Si powder, halide activator (NaF) and inert filter (Al₂O₃ powder) were weighed, mixed and ground. The average particle sizes of Ge, Si, NaF and Al₂O₃ powders were all less than 100 mesh (149 microns). The

pack 16Si–8Ge–5NaF–71Al₂O₃ (wt.%) was used to co-deposit Si and Ge. Packs were prepared by burying the substrates in a well-mixed pack powder mixture in a cylindrical alumina retort of 20 mm diameter and 35 mm length, which was then sealed with an alumina lid and cement. After that, the pack was loaded into an alumina tube furnace circulated with argon. The furnace was raised to 1300°C at a heating rate of 5°C min⁻¹ and sustained for 10 h, then, cooled down to room temperature naturally by switching off the power supply while keeping the argon flowing. The coated specimens were retrieved from the pack and cleaned in an ultrasonic water bath to remove any residual powders on their surface.

A significant issue in the creation of niobium silicide-based composites is processing. To achieve the desired balance of properties, a specific microstructure needs to be created, and this microstructure should remain stable under extreme conditions of high temperature and stress. Conventional processing modifies the microstructure. The challenge is to develop processing methods that yield the desired final microstructure during initial alloy synthesis. Innovative powder metallurgy processing is viewed as a practical approach to achieve a large-scale synthesis of uniform multiphase microstructures [2].

A promising processing method, from this standpoint, is self-propagating high-temperature synthesis (SHS) [5,30], which is described in the next section. The feasibility of using SHS for the fabrication of niobium silicides from elements is based on thermodynamics [8]. Nb₅Si₃ and NbSi₂ have relatively high negative enthalpies of formation, – 60.7 kJ/mol and – 46.0 kJ/mol, respectively [8]. Thermodynamics predicts that Nb₅Si₃ and NbSi₂ can be obtained from elemental niobium and silicon by exothermic reactions described by the following equations:



For successful implementation of SHS approaches, it is important to understand what factors are responsible for the formation of certain phases and how one can tune the operating parameters toward the formation of the desired product [10].

2.2 Self-Propagating High-Temperature Synthesis (SHS)

2.2.1 History of SHS

Combustion synthesis takes advantage of the high heat release of chemical reactions between certain elements and compounds to generate high temperature and convert the reactants into the desired products [30]. Some of the advantages of combustion synthesis, compared with traditional solid-state synthetic routes, are the low energy consumption, short process times, high purity of the products, and low cost of experimental apparatus [30,31]. Combustion synthesis includes several methods developed for solid, liquid, and gaseous reactants [30]. Among these methods, the so-called self-propagating high-temperature synthesis (SHS) has been used extensively for the synthesis of various compounds from powders.

The concept of SHS was developed in the 1960s as a byproduct of research on the combustion of condensed, solid-state systems in the Former Soviet Union [32]. Figure 2.2 [33] shows the background and main steps of this development. In an attempt to model complex combustion of thermites, Merzhanov and his team used a mixture of Ti and B, with the goal of obtaining a simple, gasless combustion. The product of the combustion was pure TiB_2 ; the sample retained its original shape and was hard and dense [32, 34]. Normally, TiB_2 is made by gradually heating a powder mixture of Ti and B to 1500°C in a high temperature furnace for several hours. Merzhanov realized that this method could be used for synthesis of various materials [32].

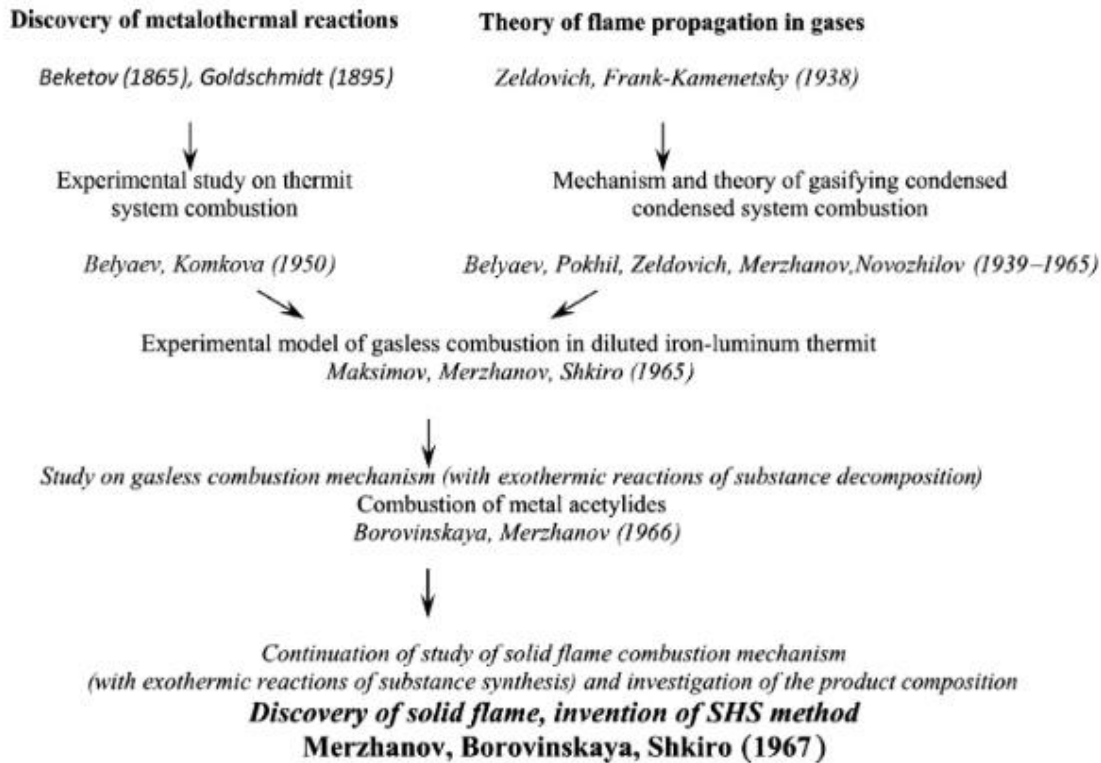


Figure 2.2: A schematic concept of the historical discovery of SHS [33].

By now, over 700 kinds of inorganic compounds and materials have been fabricated by SHS [35]. Considerable interest in the method has been generated in the US, Japan, France, Italy, China, Korea, Taiwan, and other countries [36]. SHS-production of a large number of materials has been scaled up and commercialized [31]. Industrial SHS reactors (Fig. 2.3) have been developed in the former USSR and used in plants located in that country and Spain [37-38]. In 1990, the amount of SHS products manufactured in the USSR was as large as several thousand metric tons [36]. Large-scale (over 10,000 metric tons annually) production of ceramic-lined steel pipes (Fig. 2.4) by the so-called centrifugal SHS has been organized in China [17].

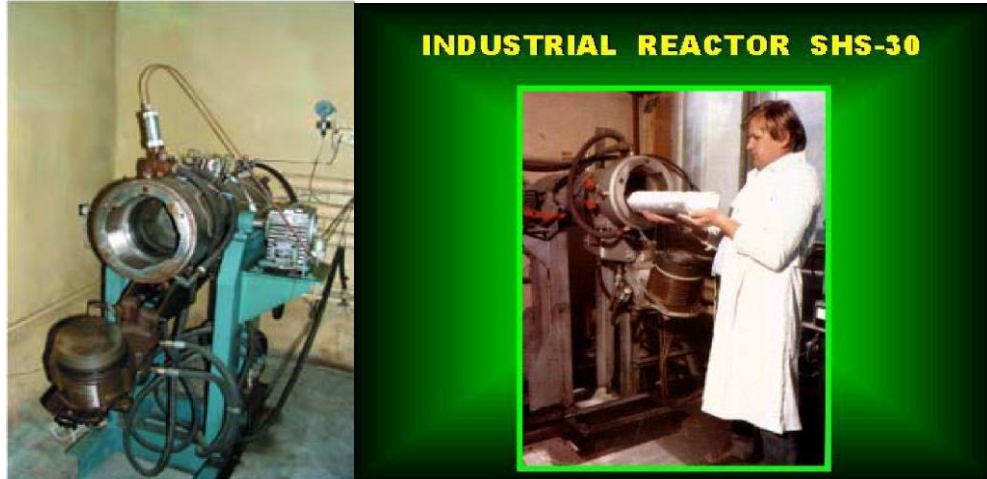


Figure 2.3: An industrial SHS reactor, from [38].



Figure 2.4: Large-scale ceramic-lined steel pipes produced using SHS [17].

2.2.2 Combustion Wave in the SHS Process

In the SHS process, the reactants are typically fine powders that are mixed and pressed into a pellet to increase their contact. The pellet is then placed inside a closed chamber and ignited in vacuum or inert atmosphere [39]. At the laboratory scale, the SHS process usually involves the combustion of a small pellet of the initial powder mixture in a specific gas environment (e.g., argon at 1 atm pressure). The pellet is ignited at the top using a hot wire, a laser beam, or some other source of energy. This provides the heat impulse needed to initiate the chemical reaction in the

heated surface layer. Upon ignition, a combustion wave forms and propagates downward, leading to the formation of desired products (Fig. 2.5). Only a small amount of energy is required for the ignition, while the combustion process utilizes the reaction heat release, thus dramatically reducing energy consumption [32].

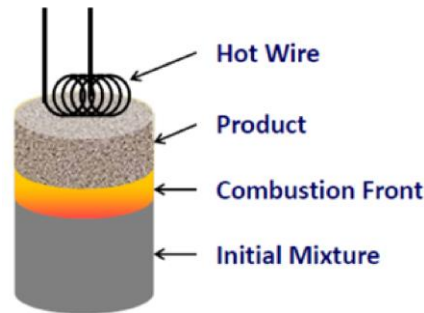


Figure 2.5: Schematic of the SHS process.

For most SHS processes, the combustion front presents a smooth surface that propagates layer-to-layer with a constant velocity. The combustion front is considered to be the "fire" part of the wave and is followed by extended zones of chemical reactions and various physico-chemical conversions. These chemical reactions and conversions taking place imply how the propagation front will react [40].

The combustion wave in a typical SHS process consists of several zones as shown in Fig. 2.6 [41]. The preflame zone is characterized by a high thermal gradient. In this zone, intense heat transfer takes place though the main chemical reactions do not occur. Phase transformation and side reactions can take place. In the main heat release zone, the main reactions occur. The velocity of combustion front propagation is determined by the heat release in the zone of main heat release and heat transfer in the preflame zone. Heat losses from the main heat release zone to the surroundings may also play an important role. If they are significant, the combustion may be

extinguished. This is called “quenching”, and it can be used to study the products formed in the main heat release zone [17]. If the reaction occurring in the main heat release zone is not complete, zones of delayed combustion and structure formation follow.

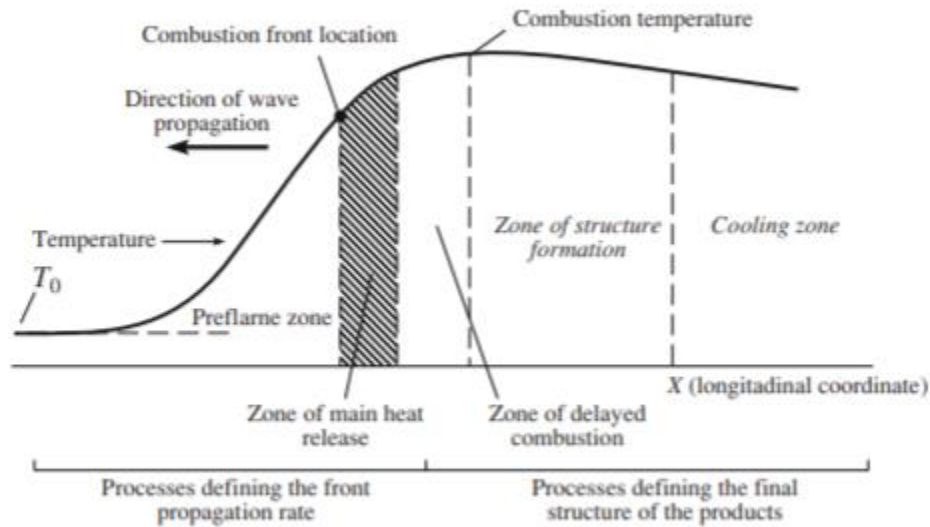


Figure 2.6: Typical structure of combustion wave in the SHS process [41].

The presence of the structure formation zone is a characteristic of SHS that distinguishes it from combustion of propellants and other energetic materials. Several processes, such as crystallization, product condensation, phase transformation, etc., that can take place in this zone do not affect the combustion wave velocity. They do, however, strongly influence the structure of the product [18, 41].

The temperature profiles obtained during combustion carry valuable information. In studies conducted by Zenin and Maltsev [40, 42, 43], microthermocouple and optico-spectral methods were used to determine the temperature profiles. These investigations showed that SHS temperature profiles consist of four types, shown in Fig. 2.7 [40]. Type I is a classical case, where

the combustion wave consists of a heated layer and a reaction zone (shaded area), which is narrower than the former [40, 44]. Type II signifies profiles with a wide reaction zone; in this case there are two subzones known as "propagation" and "post-combustion". The propagation sub-zone promotes the combustion front displacement. This type of temperature profile is typical in processes such as SHS [40]. Type III is distinguished by a point of inflection in the temperature profile curve. The presence of two zones of chemical reaction is necessary for its existence with the front propagation only affected by the first zone of reaction. These profiles typically occur with complicated reactions occurring in the combustion wave. The final type is Type IV; this is characterized by the presence of an isothermal region. This region appears as a plateau and shows the thermal action of the profile high temperature regions from the combustion front. The temperature plateau results from the simultaneous action of the chemical reaction and phase transition (ex. reactant melting) [40].

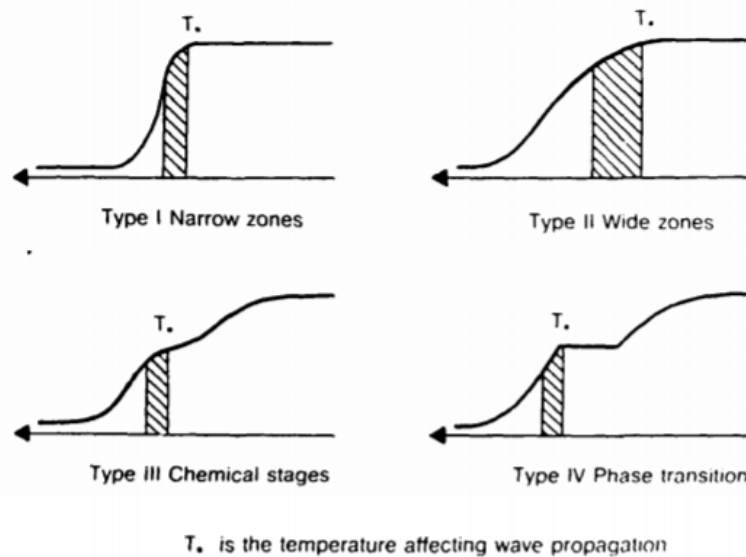


Figure 2.7: Types of temperature profiles [40].

Stationary layer-to-layer propagation of the combustion wave is not always obtained during SHS. In some cases, researchers observed oscillatory combustion and spin combustion. During oscillatory combustion, the layer-to-layer propagation of combustion is retained, but the front propagates in an oscillatory regime, i.e. it consists of successions of rapid displacements and stops. In spin combustion, the layer-to-layer regime is distorted, and observations show one or several hot spots, which propagate at a certain velocity along a definite trajectory (often a helical path for cylindrical samples) [40]. Oscillations result from process sensitivity to the longitudinal minor perturbation, and spin results from sensitivity to transverse perturbations. In both cases, the heated layer, formed ahead of the combustion front due to the heat transfer, burns out. During oscillatory combustion the layer burns out in the longitudinal direction and then forms again, but during spin combustion it fully burns out in the transverse direction [40].

Researchers have used various approaches to describe and explain spin combustion using one- and two-dimensional (1D and 2D) investigations of spinning waves [45-47]. Often they neglected radial heat transfer and considered a model for combustion of a thin, cylindrical shell. To describe the inner structure of the three-dimensional (3D) spinning wave (the motion of reaction zones inside a cylinder), Ivleva and Merzhanov took into account all components of heat transfer (longitudinal, tangential, and radial) [48, 49]. Their modeling showed the possibility of different modes of spin combustion, briefly described below.

The simplest mode is a steady one-spot combustion wave. The front profile is controlled by a high-temperature area (hot spot). Figure 2.8 shows (a) the structure of the combustion front, (b) the distribution of the dimensionless temperature, θ , and (c) the distribution of the conversion degree, η , at the same moment of time in a cross section bearing a point with θ_{\max} . This cross section is front-bound and moves downward as the sample burns out. The distribution of θ is not

uniform and has a hot spot where temperature is greater than the combustion temperature ($\theta > 0$). If θ is sufficiently high, the heat flux from the hot spot becomes sufficient for ignition of the unreacted mixture nearby, so the hot spot shifts into this zone, resulting in a clockwise motion of the hot spot. Since the entire front is also moving downward, a screw trajectory is obtained as a result. Figure 2.8 (d) shows the distribution of θ in the form of isotherms over a cross section of the sample at some moment of time (the brighter the area, the higher the temperature). During steady propagation of the combustion wave, the configuration of the front and the distributions of both θ and η remain unchanged and only rotate when moving downward [49].

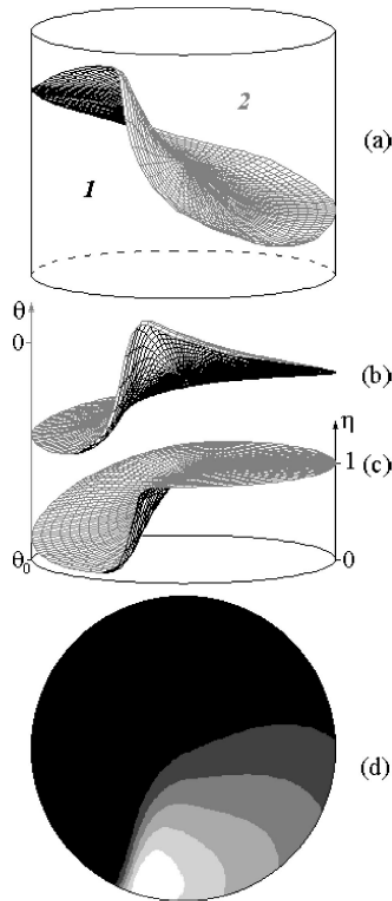


Figure 2.8: Steady one-spot spinning wave: (a) wave front structure, spatial distribution of (b) θ and (c) η in the cross section of θ_{\max} , and (d) the distribution of θ in the form of isotherms [49].

Spinning waves with two spots on the surface are also possible, where two hot spots move steadily over a screw trajectory. Steady one- and two-spot combustion modes were obtained at a relatively low ratio of the sample radius to the characteristic length of the reaction zone. With increasing the radius, the wave propagation becomes unsteady (symmetric periodic, asymmetric periodic, and aperiodic). The symmetric periodic two- or three-spot spinning waves move along the sample axis in a pulsating mode, while near the surface the spots move in a spinning mode. In the asymmetric periodic wave, the inner areas burn in a pulsation mode, while a flickering spot moves in the near-surface layer; this spot varies in its shape and size. The asymmetric periodic wave with three spots was also obtained. Here the spots dive in the depth of the sample, merge, separate, appear on the surface, etc. Note that the merger of two spots gives birth to two new spots that move in opposite directions. With a further increase in the radius, the spinning wave becomes aperiodic (chaotic), with a complicated motion of many spots. The chaotic modes are strongly dependent on the initial conditions.

It should be noted that the combustion modes obtained by Ivleva and Merzhanov did not include the motion of two counterpropagating hot spots, which was often observed experimentally. This was however described in a 2D model (combustion only on the surface of the cylinder) by Bayliss and Matkowsky [46]. The computations of solutions involving counterpropagating hot spots have shown that when the spots collide, they undergo one of three possible interactions: (i) a strong (hot) spot collides with a weak (cooler) spot with both the strong and weak spots continuing to rotate in the same direction as before the interaction, (ii) two strong spots collide to produce two weak spots, and (iii) two weak spots collide to produce two strong spots. The latter two interactions describe the phenomena of apparent annihilation and creation of hot spots, respectively, which have been observed in experiments.

Recently, spin combustion of Mo/B/Si mixtures has been studied experimentally [50]. The following modes were observed: a single hot spot, two counterpropagating hot spots, three hot spots moving in the same direction, and multiple hot spots. Characteristics of spin combustion such as axial velocity (u), pitch (z), frequency (f), number of spin heads (n), and tangential velocity (v) were determined based on video records of the combustion process. Parameters were checked for accuracy using the mass conservation equation: $v = \pi \cdot d \cdot u \cdot n \cdot z^{-1}$, where d is the pellet diameter. There is also a relationship between the characteristics u , f , and z : $u = f \cdot z$. The measurements have revealed that the product $u \cdot z$ (or $u^2 \cdot f^{-1}$) remains approximately constant. This was experimentally shown in an early work on spin combustion [51]. According to a simplified theory developed by Novozhilov [45], the product $u \cdot z$ (or $u^2 \cdot f^{-1}$) is a constant and is of the same order of magnitude as the thermal diffusivity of the medium. This is explained by the role the pitch plays in the preheat zone in the flame. Many powdered mixtures used in SHS have thermal diffusivity in the order of $1 \text{ mm}^2/\text{s}$, thus the obtained values of $u \cdot z$ maintain the same order of magnitude as the thermal diffusivity.

The effects of spin combustion on the properties of the products are not well documented in literature. The velocity of the propagation front of the sample would be dependent on the mixture composition and combustion temperature. During spin combustion, the temperature is relatively low because of a lower exothermicity [50]. This lesser temperature alone may change the product composition.

Along with a “normal” SHS, there is one more combustion synthesis technique, which apparently has not been used for the Nb-Si system yet. This is known as the "chemical oven" technique [52], where the sample is surrounded by a layer of a highly exothermic mixture such as Ti/C or Ti/B (Fig. 2.9). Combustion of this layer releases enough heat for enabling ignition and

combustion of the core material even for mixtures with very low exothermicities. The combustion products of the shell, such as TiC and TiB₂, are also valuable products and can be utilized. Recently, the "chemical oven" technique has successfully been used for the synthesis of several Mo-B-Si materials that could not be obtained by conventional SHS [52].

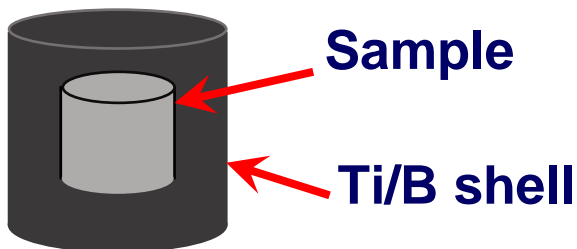


Figure 2.9: Diagram of chemical oven technique.

2.2.3 SHS of Niobium Silicides

SHS of niobium silicides was studied as far back as 60 years ago in work by Sarkisyan *et al.* [53]. The Nb:Si mole ratio was varied over a range from 5:1 to 1:4. Despite the relatively high adiabatic flame temperatures, self-sustained combustion was achieved only after preheating the mixtures. The mixture of 1 mol Nb and 2 mol Si required the lowest preheating temperature, 250 °C (523 K), and the products contained NbSi₂ and unreacted Nb. The mixture of 5 mol Nb and 3 mol Si required preheating at 450 °C (723 K), and the products contained NbSi₂, Nb, and two phases (α and β) of Nb₅Si₃. Mixtures with Nb contents higher than in Nb₅Si₃ required higher preheating temperatures. It is interesting that both α and β phases of Nb₅Si₃ were observed in the products obtained for Nb:Si mole ratios from 5:1 to 2:3. The presence of the high-temperature β phase was noted but not understood because the measured combustion temperatures were lower than the phase transition temperature of 1940 °C (2213 K).

More recently, SHS of Nb_5Si_3 with preheating was studied by Yeh and Chen [35, 54]. It was reported that preheating at 300 °C allowed for the mixture to be ignited, which led to the formation of α - Nb_5Si_3 and β - Nb_5Si_3 phases. Limited data on the SHS with preheating of $\text{Nb}_5\text{Si}_3/\text{Nb}$ composites were also reported [54]. The authors have investigated some additional factors, such as the mixture density and reported observations of different modes of the combustion wave (spinning vs. planar), but, in general, the results were similar: preheating was necessary, and the final product contained multiple phases including the high-temperature β phase.

The addition of Joule heating to the reaction zone has been investigated at the University of California – Davis to enable combustion synthesis of Nb_5Si_3 with no preheating [55]. Specifically, the so-called field-activated combustion synthesis (FACS) was used, where an electric field is applied perpendicular to the direction of the combustion wave. The mode of wave propagation and the nature of the obtained product depended on the field magnitude. At higher fields, a steady propagation of a planar combustion front occurred, and the product contained α and β modifications of Nb_5Si_3 , with no other phases. The relative concentrations of α and β phases were dependent on the applied field and the mixture density. At lower fields, a spinning combustion wave was observed, leading to the formation of a multiphase product that included α - Nb_5Si_3 , NbSi_2 , and unreacted Nb.

Later, the UC-Davis team had performed simultaneous synthesis and densification of niobium silicide/niobium composites using two techniques – FACS and spark plasma sintering (SPS) [21]. The two techniques are, actually, very similar to each other. The SPS facility used involved a pulsed DC power supply, which generated 15 V, 5000 A, while the FACS applied 60 Hz AC, 10 V, 1750 A current. Each facility included a uniaxial 100 kN press. Dense Nb_5Si_3 and $\text{Nb}_5\text{Si}_3/\text{Nb}$ composites were obtained. SPS and FACS are feasible only for mixtures that are good

electrical conductors. For example, the attempt to use FACS for synthesis of NbSi₂ failed because of a very low electrical conductivity of the mixture [21].

A more universal approach to enabling SHS of niobium silicides with no preheating is based on the use of mechanical activation of the reacting mixture. Mechanical activation is a short-term, high-energy ball milling step before the SHS process. It has been shown that mechanical activation facilitates the ignition and ensures stable combustion of low-exothermic mixtures. The entire process is commonly called mechanical activation-assisted SHS or mechanically activated SHS (MASHS) [5,30]. It has been used for the synthesis of various compounds. Recently, MASHS was used for the fabrication of molybdenum silicides and borosilicides [50,52], magnesium silicide [56], and zirconium diboride [57].

MASHS of niobium silicides has been studied by researchers in Italy [58], China [59], and Russia [60-64]. The Italian team has investigated the effect of milling on the reactivity of mixtures corresponding to stoichiometries of reactions for synthesis Nb₅Si₃ and NbSi₂, described by Eqs. (1) and (2). A shaker mill (Spex Certiprep 8000) was used. For each mixture, after sufficiently long milling, self-sustained combustion was achieved with no preheating. In contrast with the results for preheated mixtures [53], only one compound, corresponded to the expected reaction, was observed in the products. Similarly, to the experiments with preheating, both α and β phases of Nb₅Si₃ were detected. It was found that increasing the milling time increased the amount of β phase with respect to α phase.

Work by Maglia *et al.* [58] has also provided insight into the understanding of the difficult ignition of Nb/Si mixtures and explained the observed positive effect of mechanical activation. Briefly, two factors may be responsible for the poor ignition of the Nb-Si system despite the relatively high exothermicity. First, the solubility of Nb in molten Si is limited, and this decreases

the rate of this dissolution. Second, the melting points of both Nb_5Si_3 and NbSi_2 are much higher than the combustion temperatures. It has been suggested that the first step in the reaction mechanism in the composition $\text{Nb}:\text{Si} = 5:3$ is the reaction of liquid Si with abundant solid Nb, leading to the formation of NbSi_2 . After that, the formed solid NbSi_2 slowly reacts with the residual solid Nb. This explains the observed difficulty of obtaining the Nb_5Si_3 phase by combustion, despite its significant negative enthalpy of formation and high adiabatic flame temperature. The mechanical activation step increases the surface contact area of the powders and decreases the critical diffusional lengths required for completion of the solid-state reaction, thereby enhancing the overall reactivity of the Nb-Si system.

Song *et al.* [59] mixed Nb and Si powders in a 1:2 mole ratio in a planetary ball mill at 450 rpm for 240 min using Al_2O_3 milling beads and alcohol. The subsequent SHS process fully converted the compacted mixture to NbSi_2 , with no additional phases.

A team from Tomsk Research Center [60-64] used a planetary mill to activate Nb/Si mixtures. One interesting result of these studies was a short time of mechanical activation as compared with the studies [58,59]. For example, in [58], full conversion of $5\text{Nb} - 3\text{Si}$ mixture to Nb_5Si_3 by SHS required at least 120 min of milling, while the optimal time of mechanical activation in a planetary mill was in the range 0.5 – 2 min [61-64]. This indicates that the choice of type and parameters of mechanical activation is crucial for successful MASHS of niobium silicide-based composites.

The planetary ball mill AGO-2 has shown shorter milling times when compared to most other mills. In a study comparing the AGO-2 and the Fritsch Pulverisette 7 planetary ball mills and their times to synthesize ZnFe_2O_4 from ZnO and Fe_2O_3 , it was shown that the AGO-2 took 2 h compared to the 4 h needed from the Pulverisette 7 [65].

A study by Voloskova *et al.* on the mechanochemical synthesis of calcium orthosilicate from high-calcium fly ash provides a direct comparison of the AGO-2 and the Fritsch Pulverisette 5 “classic line” mills [66]. The milling times to produce calcium oxide content (W_{CaO_f}) can be seen in Fig. 2.10.

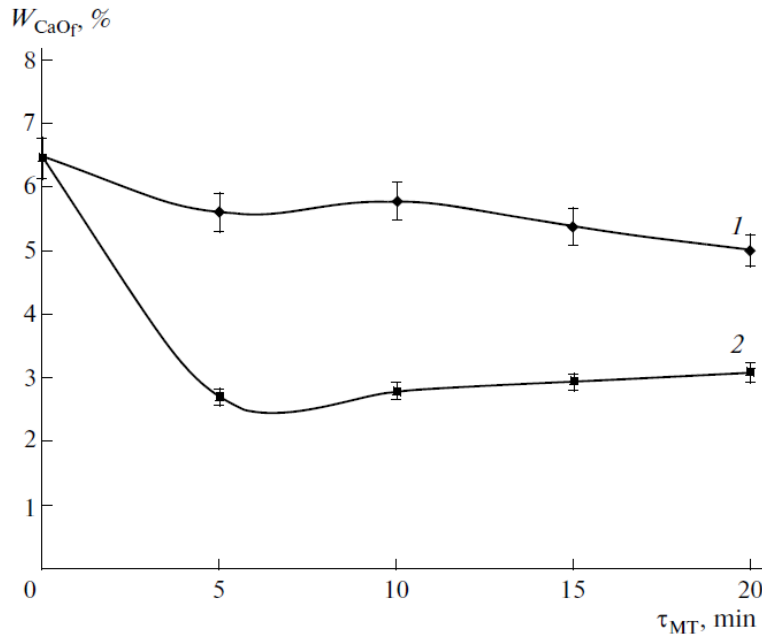


Figure 2.10: Dependence of the free calcium oxide content (W_{CaO_f}) of fly ash on the time of mechanochemical treatment (τ_{MT}) in (1) AGO-2 and (2) Fritsch Pulverisette 5 classic line [66].

When comparing specifications, the AGO-2 mill has the largest power per gram of charges; it is able to reach up to 3.0 W/g compared to the 1.6 W/g of the Pulverisette G5 planetary mill, which explains the shortened milling times during mechanical activation. However, the Pulverisette G5 planetary mill has a larger ball velocity reaching 11.24 m/s compared to 8.24 m/s produced by the AGO-2 [67]. The Pulverisette 7 premium line mill generates a centrifugal acceleration of 95 g ($g = 9.81\text{m/s}^2$), whereas the AGO-2 can reach only 60 g [68]. To summarize,

The choice of the mill that should be based on the need of the user, as well as availability of the mill.

From the scientific viewpoint, it is remarkable that virtually all studies on SHS of Nb_5Si_3 have reported the formation of the high-temperature $\beta\text{-Nb}_5\text{Si}_3$ phase despite the fact that the temperatures were well below its existence domain in the Nb-Si phase diagram. An example of this is shown in work by Maglia *et al.* [58], which shows that in the composition of Nb:Si = 5:3, $\beta\text{-Nb}_5\text{Si}_3$ appeared in every milling case (Table 2.1). When comparing to the obtained temperature profiles (Fig. 2.11), all temperatures are below the $\beta\text{-Nb}_5\text{Si}_3$ phase transformation temperature of 1940 °C (2213 K).

Table 2.1: Effect of milling on product composition [58].

Milling time (min)	Product composition (%)					
	NbSi ₂	Nb	Si	$\alpha\text{-Nb}_5\text{Si}_3$	$\beta\text{-Nb}_5\text{Si}_3$	C-Nb ₅ Si ₃
Nb:Si = 1:2						
0	97.76	0.75	1.48	0	0	0
60	99.91	0.088	0	0	0	0
180	99.79	0.203	0	0	0	0
360	99.77	0.25	0	0	0	0
540	94.35	0.163	0	0.463	0.16	4.85
Nb:Si = 5:3						
0	35.02	32.6	1.47	25.82	2.81	2.25
80	15.89	18.06	8.87E - 4	41.03	13.89	11.1
120	0	0	0	75.41	13.56	11.02
240	0	0	0	72.97	9.32	17.7
285	0	0	0	48.06	23.34	28.58

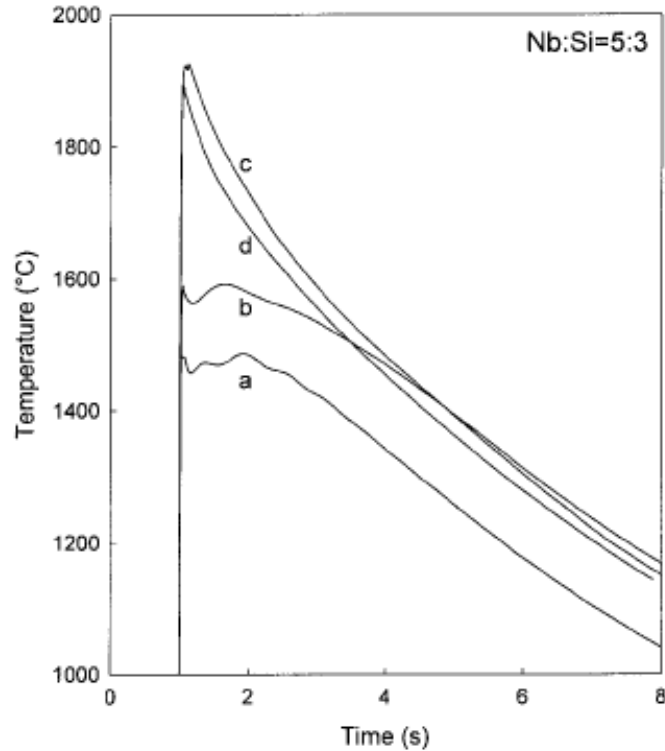


Figure 2.11: Temperature profiles for the composition Nb:Si = 5:3, for the milling times (min): (a) 80; (b) 120; (c) 240; and (d) 285 [58].

The formation of the β -Nb₅Si₃ phase during combustion may be related to the high rates of the SHS process, which lead to the formation of non-equilibrium products. This interesting result may also have a significant importance for applications as the β -Nb₅Si₃ phase may provide better mechanical properties.

The goal of the present work is not only development of niobium silicides, but also the formation of niobium silicide-based composites. Different additives may affect the SHS process outcomes. Additives with very high melting points and non-reactive ones may create additional difficulties. On the other hand, the addition of elements with low melting points (e.g., Sn) may help overcome diffusion difficulties. Some additives may exhibit exothermic reactions between each other or with Nb or Si, which also may promote ignition and combustion.

As noted in Section 2.1, binary Nb-Si alloys are brittle, and an approach to improving toughness in the Nb₅Si₃ is to make a composite with a more ductile phase, such as Nb. In such a composite, grains of Nb solid solution in the Nb₅Si₃ matrix provide toughness at ambient temperature, while the silicide supplies strength at high temperatures.

To increase the mechanical properties, the material should include more Nb than in the Nb₅Si₃ stoichiometry. Niobium silicide composites typically contain only 12–25 at% Si [9-10,16], while Nb₅Si₃ contains 37.5 at% Si. It should be noted that a study by Yeh and Chen [19] showed that the combustion behavior of Nb/Si powders is not particularly affected by the variation of experimental parameters (sample density, preheating temperature, and starting composition).

To improve the properties of niobium silicide-based composites, the addition of Ti, Hf, Cr, Al, and other elements has been studied extensively [7]. The concentration of titanium in these materials is as high as 19 – 34 at% [7], much higher than any other additive. Due to the high atomic percentage of Ti, it is worth exploring the feasibility of using MASHS for fabricating the composites of Nb, Ti, and their silicides from ternary Nb/Ti/Si mixtures.

The addition of Ti should help ignite mixtures with a lower content of Si. The standard formation enthalpy of Ti₅Si₃ per mole of atoms (-78.1 ± 5 kJ [69]) is greater than that of Nb₅Si₃ (-64.6 ± 2.4 kJ [70]), leading to higher combustion temperature. Since the melting point of Ti is 1668 °C, during SHS of Ti₅Si₃, both Ti and Si are liquid in the reaction zone, allowing their rapid reaction with no preheating or mechanical activation [71-74]. In mechanically activated Ti/Si mixtures, the combustion wave propagated at a temperature as low as 1270 °C, i.e. with solid Si in the reaction zone [73]. Thus, it is expected that ternary Nb/Ti/Si mixtures can be combustible at Si concentrations below 25 at%.

Chapter 3: Experimental Procedures and Facilities

3.1 MASHS Procedures

3.1.1 Mixing

Niobium, titanium, and silicon powders were obtained from Alfa Aesar; they were –325 mesh and have purities of 99.8, 99.5, and 99.5%, respectively. Initially, 6 g samples were prepared. Later, the sample mass was increased to 18.5 g. Tables 3.1 and 3.2 show the masses of powders for making various mixtures studied in the present work.

Table 3.1: Masses of powders used for making 6 g samples.

Mixture	Nb	Si
	g	g
Nb/Si (1.67:1)	5.080	0.920
Nb/Si (1.70:1)	5.094	0.906
Nb/Si (1.75:1)	5.116	0.884
Nb/Si (1.81:1)	5.141	0.859
Nb/Si (1.89:1)	5.173	0.827
Nb/Si (2.00:1)	5.212	0.788
Nb/Si (2.17:1)	5.266	0.734

Table 3.2: Masses of powders used for making 18.5 g samples.

Mixture	Nb	Si	Ti
	g	g	g
Nb/Si (1.67:1)	15.66	2.84	-
Nb/Si (2:1)	16.071	2.429	-
Nb/Si (3:1)	16.806	1.694	-
Nb/Si/Ti (3:1:1)	14.538	1.465	2.497
Nb/Si/Ti (2:1:1)	13.132	1.985	3.383
Nb/Si/Ti (1:1:1)	10.179	3.077	5.244

The powders were mixed in a three-dimensional inversion kinematic tumbler mixer (Inversina 2L, Bioengineering, Fig. 3.1). Stainless steel bowls coated with zirconium oxide (Fig. 3.2) were used for powder containment and chosen based on the amount of powder needed, 20-mL bowls for 6 g and 80-mL bowls for 18.5 g. Powder mixtures were prepared inside a glovebox (Terra Universal, Series 300, Fig. 3.3) and removed once the bowl was fully locked and sealed. The used bowls were equipped with lids that have valves. Using these valves, the bowls were filled with ultra-high purity argon to avoid oxidation of the powders while mixing. Once the bowls were purged, they were positioned and locked into the mixer to be individually mixed for 60 mins.



Figure 3.1: Mixer (Inversina 2L, Bioengineering) with (a) closed and (b) open protective shield.



Figure 3.2: Bowl with purging valves.



Figure 3.3: Glovebox (Terra Universal, Series 300).

3.1.2 Mechanical Activation

The mixed powders were mechanically activated in a high-energy planetary ball mill (Fritsch Pulverisette 7 Premium Line, Fig. 3.4) using the same bowls that were used for mixing, but now with zirconia grinding balls (diameter: 5 mm). The balls-mixture mass ratio was 5:1. Before milling, the bowls were purged with ultra-high purity argon to avoid oxidation of the powders during mechanical activation. The milling speed was 1000 rpm and four milling times were used: 1, 2, 5, and 10 min. To prevent high temperatures and reaction during the milling process, a 60-min cooling pause was given after every minute of milling (e.g., a total milling time of 10 min was divided into 10 cycles). After completing the milling procedure, the powders were removed from the bowl inside the glovebox in an atmosphere composed of 5% O₂ and 95% N₂.



Figure 3.4: Planetary ball mill (Fritsch Pulverisette 7 Premium Line).

If the reactions between the powders occur during milling, the released heat may increase the temperature and hence pressure of argon in the bowl, which is dangerous. The locking hooks for the lid (see Fig. 3.2) withstand an internal pressure of up to 40 bar. The bowls are also designed with a safety feature providing overpressure relief at 20 bar. To ensure that pressure remains sufficiently low during milling even if the entire mixture has completely reacted, thermodynamic calculations for adiabatic combustion at constant volume were conducted using THERMO (Version 4.3) software [75].

The calculations were first conducted for Nb/Si (5:3 mole ratio) mixture and the following parameters.

Volume of the bowl: **20-mL**

Diameter of a ball: 5 mm

Number of balls: 80 (Mass of the balls: 29.6 g)

Initial pressure of Ar in the bowl: 1 atm

Mass of Nb/Si mixture: 1 g, 2 g, 3 g, 4 g, 5 g, 6 g, 7 g, 8 g, 9 g, 10 g

Volume of the bowl: **80-mL**

Diameter of a ball: 5 mm

Number of balls: 250 (Mass of the balls: 92.5 g)

Initial pressure of Ar in the bowl: 1 atm

Mass of Nb/Si mixture: 18.5 g

The volume of the gas was calculated as the volume of the bowl minus the volume of balls minus the volume of the initial reactants.

The calculations have shown that Nb_5Si_3 is the only product. Table 3.3 shows the obtained values of the adiabatic flame temperature and final pressure. It is seen that the final pressure is almost the same in all the calculations, and it is in the range from 7.83 to 7.93 atm (1 atm = 1.01325 bar). The low sensitivity of pressure to the variation of the mixture mass is explained by (1) the low variation of the adiabatic flame temperature because of the relatively low mass of argon and (2) the low volume of the solid materials as compared with the volume of argon gas in the bowl.

Table 3.3: The adiabatic flame temperature and pressure of Nb/Si mixtures calculated at constant volume (20 mL and 80 mL).

Mass	Adiabatic Flame Temperature	Pressure
g	K	atm
Volume: 20 mL		
1	2257	7.83
2	2273	7.88
3	2278	7.91
4	2281	7.91
5	2283	7.91
6	2284	7.92
7	2284	7.93
8	2286	7.92
9	2286	7.92
10	2286	7.92
Volume: 80 mL		
18.5	2282	7.91

The calculations were also conducted for combustion of ternary Nb/Si/Ti mixtures, listed in Table 3.2, with a mass of 18.5 g. The results are shown in Table 3.4. It is seen that the pressure is about 8 atm in the 1:1:1 mixture and decreases with increasing the mole fraction of Nb.

Table 3.4: The adiabatic flame temperature and pressure of Nb/Si/Ti mixtures calculated at constant volume (80 mL).

Nb/Si/Ti Ratio	Adiabatic Flame Temperature	Pressure
	K	atm
3/1/1	1539	5.38
2/1/1	1830	6.42
1/1/1	2243	7.93

Thus, according to the thermodynamic calculations, in the unlikely case of ignition inside the bowl, pressure will be about 8 bar, i.e. way below the value of 40 bar at which the locking hooks may fail as well as below the value of 20 bar at which the overpressure relief feature of the bowl activates.

3.1.3 Compaction

The powders were compacted to cylindrical pellets in a uniaxial hydraulic press (Carver, Fig. 3.5). Trapezoidal pressing dies of three diameters (6, 13, and 25 mm) were used. The pressing force was 12.7, 29.4, and 74.5 kN for pellet diameters of 6, 13, and 25 mm, respectively (the corresponding pressures were 451, 222, and 152 MPa).

In some experiments, a booster pellet of titanium/boron mixture (1:2 molar ratio) was placed at the top of the sample to facilitate the ignition and ensure identical ignition parameters. These pellets were compacted at the same pressing parameters.



(a)



(b)

Figure 3.5 Pressing equipment: (a) die set for 13 mm diameter and (b) uniaxial hydraulic press.

3.1.4 SHS Procedures

The combustion experiments were conducted in a 30-L stainless steel reaction chamber (Fig. 3.6). The pellet was installed vertically on a ceramic fiber insulator (Fiberfrax). The chamber was evacuated and filled with ultrahigh purity argon at 1 atm. The pellet was ignited at the top by a hand coiled tungsten wire (Midwest Tungsten Service, Inc.) heated with a DC power supply (Mastech HY3050EX) set at 15 V. As mentioned above, in some experiments, a Ti/B booster pellet was placed at the top of the sample.

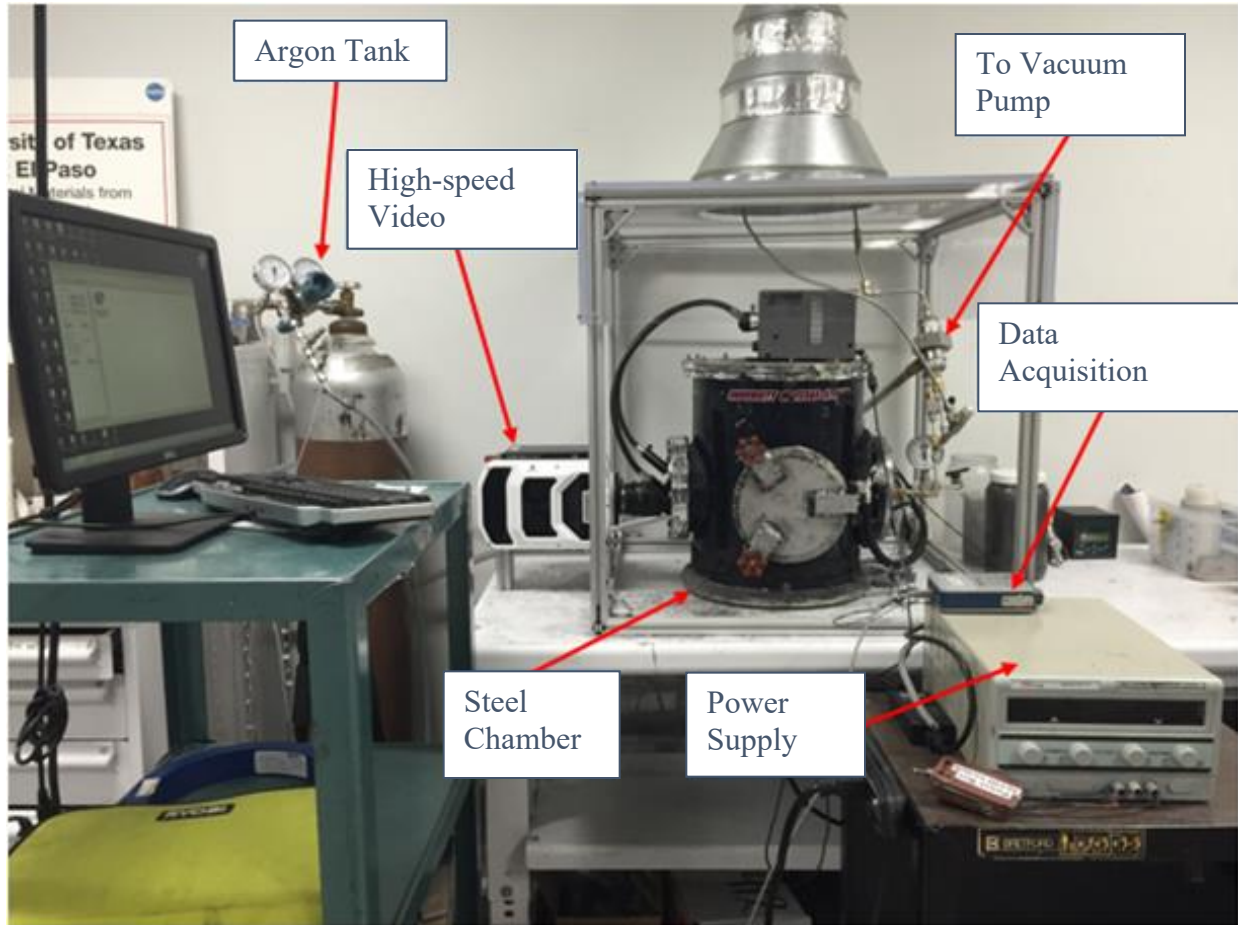


Figure 3.6: Hot-wire ignition setup.

The combustion process was observed using video recording (iPhone XS, Dual 12MP wide and Telephoto cameras) through a glass window. In several experiments, thermocouples (95%W/5%Re-74%W/26%Re, type C, wire diameter: 76.2 μm , Omega Engineering) were used to measure the temperature in the middle of the sample during the combustion process. The thermocouples, located in two channel ceramic insulators (Omegatite 450, Omega Engineering), were inserted into pellets through channels, drilled approximately midway through the sample. In some experiments, the channels were perpendicular to the pellet axis, while in the others they were drilled from the bottom along the axis. The thermocouples were connected to a USB-based data acquisition system (National Instruments USB-9211).

A series of experiments were conducted using the chemical oven technique, where the pellet consisted of a core made of the Nb/Si (5:3 mole ratio) mixture and a shell made of the Ti/B (1:2 mole ratio) mixture. To prepare the composite pellet, first the core pellet (diameter 13 mm) was made as described in Section 3.1.3. Next, a 25 mm die was partially filled with the Ti/B mixture, the core pellet was submerged into this mixture, and pressing was performed.

3.2 Characterization of Materials

3.2.1 Laser Diffraction Particle Size Analysis

Particle size distributions of the used Nb and Si powders and mixed powders after milling were determined using a laser diffraction particle size analyzer (Microtrac Bluewave, Fig. 3.7). This instrument utilizes a three-laser, multi-detector, multi-angle optical system to provide particle size analysis in the range from 0.01 μm to 2800 μm . The entire system includes a sample delivery controller (SDC) that delivers the sample powder to the particle size analyzer unit. Isopropyl alcohol (VWR International), neutral with respect to the tested powders, was used as a carrier liquid.



Figure 3.7: Particle size analyzer (Microtrac Bluewave).

3.2.2 X-Ray Diffraction Analysis

Compositions of the powders were investigated after milling and after combustion using X-ray diffraction analysis (Bruker D8 Discover XRD and Rigaku MiniFlex II Desktop XRD, Fig. 3.8). For the analysis, the products were crushed into a powder and scanned in a 2θ range of 20° to 90° , with a scan speed of $5^\circ/\text{min}$ and a step size of 0.07° .



(a)



(b)

Figure 3.8: (a) Bruker D8 Discover XRD and (b) Rigaku MiniFlex II Desktop XRD.

3.2.3 Scanning Electron Microscopy

Scanning electron microscopy (SEM) of Nb/Si mixtures and obtained products was conducted using a TM-1000 Tabletop Microscope, which utilizes a backscatter electron detector, (Fig. 3.9a) and Hitachi S-4800 Scanning Electron Microscope (Fig. 3.9b). The samples were set up using the “sprinkling method” which consists of applying a water-soluble carbon paste (Electron Microscopy Sciences, CCC Carbon Adhesive) on the specimen stub. Before the paste dries, powder was collected with a cotton swab and sprinkled onto the paste. Once the paste was completely dry, the excess powder was blown off to remove loose powders and minimize the contamination of the internal sample chamber of the instrument.



(a)



(b)

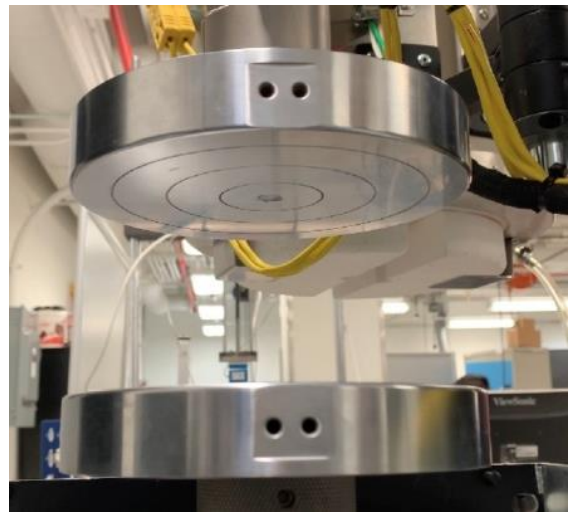
Figure 3.9: (a) TM - 1000 Tabletop Microscope and (b) Hitachi S-4800 Scanning Electron Microscope.

3.2.4 Compressive Strength Testing

Compression testing was conducted using an Instron 5969 Universal Test Machine (Fig. 3.10a) in accordance with ASTM standard E9 [76]. For testing, the middle section of the pellet was extracted using a diamond saw. The sample was then polished to ensure the top and bottom surfaces were flat. Compression plates were fitted onto the machine and used for sample testing (Fig 3.10b).



(a)



(b)

Figure 3.10 (a) Instron 5969 Universal Test Machine and (b) compression testing plates.

Chapter 4: Results and Discussion

4.1 MASHS of Nb₅Si₃

Experiments with Nb/Si (5:3 mole ratio) mixtures were conducted with 13-mm-diameter pellets, which had a height of about 10 mm. The relative density of the samples was in the range from 53 to 63%. Initially, the pellets were ignited using a 1-g booster pellet (thickness: about 3 mm) at the top. In the experiments with an unmilled Nb/Si mixture, the combustion front propagation stopped soon after the ignition, which correlates with prior studies [19, 53-54, 77] where preheating was required. Mechanical activation for 1 min has enabled the propagation until the bottom of the sample.

Then, experiments were conducted with no booster pellet. The mixture activated for 1 min ignited, but the combustion front stopped in the middle of the pellet. However, all other mechanically activated mixtures (2, 5, and 10 min) burned completely. Figure 4.1 shows images of the combustion propagation in the experiments with mixtures milled for 2 and 10 min. It is seen that with increasing the milling time from 2 to 10 min, the front velocity doubled, and the light emission increased dramatically.

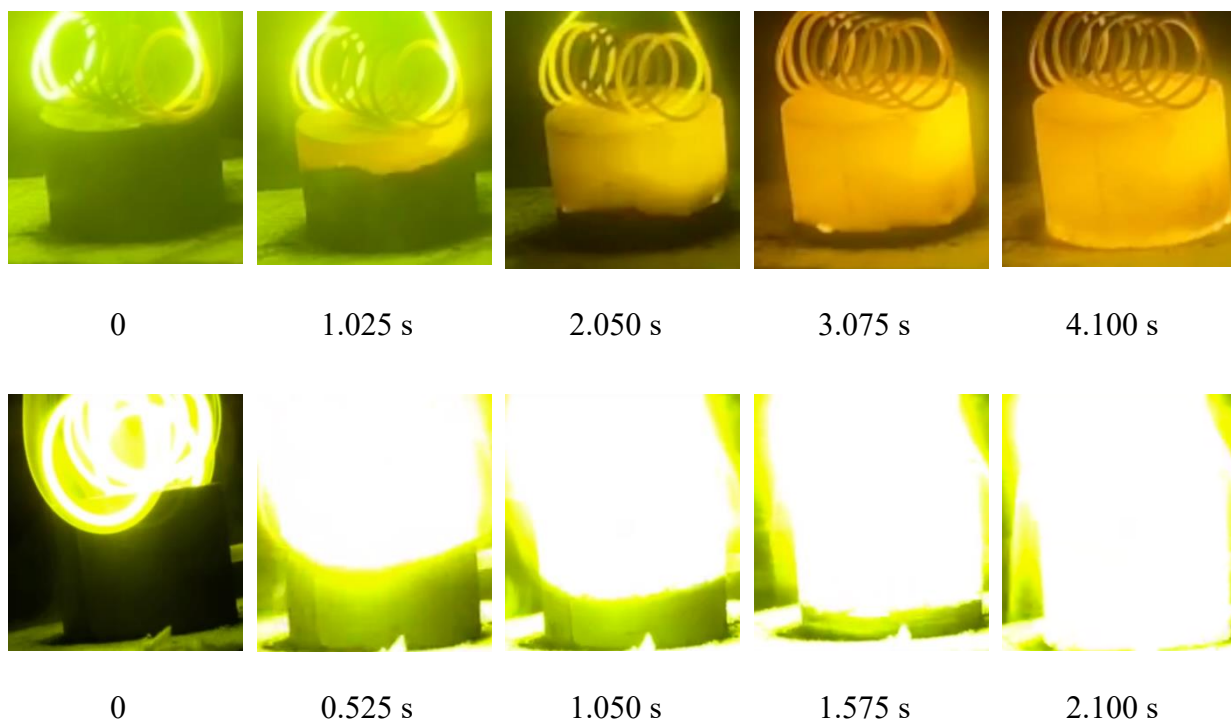


Figure 4.1: Images of combustion propagation over Nb/Si mixture (5:3 mole ratio), mechanically activated for (top) 2 min and (bottom) 10 min. Time zero was selected arbitrarily.

Figures 4.2 – 4.4 show the XRD patterns of products obtained by combustion of the mixtures activated for 2, 5, and 10 min. It is seen that the combustion products of the mixtures activated for 2 or 5 min contain four phases: α -Nb₅Si₃, γ -Nb₅Si₃, NbSi₂, and Nb. Note that the presence of unreacted Nb correlates with the formation of NbSi₂, which contains much more Si than Nb₅Si₃. With increasing the milling time from 2 min to 5 min, the concentrations of both NbSi₂ and Nb decrease. At a milling time of 10 min, their peaks are not present and a small peak at 43° appear to indicate traces of Nb₃Si (other peaks of this phase overlap with those of α -Nb₅Si₃ and γ -Nb₅Si₃ phases).

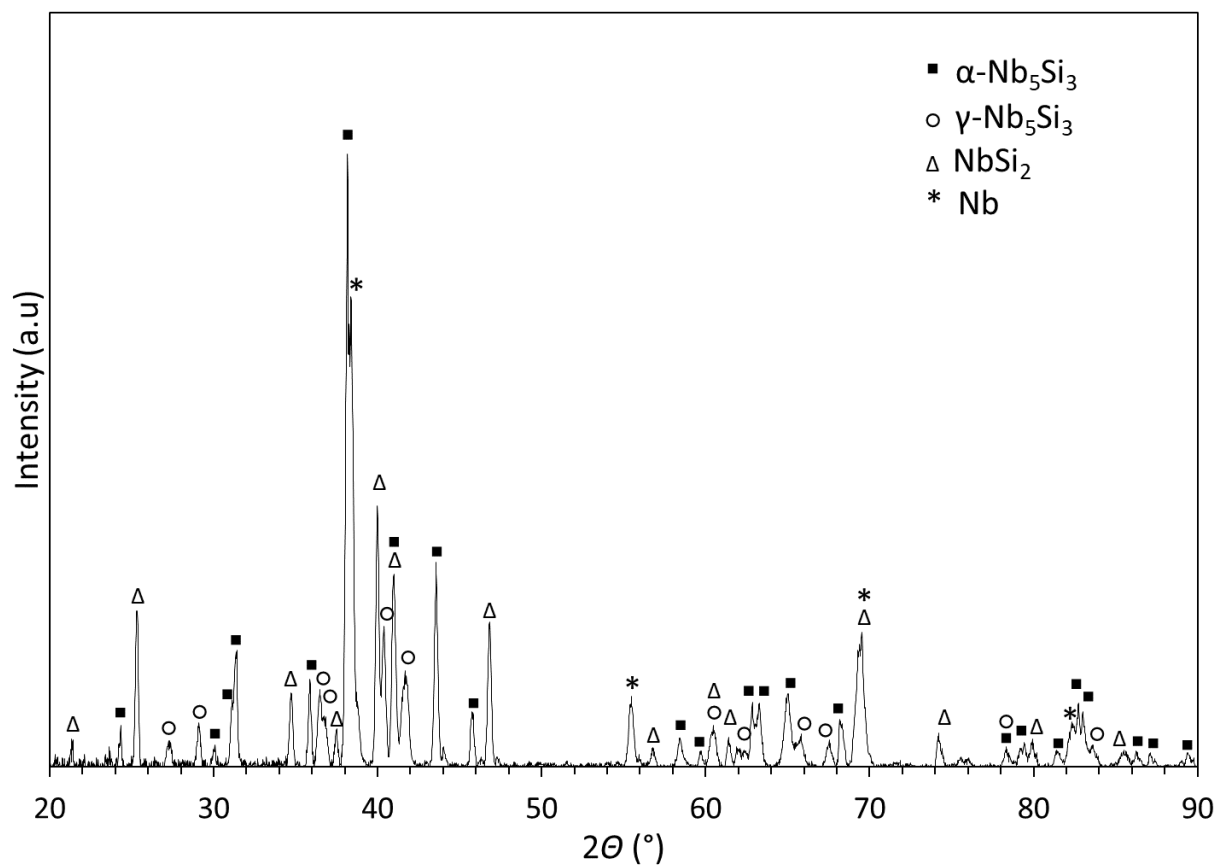


Figure 4.2: XRD pattern of combustion products of Nb/Si mixture milled for 2 min.

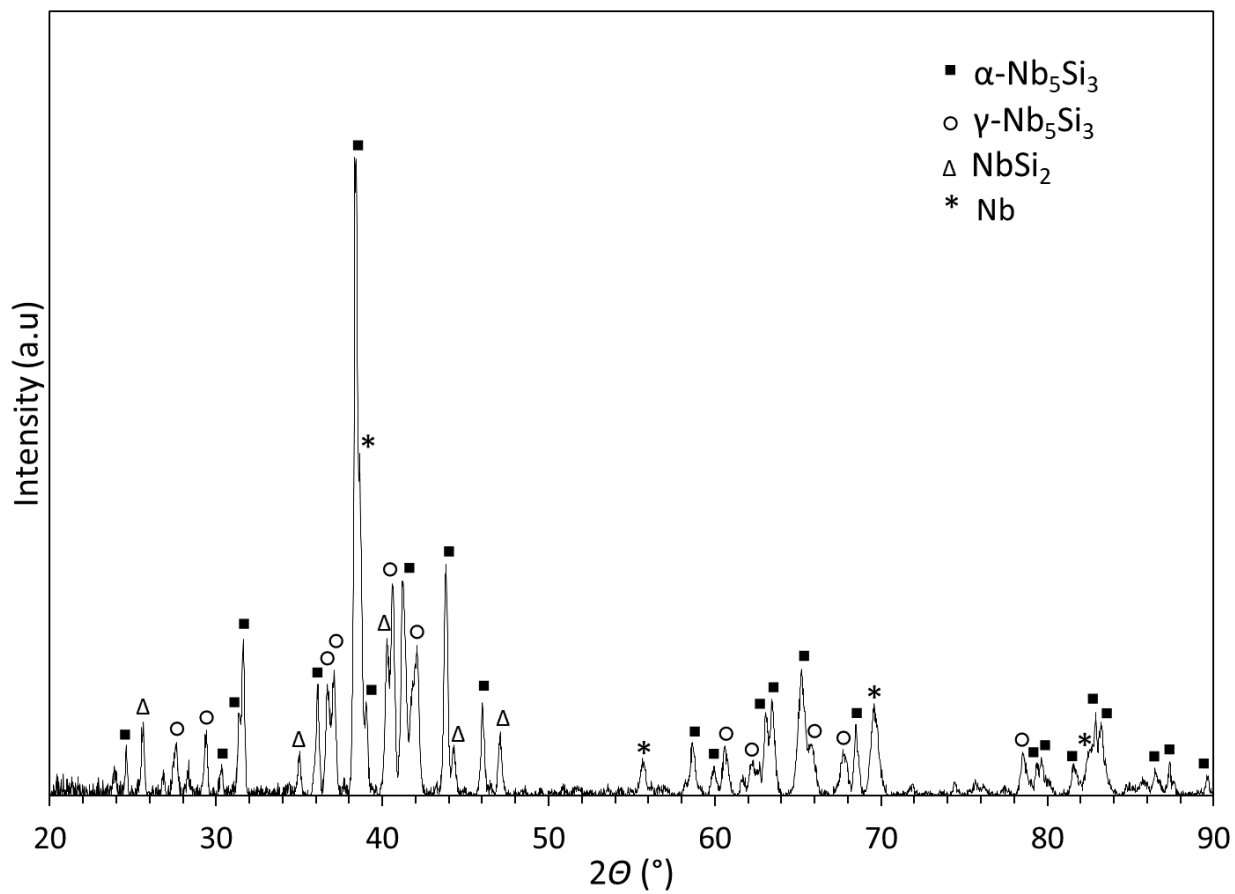


Figure 4.3: XRD pattern of combustion products of Nb/Si mixture milled for 5 min.

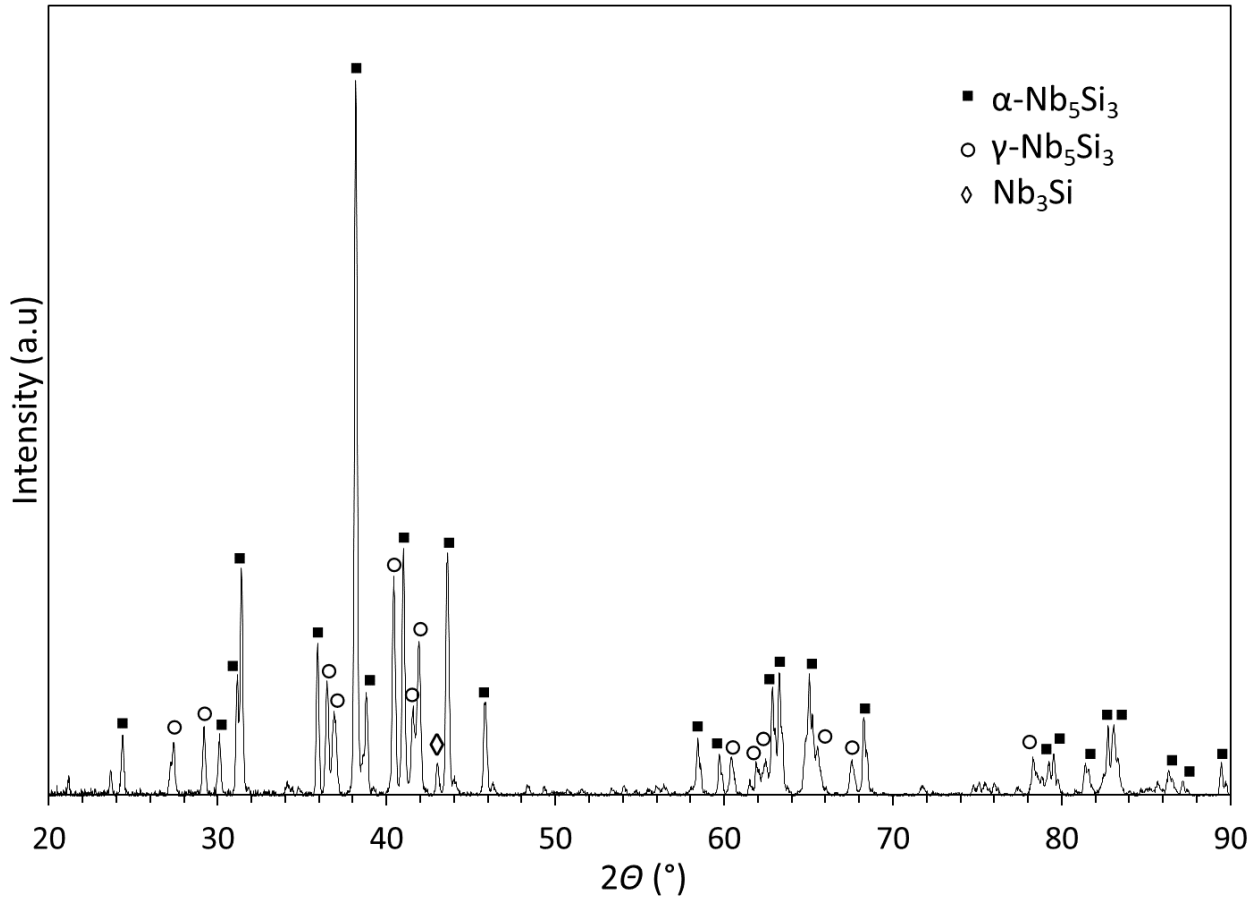


Figure 4.4: XRD pattern of combustion products of Nb/Si mixture milled for 10 min (diameter 13 mm).

The product obtained by MASHS with 10-min milling consists of α - Nb_5Si_3 and γ - Nb_5Si_3 phases with traces of Nb_3Si . Increasing the milling time to 15 min has not changed the product composition. The formation of NbSi_2 at shorter times of milling correlates with the aforementioned mechanism of Nb_5Si_3 synthesis, which includes the formation of NbSi_2 as an intermediate product [58].

This effect of the milling duration on the phases obtained during the combustion process is in qualitative agreement with the prior study on MASHS of Nb_5Si_3 , where the mixture was mechanically activated in a shaker ball mill at 875 cycles/min [58]. It was shown in that work that

longer milling leads to a higher temperature and a faster propagation of the combustion wave. Since the formation of NbSi_2 is the initial step in the formation mechanism of Nb_5Si_3 , it occurs at a relatively low temperature, but complete transformation to the final Nb_5Si_3 product requires a higher temperature. Our observations of the accelerating effect of milling duration on the front propagation align with these results. However, the formation of Nb_5Si_3 phases with no NbSi_2 and Nb required only 10 min of milling in the planetary mill vs. 120 min of milling in the shaker mill [58]. Thus, the use of a planetary mill is more effective for MASHS of Nb_5Si_3 than the use of a shaker mill.

It was shown [58] that the mechanical activation step increases the reactivity of the Nb-Si system by increasing the surface contact area of the powders and decreasing the critical diffusional lengths required for completion of the solid-solid reaction. To investigate how mechanical activation affected the powders in the present work, particle size analysis was conducted for an unmilled Nb/Si mixture and after each of the milling times 2 min, 5 min, and 10 min. The initial Nb and Si powders were examined as well.

The analysis has shown that all tested powders have a unimodal particle size distribution. Table 4.1 shows the parameters that are commonly used for the characterization of powders: the mean volume diameter, the median diameter, and the surface area per unit volume (calculated by the instrument's software assuming that all particles are spherical). The data on the median diameter and surface area indicate that the particle size decreased after 2-min milling, but the longer times did not affect it much.

Table 4.1: Particle size distribution parameters.

Specimen	Mean Volume Diameter	Median Diameter	Surface Area per Unit Volume
	μm	μm	m²/cm³
Nb	16.0	2.63	0.77
Si	13.8	3.31	0.72
Nb/Si, no milling	15.2	3.41	0.75
Nb/Si, 2 min milled	17.7	1.27	1.15
Nb/Si, 5 min milled	20.1	1.20	0.97
Nb/Si, 10 min milled	13.9	1.73	1.00

The relatively low decrease in the particle size after milling implies that significant agglomeration could take place. To verify this, scanning electron microscopy was done. Figure 4.5 shows SEM images of an unmilled mixture and of a mixture milled for 10 min. In the former case (Fig. 4.5 a), a clear difference can be seen between the Si (gray) and Nb (white) powders, while in the milled sample (Fig. 4.5 b) the particles are of the same shade though of different sizes, which suggests uniform mixing and significant agglomeration of the milled powder. Apparently, the particle size analysis determined the size of agglomerates and so the surface area was also determined based on the size of agglomerates.

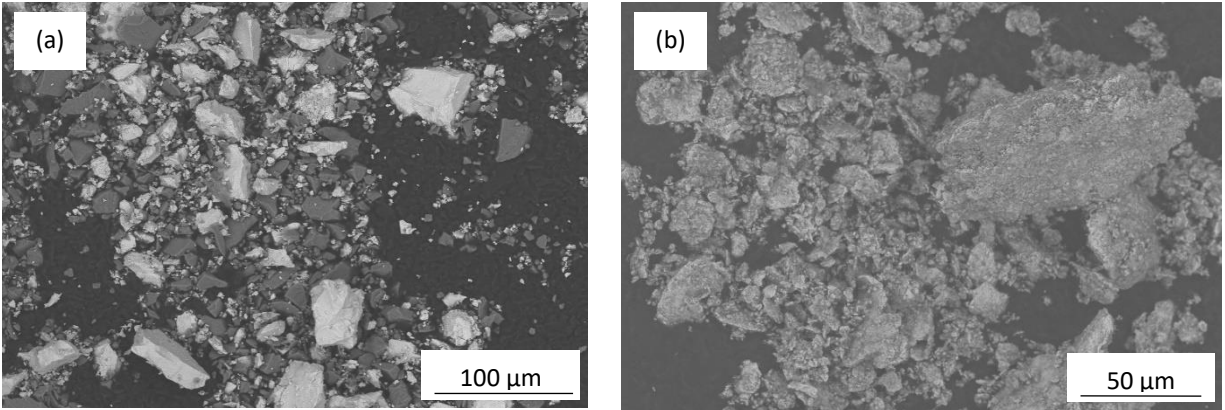


Figure 4.5: SEM images of (a) non-activated mixture and (b) mixture milled for 10 min.

It can be concluded that not only does milling grind coarse particles that are present in the initial powders, but it also creates a powder that consists of agglomerates where the two components, Nb and Si, are uniformly mixed. Agglomeration clearly improves conditions for effective solid-solid reactions between the two components. It should be noted that mechanical activation is a complex phenomenon that may also include other processes, such as the increase in the dislocation density and crystallographic defect concentrations within the powders, which improves high-temperature diffusion kinetics through short circuit diffusion [30]. The analysis of such processes is beyond the scope of the present work.

In contrast with the prior studies on SHS of Nb_5Si_3 [19, 53-55, 77], β phase was not detected in the XRD patterns of the products. It is possible that in the prior studies, preheating [19, 53-54, 77], the Joule heat [55], and a large thermite booster pellet [55] increased the combustion temperature leading to the formation of the high-temperature β phase.

In contrast, γ phase was always detected in the present work and in the prior MASHS of Nb_5Si_3 [58] as well. The formation of the metastable γ phase could be related to a relatively high cooling rate after the SHS process. Since the cooling rate depends on the pellet diameter, the

experiments, with pellets of smaller and larger diameters (i.e. 6 and 25 mm) were performed to verify this hypothesis, with a milling time of 10 min.

Figures 4.6 and 4.7 show XRD patterns of the products obtained by combustion of pellets with a diameter of 6 and 25 mm. Figure 4.8 shows the intensity ratio of the highest peak of γ phase to the highest peak of α phase in the XRD pattern as a function of the pellet diameter. Each point is the average of values obtained in six experiments, and the error bars show the standard deviations. It is seen that the decrease in the diameter from 13 to 6 mm resulted in a higher average γ -to- α ratio. While the sample with the 25 mm diameter showed a similar average to the 13 mm, there was a larger deviation in the ratios. These changes in ratios can be seen in XRD patterns between 60-70°, as the γ phase decreases. Since the cooling rate increases with decreasing the diameter, the observed increase in the concentration of γ phase supports the explanation based on its metastability.

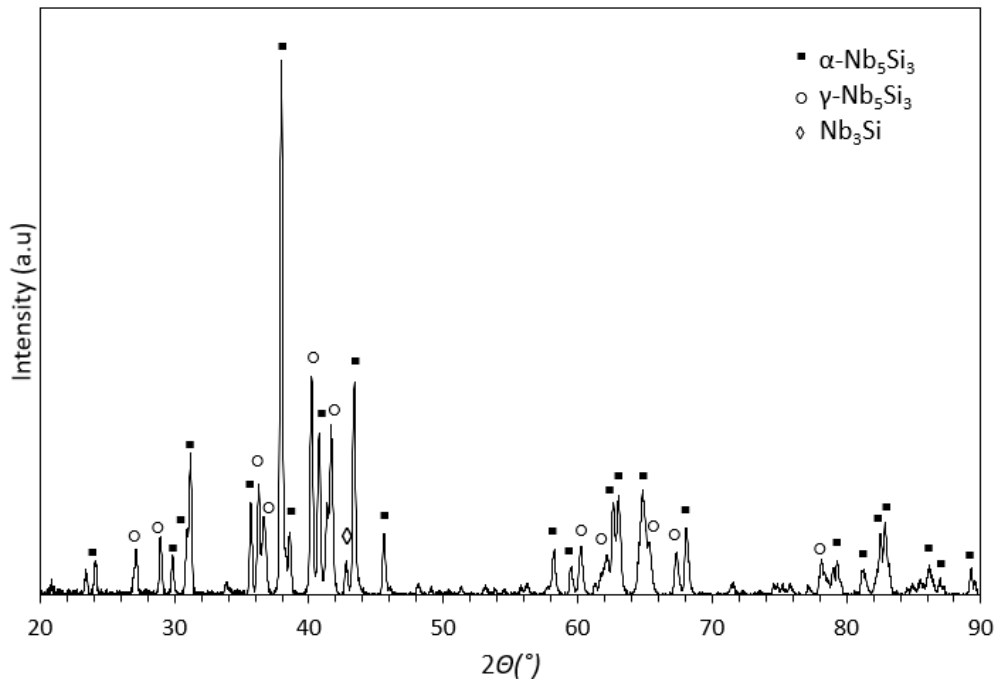


Figure 4.6: XRD pattern of combustion products of Nb/Si mixture milled for 10 min (diameter 6 mm).

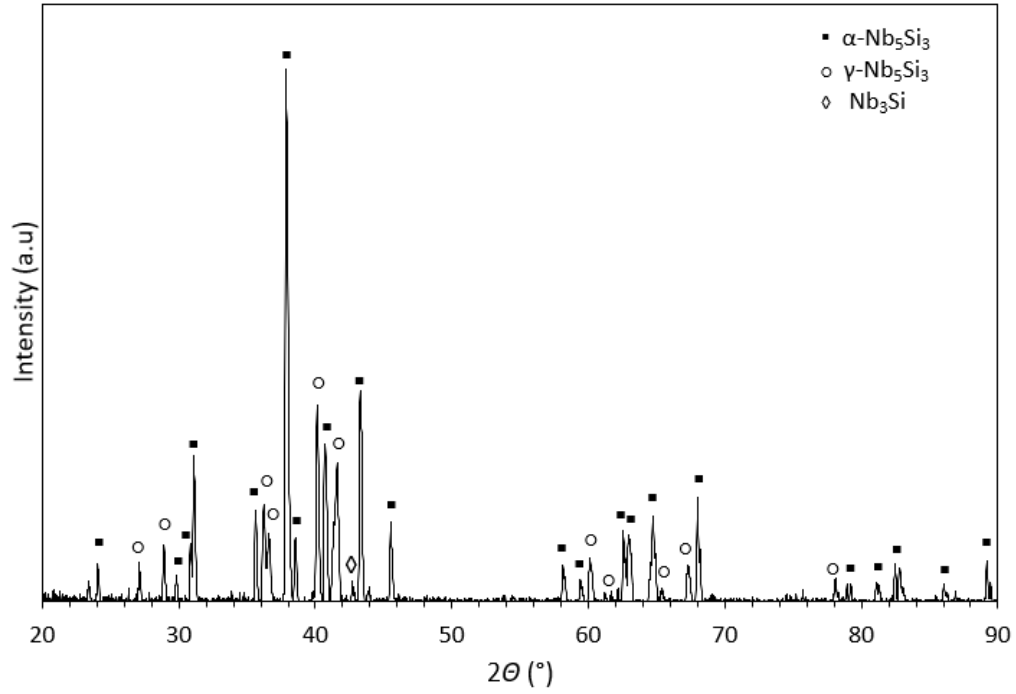


Figure 4.7: XRD pattern of combustion products of Nb/Si mixture milled for 10 min (diameter 25 mm).

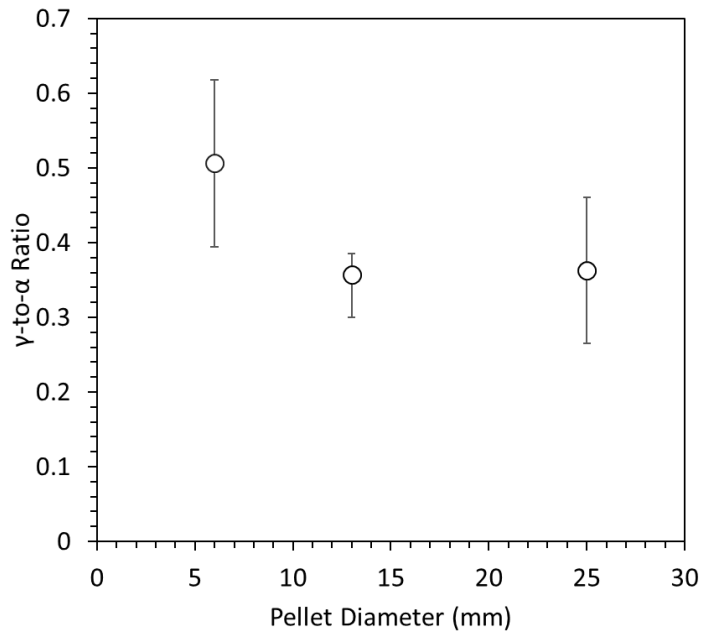


Figure 4.8: The γ -to- α peak intensity ratio in the combustion products of Nb/Si mixture vs. the pellet diameter.

Experiments were conducted using the “chemical oven” technique in an effort to obtain the high-temperature β -Nb₅Si₃ and reduce the concentration of γ phase. The adiabatic flame temperature of Ti/B (1:2 mole ratio) is 3193 K [52], which is much higher than the calculated adiabatic flame temperature of 2289 K for Nb/Si (5:3 mole ratio). A higher temperature could allow the sample to heat above the α - β transition point (1935°C, [8]), however this may not be the case due to heat losses which could make the combustion temperature closer to the transition temperature of the sample. A higher temperature is expected because the sample is being insulated by the highly exothermic TiB₂ shell, which will increase combustion temperature. The higher temperature caused by the wrapping with TiB₂ also has the potential to greatly increase the sample cooling time, hence decreasing the concentration of the γ phase.

For XRD analysis, the outer TiB₂ shell was removed and the core was analyzed. Figure 4.9 shows the obtained XRD pattern of the products. As in the standard technique (Fig. 4.4), three phases appeared: α -Nb₅Si₃, γ -Nb₅Si₃, and Nb₃Si. Here the α phase is also dominant, but the γ -to- α ratio is equal to 0.16, which is, indeed, much less than in the standard technique (0.36, see Fig. 4.6). However, still no β -Nb₅Si₃ was detected in the products. The β phase probably did form during the process, but was transformed to α phase, resulting from a steep temperature drop to less than 1935°C during the prolonged cooling period.

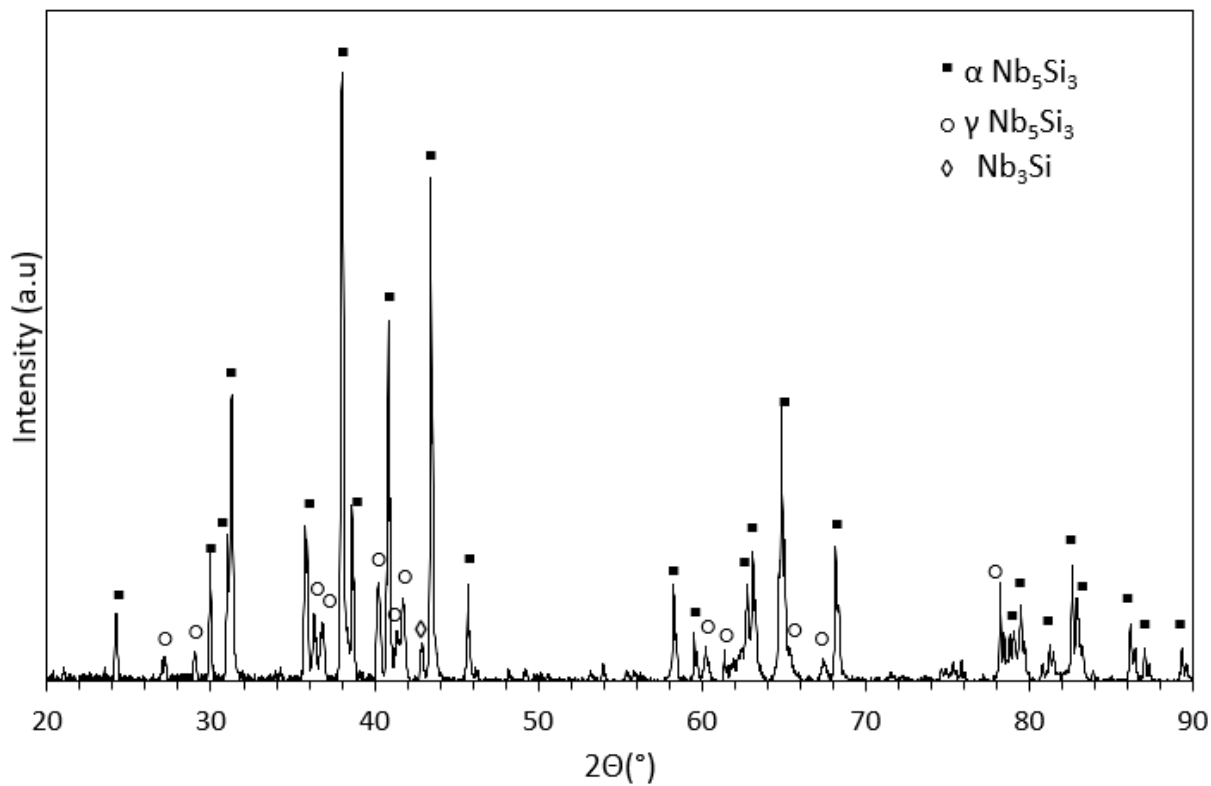


Figure 4.9: XRD pattern of combustion products of Nb/Si mixture obtained using the chemical oven technique

4.2 MASHS of Nb₅Si₃/Nb Composites

Prior to MASHS experiments, thermodynamic calculations of the adiabatic flame temperature and combustion products were conducted using THERMO (version 4.3) software. This software is based on the Gibbs free energy minimization and contains a database of approximately 3000 compounds [75]. In the calculations, the temperature of the initial reactants was set to 298 K and the pressure was maintained constant at 1 atm.

Initially, calculations were conducted for the mole fractions of excess Nb in the initial mixture varied from 0 to 1 (i.e. no excess Nb means Nb:Si mole ratio is 5:3 = 1.67). The results showed that for all mixtures, the combustion products consist of Nb₅Si₃ and Nb. It should be noted, however, that the software database does not include thermochemical properties of Nb₃Si, so caution should be exercised in the analysis of the obtained results.

Figure 4.10 presents the adiabatic flame temperature vs. the mole fraction of excess Nb in the initial Nb/Si mixture. It is seen that the adiabatic flame temperature decreases with the addition of more Nb, but the decrease is relatively small up to very high contents of excess Nb. For example, increasing the Nb/Si mole ratio from 0 to 1.89 (40% excess Nb) and then further increasing to an Nb/Si mole ratio of 3 (80% excess Nb), the adiabatic flame temperature decreases from 2289 K to 2151 K and 1677 K, respectively. This implies that the mixtures with relatively high contents of excess Nb may remain combustible.

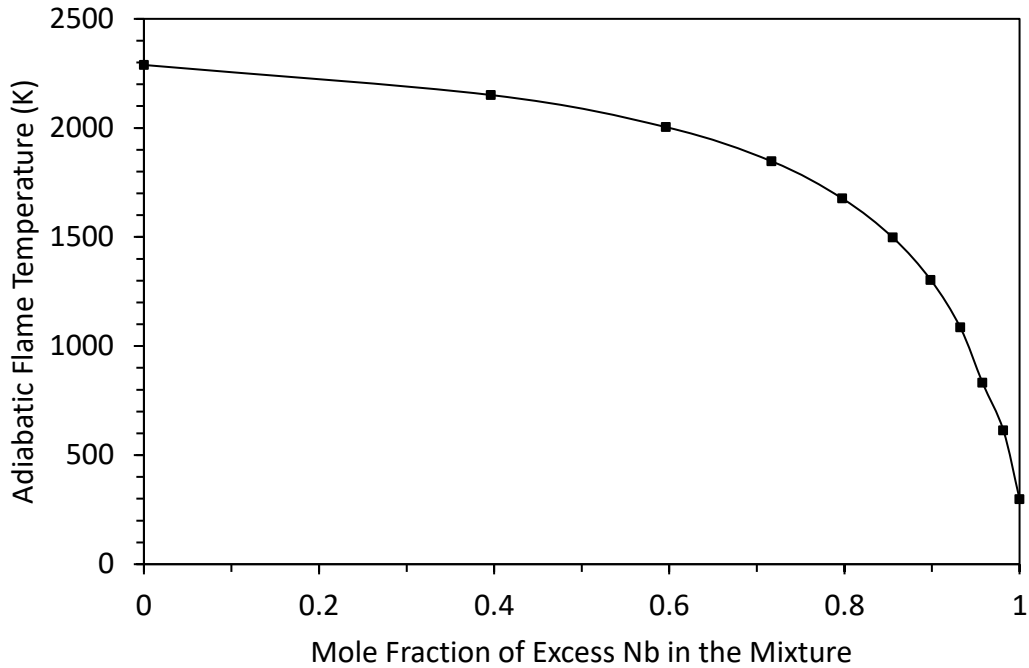


Figure 4.10: The adiabatic flame temperature vs. the mole fraction of excess Nb in the initial mixture.

The experiments on MASHS of Nb₅Si₃/Nb composites were conducted with 13-mm-diameter pellets. Initially, the pellet height was about 10 mm and the relative density was 53-63%. The mole fraction of additional Nb was increased incrementally (by 0.1) from a zero to 0.7, which corresponds to increasing the actual Nb/Si mole ratio in the initial mixture from 1.67 to 2.44. Mechanical activation was performed as ten cycles with the total milling time of 10 min.

The initial experiments were conducted without a booster pellet. However, at a certain concentration of Nb, short-circuiting of the tungsten coil by the pellet was noticed, which created an uncertainty in the results due to a longer ignition time and Joule's heat release in the pellet (Fig. 4.11).

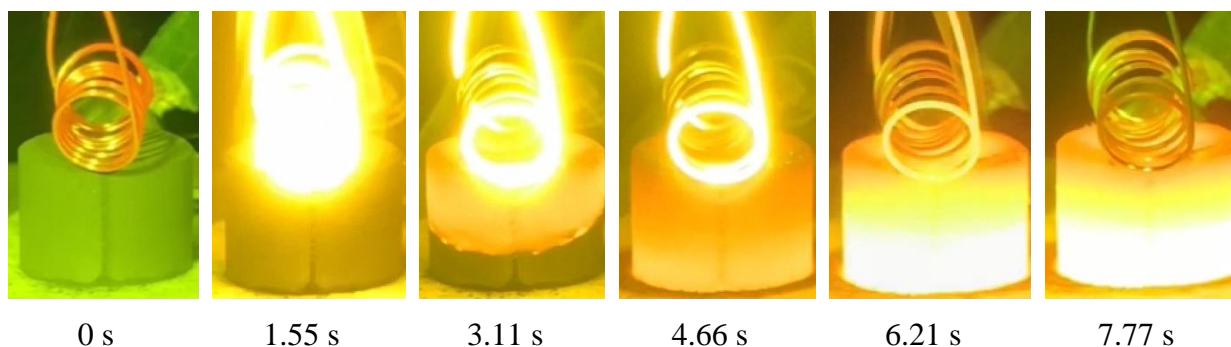


Figure 4.11: Short-circuiting of a coil during combustion of the mixture with Nb/Si mole ratio of 1.89 (40 mol% excess Nb). Time zero was selected arbitrarily.

For this reason, the experiments with excess Nb were conducted with Ti/B (1:2 mole ratio) booster pellets (mass: 1 g). They have shown that increasing the mole fraction of excess Nb to 0.7 has not led to a significant change in the combustion front velocity, which was in the range of 4-5 mm/s for all samples (Table 4.3).

Table 4.3: Combustion front velocities of samples with excess Nb.

Excess Nb Mole Fraction	Velocity (mm/s)
0	4.87
0.1	4.62
0.2	4.13
0.3	4.35
0.4	4.96
0.5	4.01
0.6	4.13
0.7	4.21

The XRD patterns of the products were obtained for all mixtures and compared with that of the product obtained from the stoichiometric (Nb_5Si_3) mixture (Fig. 4.4). Figure 4.12 shows the XRD pattern of products obtained by combustion of a mixture with Nb/Si mole ratio of 1.70, i.e. 10 mol% excess Nb in the expected $\text{Nb}_5\text{Si}_3/\text{Nb}$ mixture. It is seen that, in addition to $\alpha\text{-Nb}_5\text{Si}_3$, $\gamma\text{-Nb}_5\text{Si}_3$, Nb_5Si_3 , and Nb_3Si , the peaks of $\beta\text{-Nb}_5\text{Si}_3$ and Nb have appeared. XRD patterns of other mixtures show a growth of Nb peaks with adding more Nb. This can be seen in Figs. 4.13-4.18, which show the XRD patterns of products obtained from Nb/Si mixtures with mole ratios 1.75, 1.81, 1.89, 2.00, 2.17, and 2.44. It is also seen that the γ -to- α ratio decreases with increasing the content of Nb. The peaks of $\beta\text{-Nb}_5\text{Si}_3$ phase are not present in the patterns shown in Figs. 4.13 – 4.18. The small peak at 43° , which indicates traces of Nb_3Si , is present in all patterns. It should be noted that the presence of Nb_3Si phase has not been reported in prior research on SHS of Nb_5Si_3 .

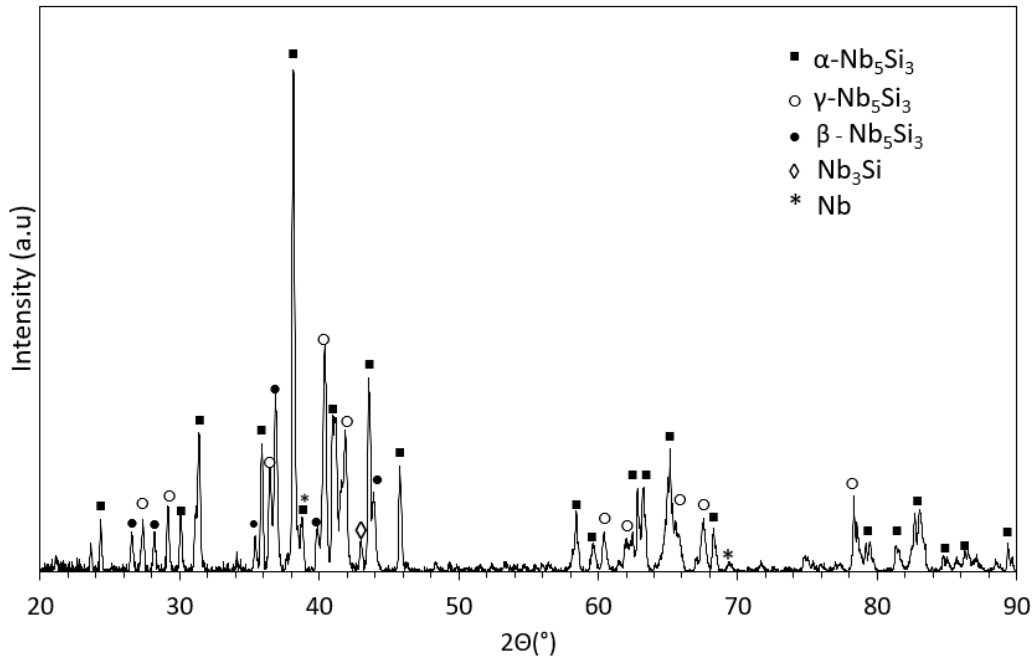


Figure 4.12: XRD pattern of combustion products; Nb/Si mole ratio: 1.70 (10 mol% excess Nb).

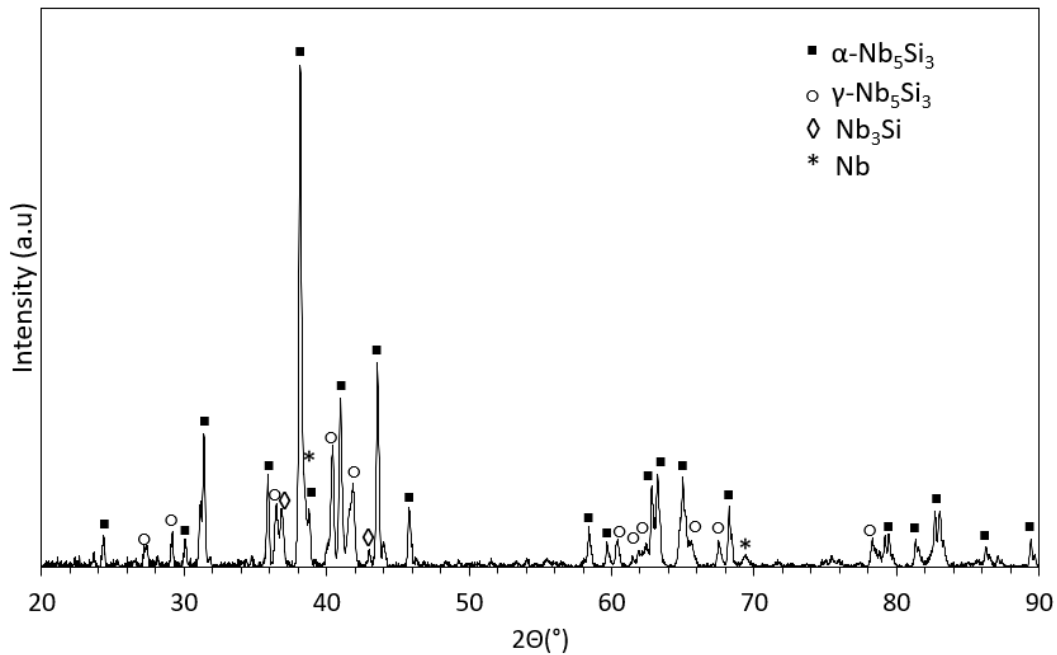


Figure 4.13: XRD pattern of combustion products; Nb/Si mole ratio: 1.75 (20 mol% excess Nb).

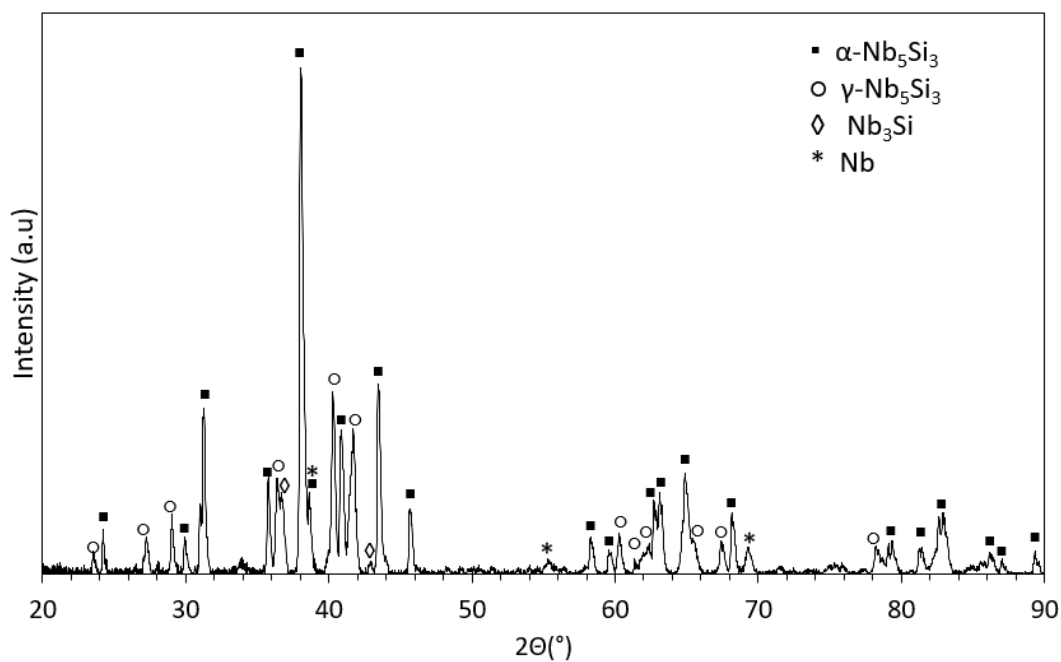


Figure 4.14: XRD pattern of combustion products; Nb/Si mole ratio: 1.81 (30 mol% excess Nb).

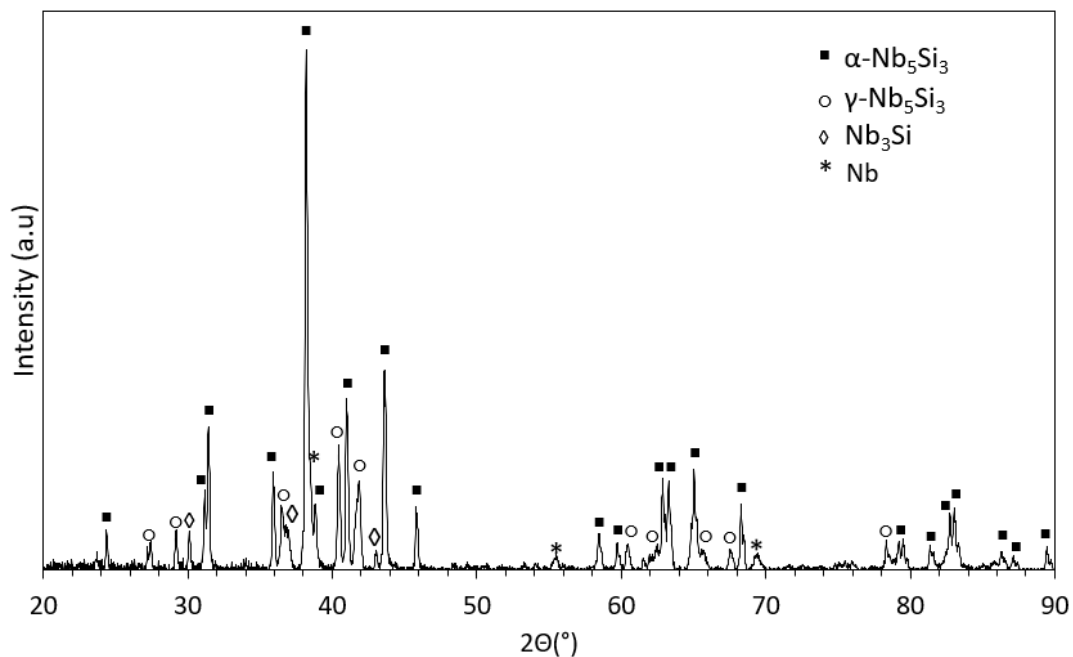


Figure 4.15: XRD pattern of combustion products; Nb/Si mole ratio: 1.89 (40 mol% excess Nb).

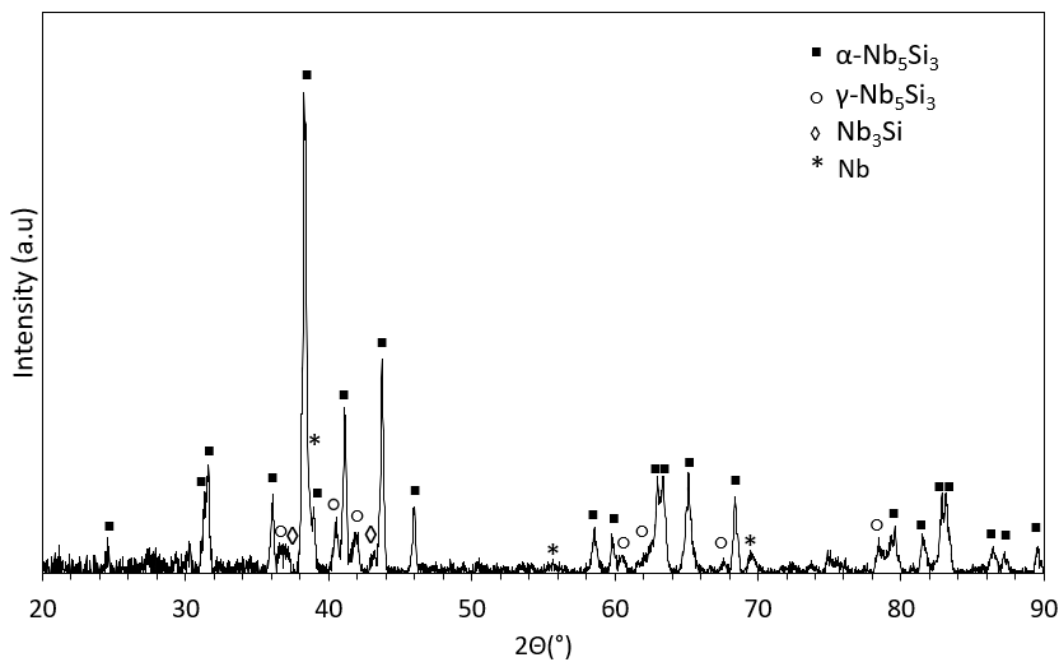


Figure 4.16: XRD pattern of combustion products; Nb/Si mole ratio: 2.00 (50 mol% excess Nb).

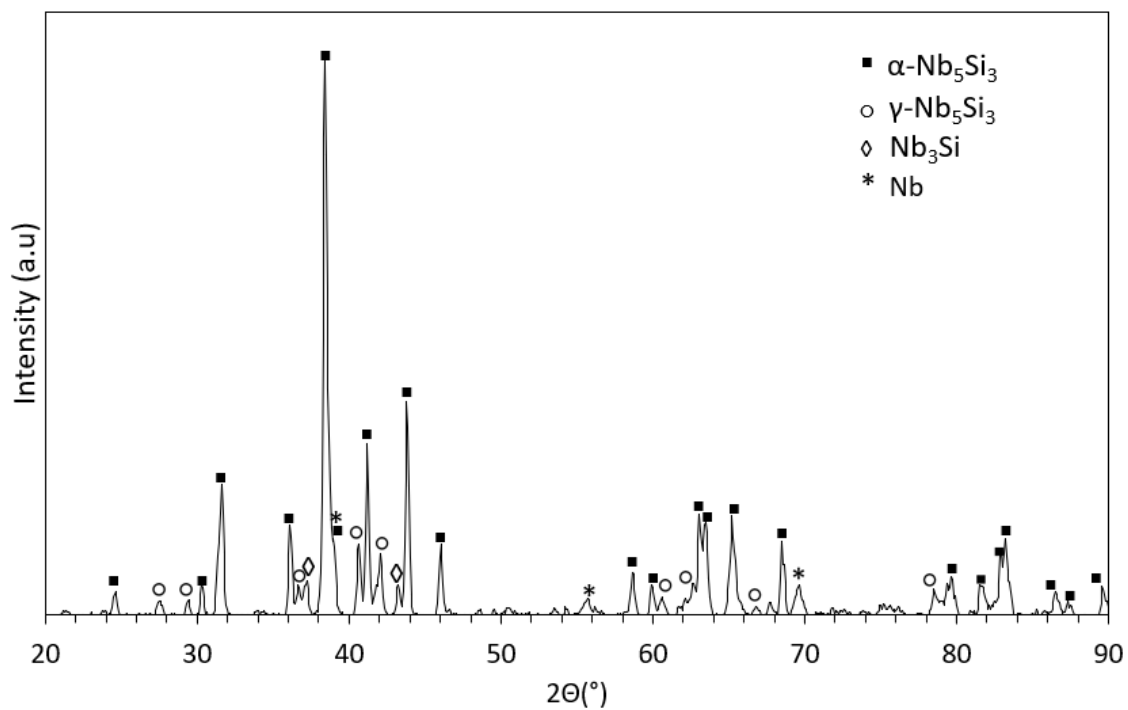


Figure 4.17: XRD pattern of combustion products; Nb/Si mole ratio: 2.17 (60 mol% excess Nb).

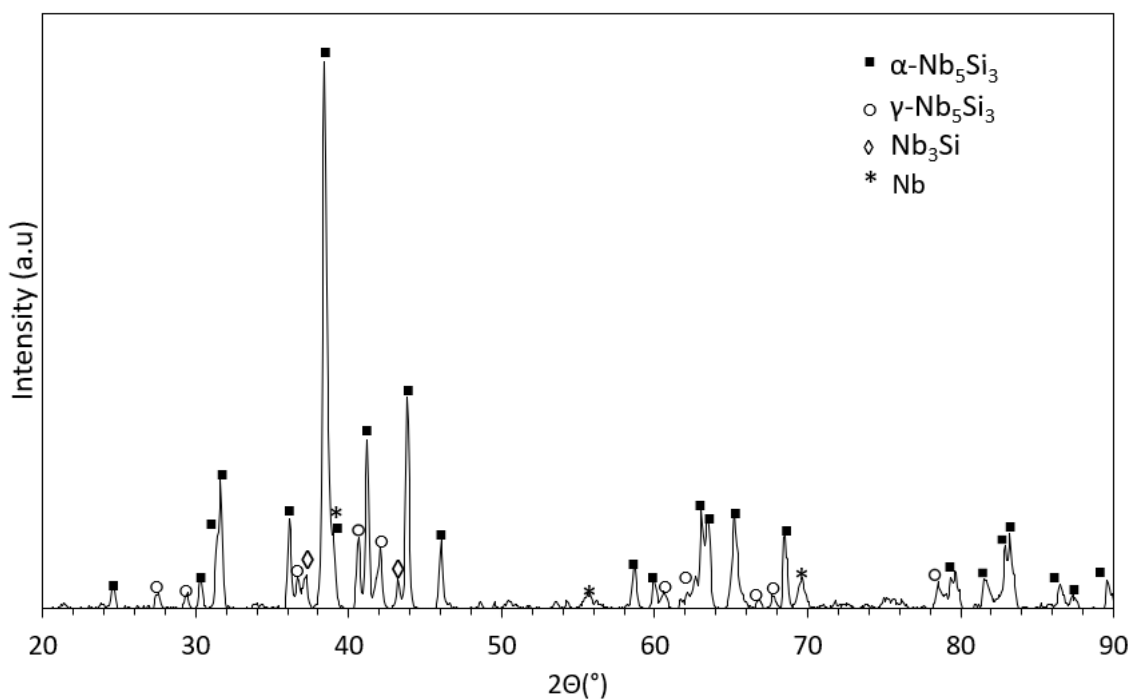
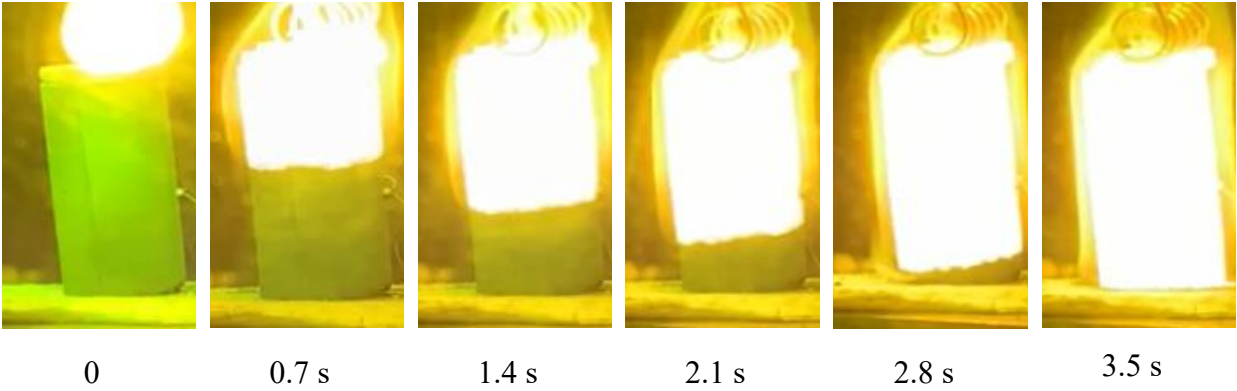


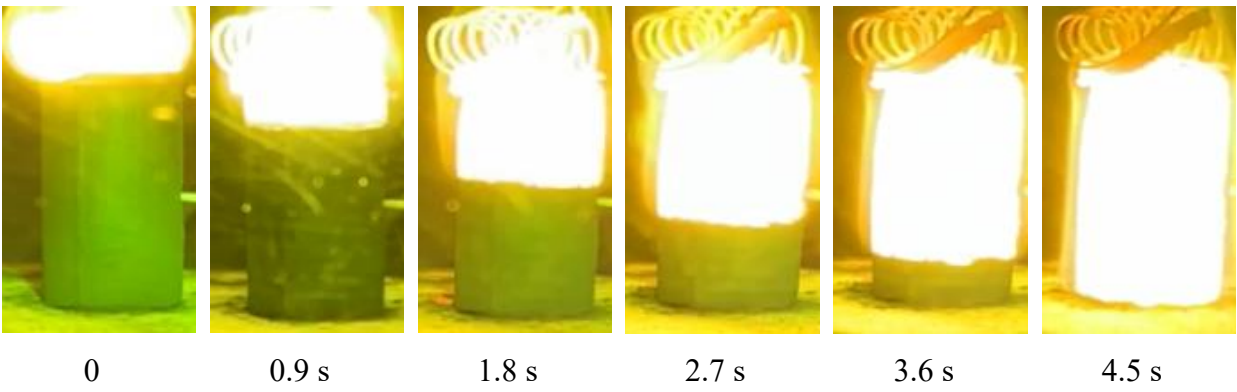
Figure 4.18: XRD pattern of combustion products of the mixture with Nb/Si mole ratio of 2.44 (70 mol% excess Nb).

The fact that the β - Nb_5Si_3 phase was present in the product obtained from the mixture with Nb/Si mole ratio of 1.70 (Fig. 4.2), but not in any other products, deserves a discussion. Apparently, the temperature was sufficiently high in that experiment for the formation of the β phase. This may be related to a relatively short height of the pellet and to the use of a too thick (i.e. too energetic) booster pellet. It is known that the end effects (both the ignition at the top and the heat loss to the support at the bottom) may significantly affect the combustion wave propagation and the product composition. To diminish the end effects, a new series of experiments were conducted where the height of the pellet was increased to 25 ± 2 mm (the diameter remained the same, 13 mm) and the mass of the Ti/B booster pellet was decreased from 1 g to 0.5 g. It is worth noting that the increase in height has led to a higher relative density, 58-70%.

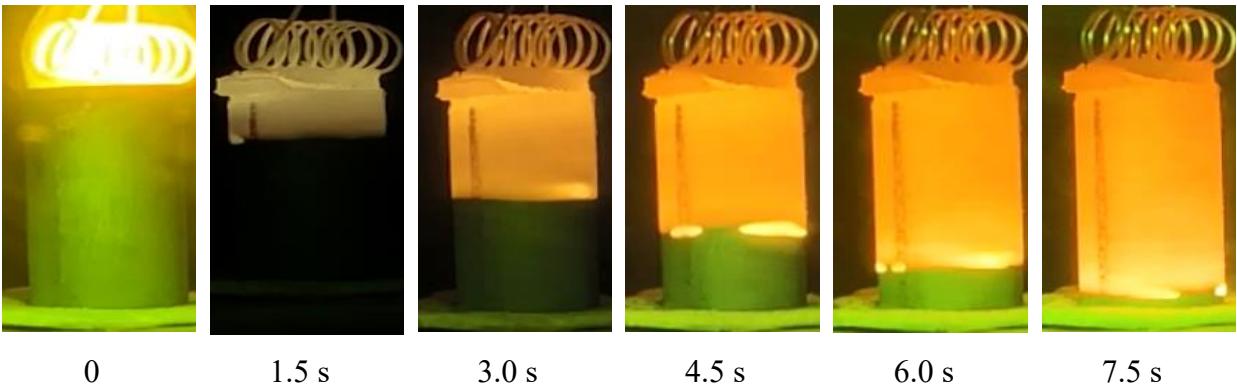
The mixtures with Nb/Si mole ratios of 1.67, 2, and 3 were tested. Note that the ratio of 3 (i.e. 25 at% Si) corresponds to either Nb_3Si or a binary mixture of 20 mol% Nb_5Si_3 and 80 mol% Nb. Figure 4.19 shows the images of combustion propagation over the pellets. It is seen that adding more Nb decelerates the front propagation. The average velocity of the combustion front propagation was 7 mm/s at Nb/Si=1.67 and 5 mm/s at Nb/Si=2. At the Nb/Si mole ratio of 3, a spinning propagation of the combustion wave was observed where hot spots were traveling over the pellet surface and the axial velocity of combustion propagation dropped to 3 mm/s (Fig. 4.19 c). The transition to spin combustion is explained by a lower exothermicity of the initial mixture. Spin combustion of metal/silicon mixtures during MASHS of molybdenum borosilicides has been reported recently [50, 52].



(a)



(b)



(c)

Figure 4.19: Images of combustion propagation over Nb/Si mixture pellets (height: 25 ± 2 mm) with Nb/Si mole ratios of (a) 1.67, (b) 2, and (c) 3. Time zero was selected arbitrarily.

For each composition, thermocouple measurements of the temperature in the center of the pellet were conducted during the SHS process. The sample rate was 100 Hz. Figure 4.20 shows the measured temperature profiles. The acquisition board shows only the voltage (not the temperature) for a Type C thermocouple, which has a highly non-linear temperature-voltage relationship. For this reason, the curves show the electromotive force (emf) of the hot junction relative to 0°C, while the grid lines correspond to the standard temperature-emf relationship for a Type C thermocouple (ASTM E230/E230M – 17). Time “zero” corresponds to the beginning of the temperature rise in each curve.

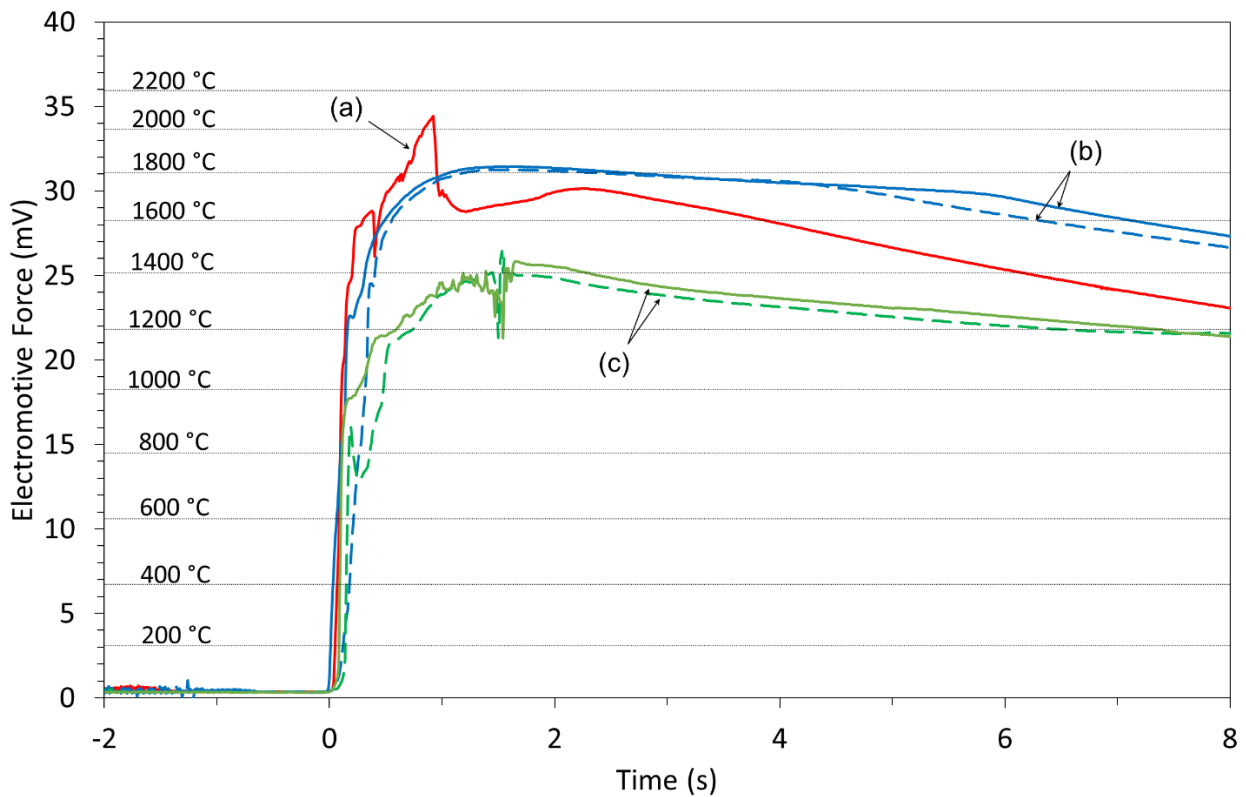


Figure 4.20: Temperature records during combustion propagation over Nb/Si mixture pellets (height: 25 mm) with Nb/Si mole ratios of (a) 1.67, (b) 2, and (c) 3.

Thermocouple measurements were conducted in several experiments with the mixture that had Nb/Si mole ratio of 1.67. All emf-time curves exhibited sudden jumps up and down. Apparently, these jumps were caused by interactions between the thermocouple wires and the initial, intermediate, or final products. Note that some of the products (Nb, Nb₅Si₃, and Nb₃Si) are electrical conductors and Nb-Si liquid may form from eutectic reactions as evident from the Nb-Si phase diagram (Fig. 2.1) [8]. For clarity, only one of the obtained curves is shown in Fig. 4.20.

Thermocouple measurements were also conducted with two mixtures that had Nb/Si mole ratio of 2 and with two mixtures that had Nb/Si mole ratio of 3. The curves for Nb/Si=2 were smooth and similar to each other. The curves for Nb/Si=3 were also similar to each other; both exhibited fluctuations near the highest point.

Figure 4.21 and Table 4.4 show the measured maximum temperatures agree with calculations for the adiabatic maximum temperature. The obtained data points are near the adiabatic flame temperatures calculated for the same mixture ratios. This was surprising because it was expected that heat losses would lower the maximum measured temperatures. The relatively low adiabatic flame temperatures were apparently obtained because of an incorrect value of the standard formation enthalpy of Nb₅Si₃ in the THERMO software database is -451.764 kJ/mol, or -56.5 kJ/(mol of atoms). The values of this property, calculated by CALPHAD modeling in five references, range from -47.7 to -64.8 kJ/(mol of atoms) [78], while the values obtained experimentally are -63.8 ± 11.5 kJ/(mol of atoms) [79] (calorimetry), -64.6 ± 2.4 kJ/(mol of atoms) [70] (calorimetry), and -62.2 ± 7.9 kJ/(mol of atoms) [80] (electromotive force measurements). Thus, the formation enthalpy of Nb₅Si₃ used in THERMO is significantly lower (by absolute value) than the experimental values, which explains the low adiabatic flame temperatures obtained in the calculations.

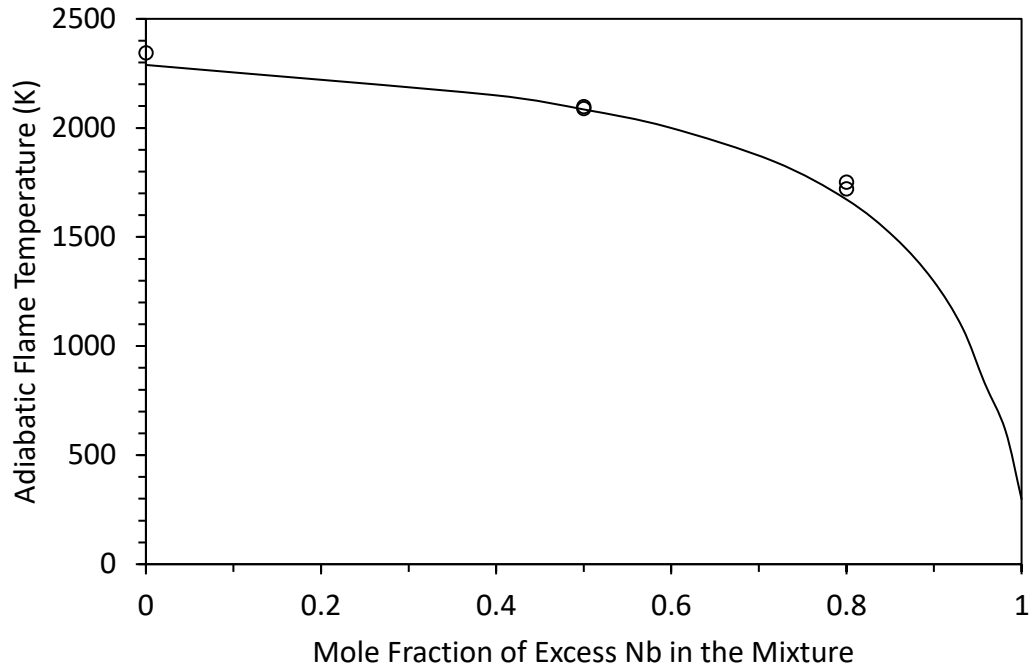


Figure 4.21: The calculated adiabatic flame temperature (curve) and measured maximum temperatures (circles) vs. the mole fraction of excess Nb in the initial mixture; the two data points at a mole fraction of 0.5 (correlating to Nb/Si ratio of 2) overlap each other.

Table 4.4: Comparison of calculated and measured temperatures for Nb/Si mixtures with mole ratios of 1.67, 2, and 3.

Nb/Si Mole Ratio	Measured Temperature (°C)	Calculated Temperature (°C)
1.67	2071	2016
2	1820	1812
3	1463	1399

Based on the measured maximum temperatures and combustion front velocities, the apparent activation energy of the occurring Nb-Si reaction was estimated. The used method is

based on the relationship between the combustion front velocity and the combustion temperature [81], and expressed by:

$$\left(\frac{u}{T_c}\right)^2 = f(n) \left(\frac{R}{E_a}\right) K \exp\left(-\frac{E_a}{RT_c}\right) \quad (3)$$

where u is the combustion front velocity, T_c is the combustion temperature, E_a is the activation energy of the reaction, R the universal gas constant, $f(n)$ a function of the kinetic order of the reaction, and K is a constant which includes the heat capacity of the product, thermal conductivity, and the heat of reaction. The Arrhenius-type plot can be obtained by plotting $\ln(u/T_c)^2$ versus $1/T_c$. The activation energy is then can be determined as the slope of this plot multiplied by $(-R)$. The use of this method in the study on SHS of Nb_5Si_3 with preheating has resulted in the activation energy of 259 kJ/mol [19].

In the present work, the average values of u were obtained based on pellet height and front propagation time, determined from the video records. Table 4.5 presents the values of the front velocity and maximum temperatures as well as the calculated parameters of the Arrhenius-type plot shown in Fig. 4.22. In the calculations of the logarithm, the values of velocity and temperature were in mm/s and K, respectively. The activation energy is equal to 60.1 kJ/mol ($7224.4 \text{ K} \cdot 8.314 \cdot 10^{-3} \text{ kJ}/(\text{mol} \cdot \text{K})$). This is about four times lower than the value reported for SHS with preheating [19], which is explained by the effect of mechanical activation in our work.

Table 4.5: The parameters used for determination of activation energy.

Nb/Si Mixture Ratio	u	T_c	$\ln(u/T_c)^2$	$1/T_c$
	mm/s	K		1/K
1.67	7	2344	-11.6	0.000427
2	5	2093	-12.1	0.000478
3	3	1736	-12.7	0.000576

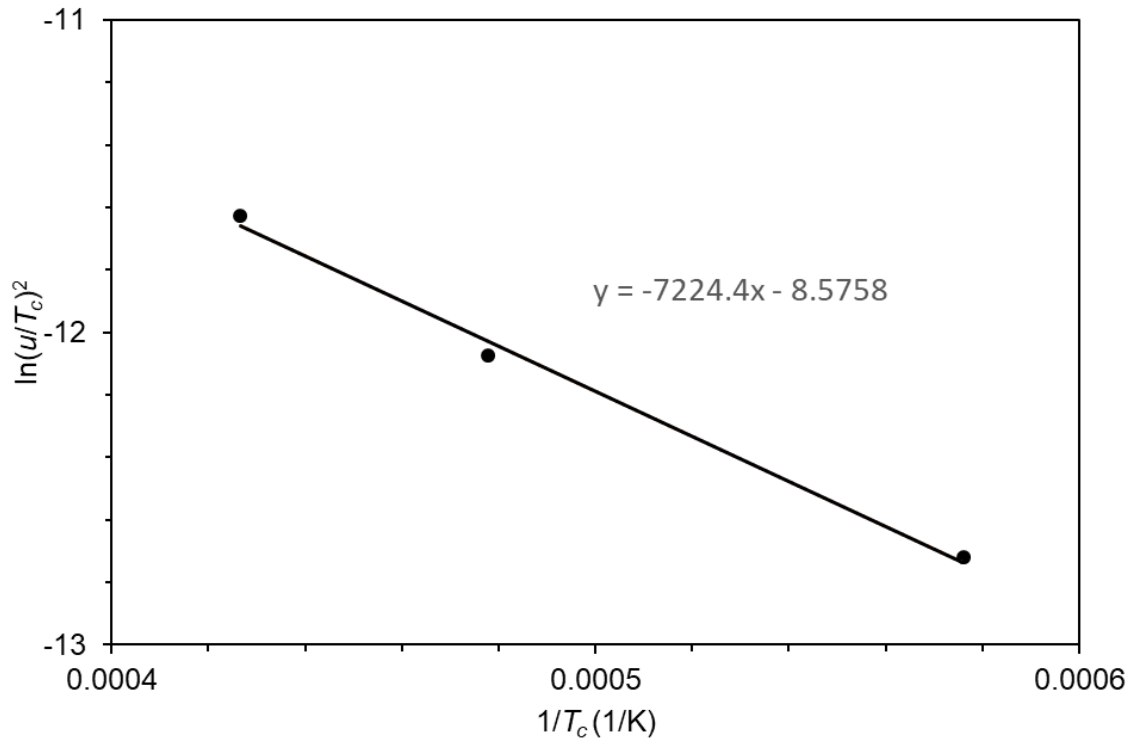


Figure 4.22: The Arrhenius-type plot for determination of activation energy of Nb-Si reaction.

Figure 4.23 shows photographs of the product pellets obtained from the mixtures with Nb/Si mole ratios of 1.67, 2, and 3. For the SEM and XRD analyses, the product pellets were cut into three parts of equal length. Their analysis has shown that XRD patterns of the top and bottom portions are slightly different from those of the middle parts, which is explained by end effects. For this reason, only XRD patterns and microstructures of the middle parts are shown in the present paper.

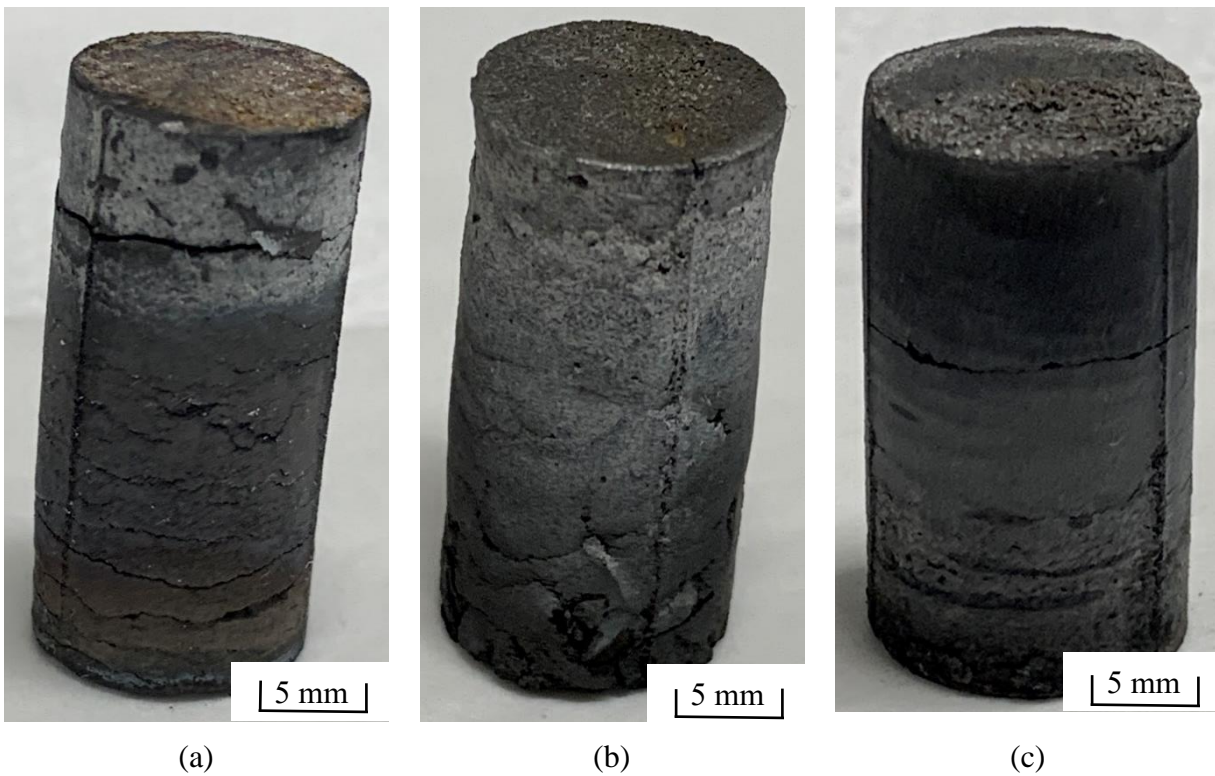


Figure 4.23: Photographs of the product pellets obtained from mixtures with Nb/Si mole ratios of (a) 1.67, (b) 2, and (c) 3.

Figure 4.24 shows the XRD pattern of the products obtained by combustion of the mixture with Nb/Si mole ratio of 1.67. As compared with the product obtained by combustion of a shorter pellet of the same mixture (see Fig. 4.4), new peaks appeared, and they belong to the β phase of Nb_5Si_3 . The appearance of the β phase may be explained by a higher temperature generated in the middle portion of the 25-mm-high pellet during combustion. Indeed, the maximum temperature measured in the experiment with this mixture (Fig. 4.21) was 2071 °C, i.e. well above the α - β transition temperature, 1935 °C [8].

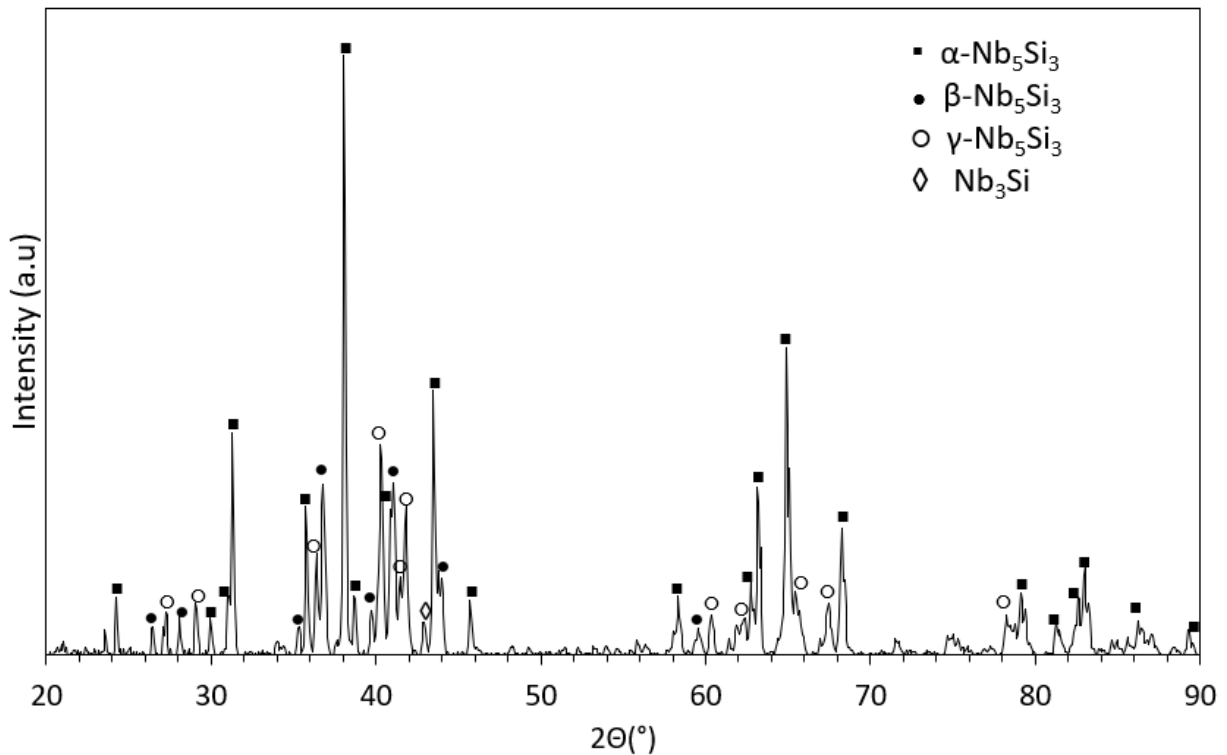


Figure 4.24: XRD pattern of combustion products of the mixture with Nb/Si mole ratio of 1.67 (height of the pellet: 25 mm).

Figure 4.25 shows the XRD pattern of the products obtained by combustion of the mixture with Nb/Si mole ratio of 2. It is seen that the β phase disappeared. This correlates with the thermocouple measurements, which showed maximum temperatures of 1816 and 1824 °C. Both of these are over 100 °C below the α - β transition temperature. Instead, Nb is now present, so the products include α - Nb_5Si_3 , γ - Nb_5Si_3 , Nb, and traces of Nb_3Si . The product composition is apparently close to 50 mol% Nb_5Si_3 (both α and γ phases) and 50 mol% Nb.

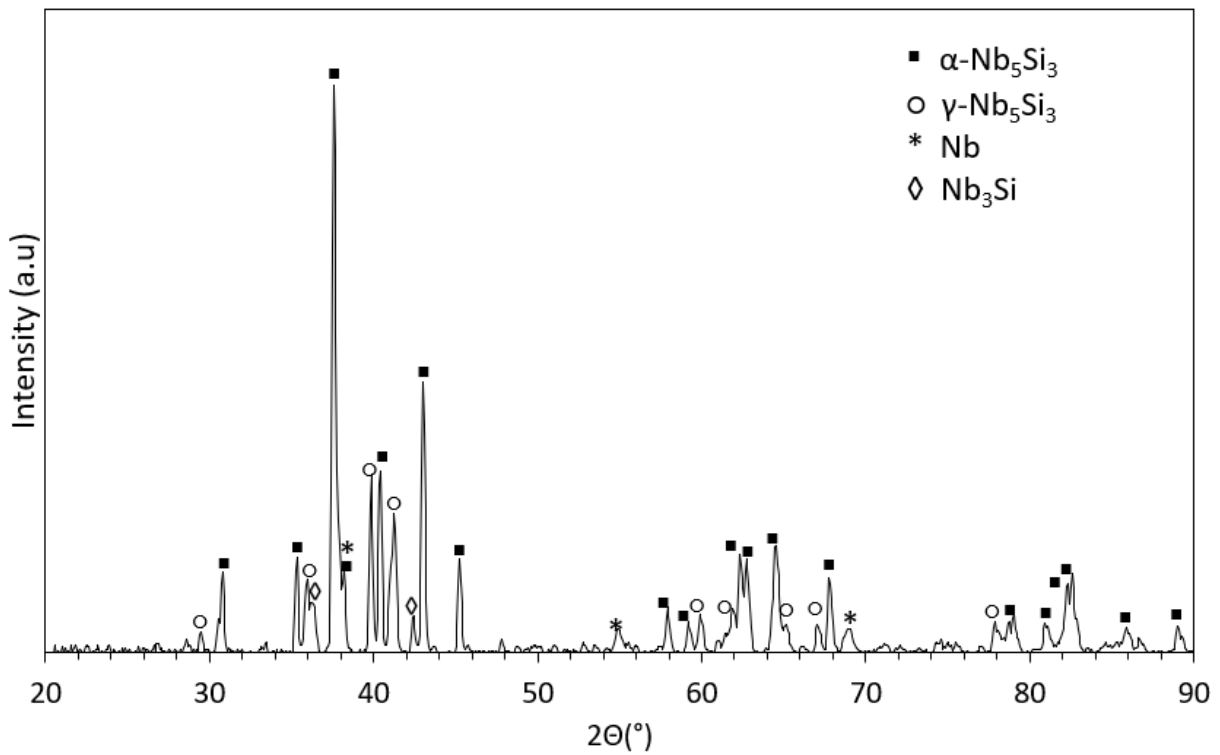


Figure 4.25: XRD pattern of combustion products of the mixture with Nb/Si mole ratio of 2 (height of the pellet: 25 mm).

Finally, Figure 4.26 shows the XRD pattern of the products obtained by combustion of the mixture with Nb/Si mole ratio of 3. The content of Nb clearly increased, while the apparent peak of Nb_3Si remained about the same. It is also notable that the peaks of the γ phase became much smaller. The γ -to- α peak intensity ratio was 0.35 and 0.31–0.32 at Nb/Si mole ratio of 1.67 and 2, respectively, and it dropped to 0.03–0.05 at Nb/Si = 3. Clearly, $\alpha\text{-Nb}_5\text{Si}_3$ and Nb are dominant phases. Although the mole ratio of 3 corresponds to Nb_3Si , the actual composition is apparently close to 20 mol% Nb_5Si_3 (primarily the α phase) and 80 mol% Nb.

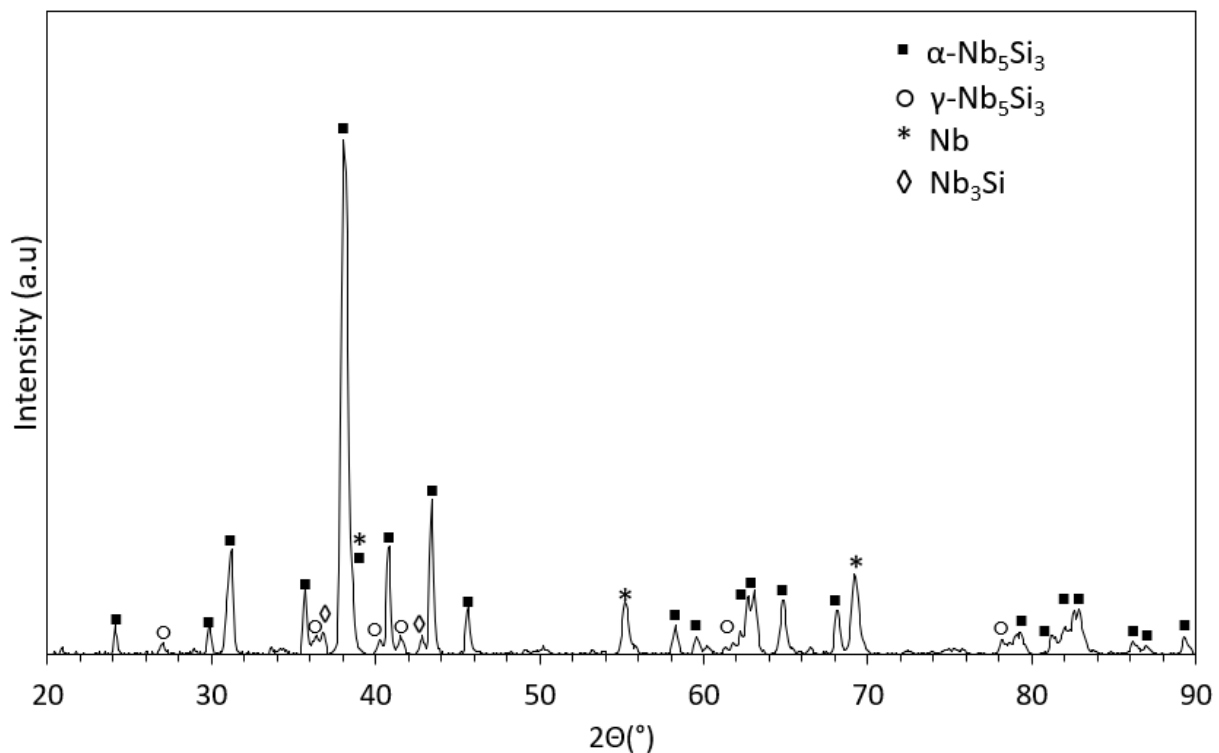


Figure 4.26: XRD pattern of combustion products of the mixture with Nb/Si mole ratio of 3 (height of the pellet: 25 mm).

Since the γ phase of Nb_5Si_3 has poor mechanical properties, the MASHS of Nb_5Si_3 -Nb composite with a low content of the γ phase is an important result. The decrease in the content of γ phase correlates with decreasing the combustion temperature. Indeed, the measured combustion temperature of the mixture with Nb/Si mole ratio of 3 is less approximately by 500 K than for the Nb/Si=1.67 mixture and by 300 K than for the Nb/Si=2 mixture (see Fig. 4.21). The lower exothermicity of the mixture and the lower temperature lead to the spinning mode of the combustion wave propagation, which is characterized by a lower axial velocity of the front propagation and, accordingly, by a longer duration of the SHS process. The decrease in the yield of the γ phase with increasing the process time implies that the γ phase is metastable, as suggested in [8], in contrast with the computational study [10].

Figure 4.27 shows SEM images of the products, crushed to powders. The products obtained from the mixtures with Nb/Si ratios of 2 and 3 appear to be agglomerates of micron-sized particles, while the Nb/Si=1.67 mixture also contains large particles of a uniform material with few pores (see Fig. 4.27d). This difference can be explained based on the temperature measurements and the Nb_5Si_3 formation mechanism [58]. This mechanism includes, as the first step, the formation of NbSi_2 , which then reacts with solid Nb. Since the temperature exceeded the melting point of NbSi_2 , 1935 °C, during combustion of the Nb/Si=1.67 mixture (see Fig. 4.21), the formed NbSi_2 phase was in the liquid state, which apparently led to the formation of large particles such as the one seen in Fig. 4.27d.

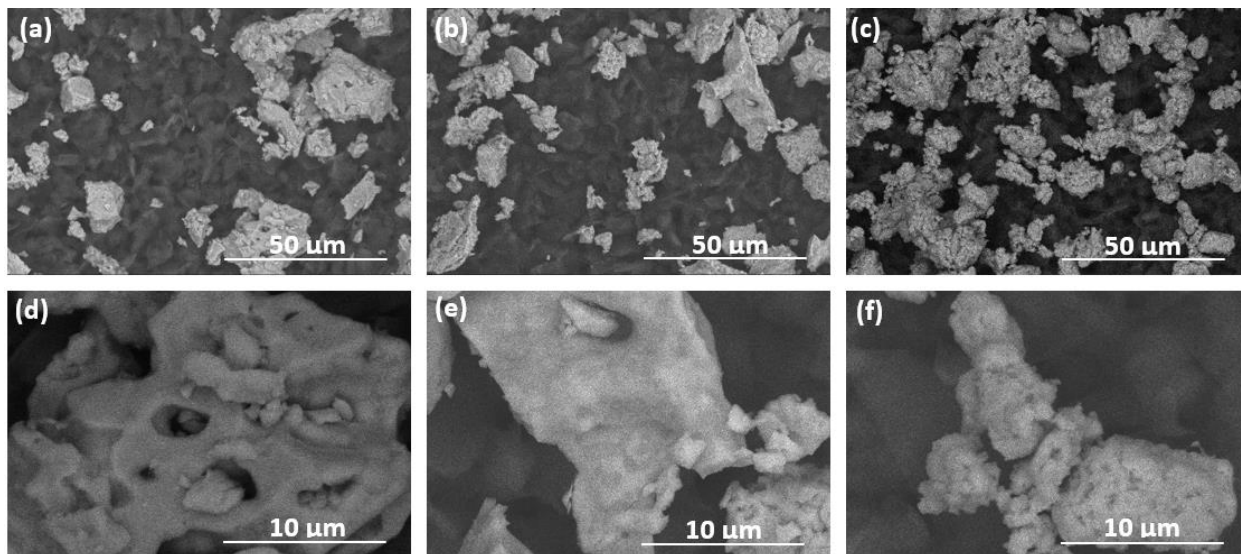


Figure 4.27: SEM images of products (crushed to powders) obtained from mixtures with Nb/Si mole ratios of (a, d) 1.67, (b, e) 2, and (c, f) 3.

Figure 4.28 shows SEM images taken from polished samples of the products. These images show dark grey patches that can be classified as phases of Nb_5Si_3 , while the lighter grey sections are classified as Nb. It is seen that in the product obtained from the stoichiometric (5:3) Nb/Si mixture (Fig. 4.28a), the amount of Nb is very small, though it does exist. Note that XRD did not detect any Nb peaks in that product (see Fig. 4.24 as well as Figs. 4.4 and 4.9), i.e. the accuracy of the XRD analysis was insufficient for detecting such a small amount. As the Nb/Si mole ratio increases, the amount of light grey patches also increases.

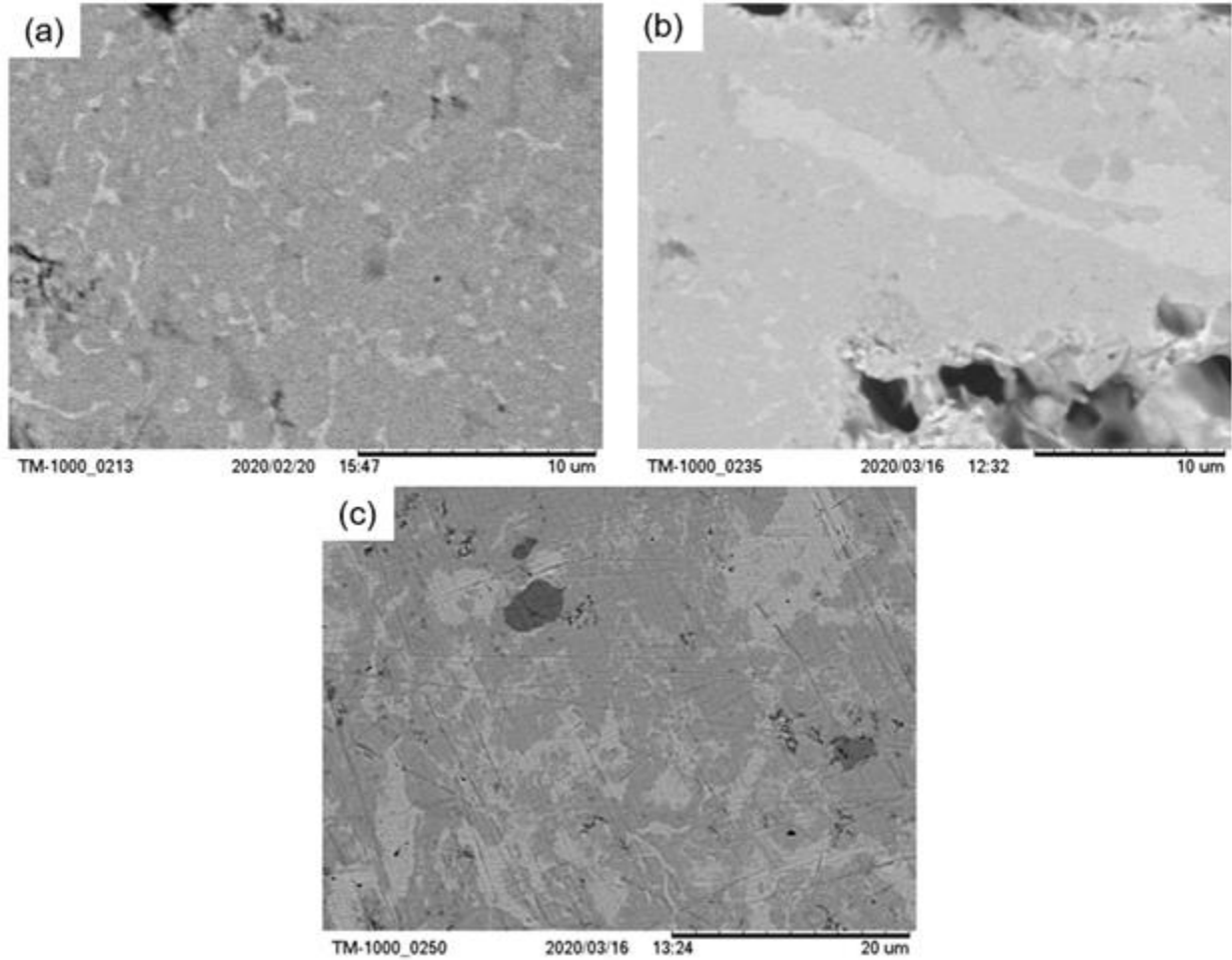


Figure 4.28: SEM images of products (polished samples) obtained from mixtures with Nb/Si mole ratios of (a) 1.67, (b) 2, and (c) 3. Products show: Nb_5Si_3 (darker grey) and Nb (lighter grey).

Handling of the pellets obtained by combustion of mixtures with various Nb/Si mole ratios and crushing them for XRD and SEM analyses have shown that the addition of extra Nb to the mixture apparently makes the products stronger. To verify these observations, the compressive strength of the product pellets (diameter: 6 mm) was measured. Figure 4.29 shows the obtained stress-strain dependencies. At the mole ratios of 1.67, 2, and 3, the compressive strength was 78 MPa, 211 MPa, and 169 MPa, respectively. All samples had a first failure point at around 60 MPa. It should be noted that niobium silicide-based alloys, obtained by conventional metallurgical

methods, exhibited compressions strengths over 1500 MPa at room temperature [9]. Therefore, the MASHS products without additional consolidation can hardly compete with them in applications where high strength is required. However, they may be sufficiently strong for various chemical engineering applications. To increase the strength, the materials could be consolidated using hot pressing or spark plasma sintering. In addition, the synthesis could be conducted in the so-called SHS compaction mode, i.e. in a special die with pressing immediately after the synthesis [50, 82].

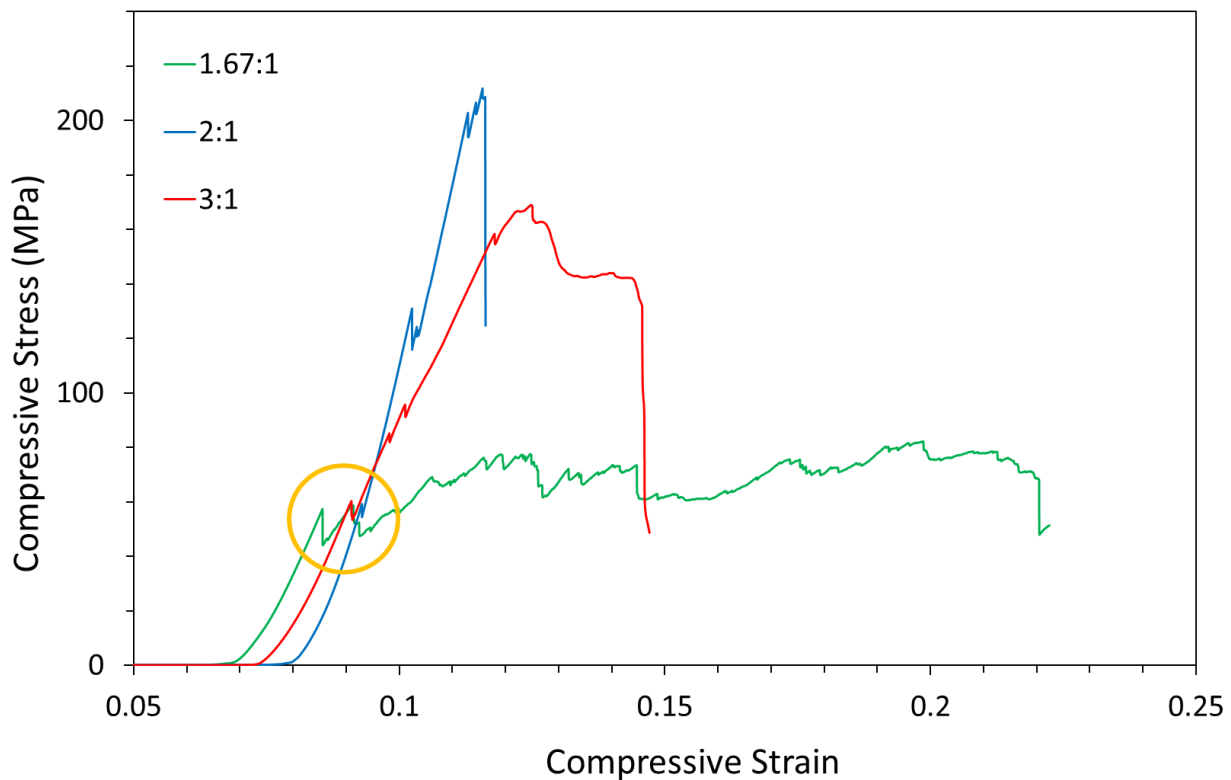
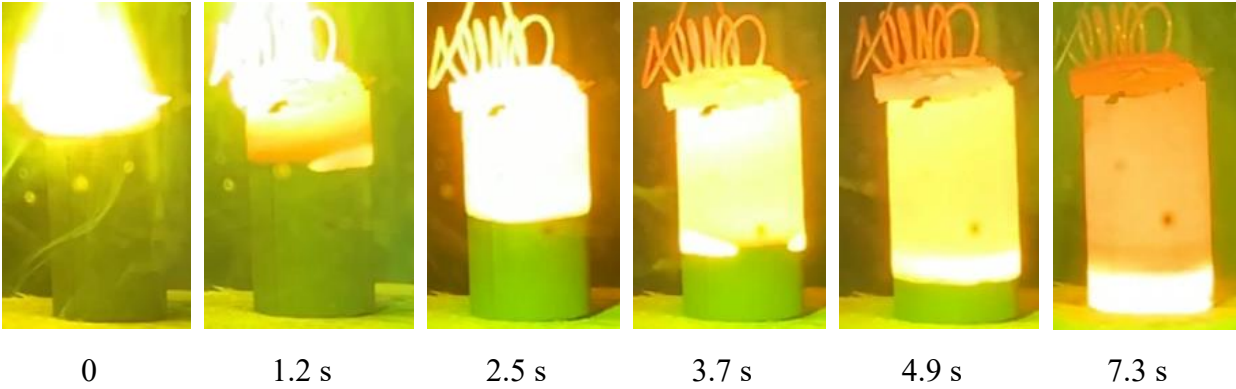


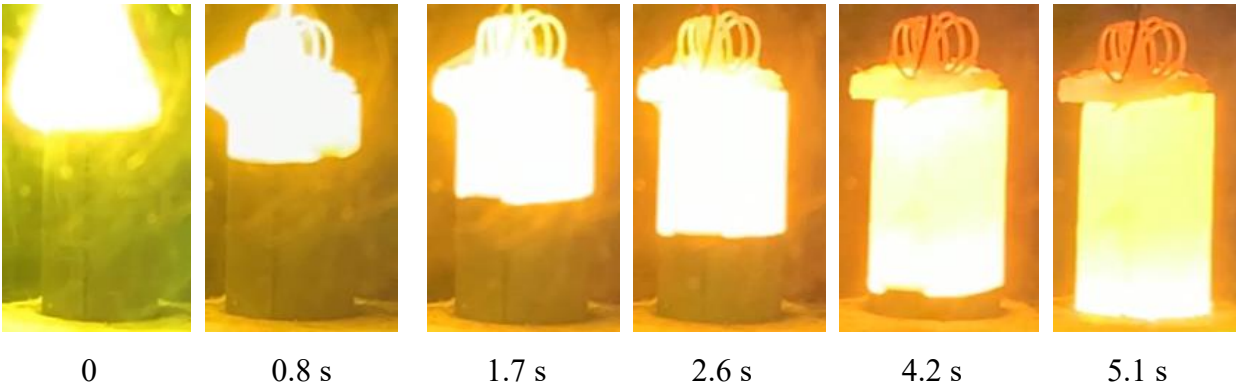
Figure 4.29: Stress-strain dependences of products obtained from mixtures with Nb/Si mole ratios of 1.67, 2, and 3.

It should be noted that the mixture with Nb/Si mole ratio of 3 burned in the spin combustion mode (see Fig. 4.19c). The unsteady propagation of the combustion wave over a low-exothermic mixture may occur in either pulsating or spinning mode [49, 82]. Both are usually considered as undesirable combustion modes that may lead to instabilities and non-uniform products. It is thus remarkable that spin combustion of the mixture with Nb/Si mole ratio of 3 led to the formation of a relatively uniform and strong product.

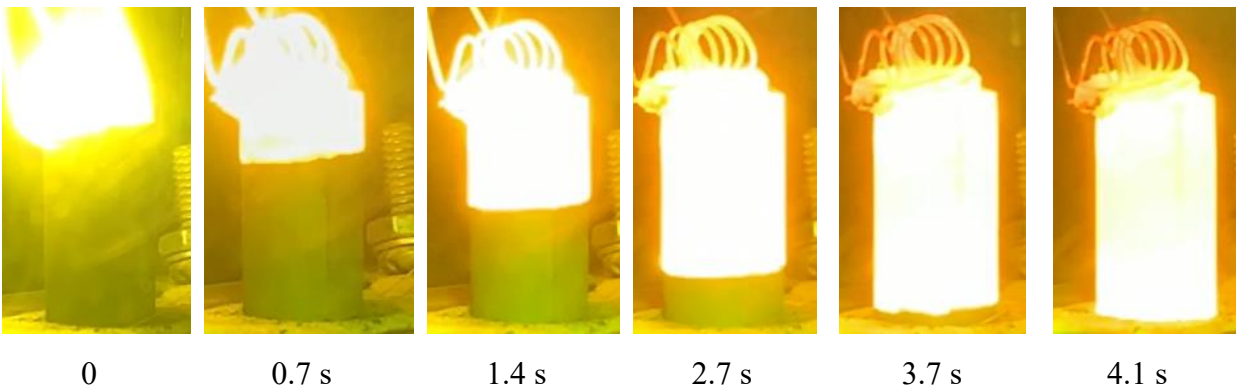
In an effort to explore the effects of spin combustion on the γ -to- α ratio of the samples, MASHS experiments were conducted with Nb/Si mixtures that contained 20–25 at% Si. The combustion wave propagated over the entire pellet when the mixture contained at least 23 at% Si. Figure 4.30 shows the images of combustion propagation over samples with 23, 24, and 25 at% Si. Based on video records for these samples, the axial velocity (u), tangential velocity (v), pitch (z), frequency (f), and number of spin heads (n) were determined. The pitch and frequency were measured using the trace on the product surface after burning.



(a)



(b)



(c)

Figure 4.30: Images of combustion propagation over Nb/Si mixture pellets (height: 25 ± 2 mm) with (a) 23, (b) 24 and (c) 25 at% Si. Time zero was selected arbitrarily.

Table 4.5 shows the obtained parameters. It should be noted that there is an obvious relationship between the axial velocity, frequency, and pitch: $u = f \cdot z$. It is seen that the u values calculated through this equation correlate with those calculated based on obtained videos. As the content of Si increases, u , v , and f also increase, z decreases and n remains the same. This is explained by the temperature increase that is occurring as more Si is added and the mixture becomes more exothermic, thus accelerating the propagation. The temperature increase with increasing Si content is confirmed by the analysis of brightness of the images in Fig. 4.30.

Table 4.5: Spin combustion parameters.

Si concentration	u	v	z	f	n	$f \cdot z$
at %	mm/s	mm/s	mm	Hz		mm/s
23	3.0	32	2.10	1.37	2	2.9
24	4.5	80	1.15	3.87	2	4.4
25	6.2	183	0.70	9.14	2	6.4

The measured values of tangential velocity, v , were confirmed using the mass conservation equation: $v = \pi \cdot d \cdot u \cdot n^{-1} \cdot z^{-1}$, where d refers to the pellet diameter. Here values of v obtained for 23, 24, and 25 at% Si were calculated as 30, 81, and 189 mm/s, respectively. These values correlate with the measured values of v shown in Table 4.5, which indicates good agreement with Novozhilov's simplified theory of spin combustion [45].

Figures 4.31 – 4.33 show the XRD patterns of the obtained products, while Table 4.6 presents the intensities of the characteristic peaks of α -Nb₅Si₃, γ -Nb₅Si₃, and Nb, as well as the intensity ratios. It is seen that as the concentration of Si decreases, the γ -to- α peak intensity ratio decreases. With decreasing Si content from 24 to 23 at%, the γ -to- α peak intensity ratio drops by three times. This is an attractive result as the γ phase has poor mechanical properties. As for Nb, the accuracy of XRD analysis does not allow to reliably detect a trend.

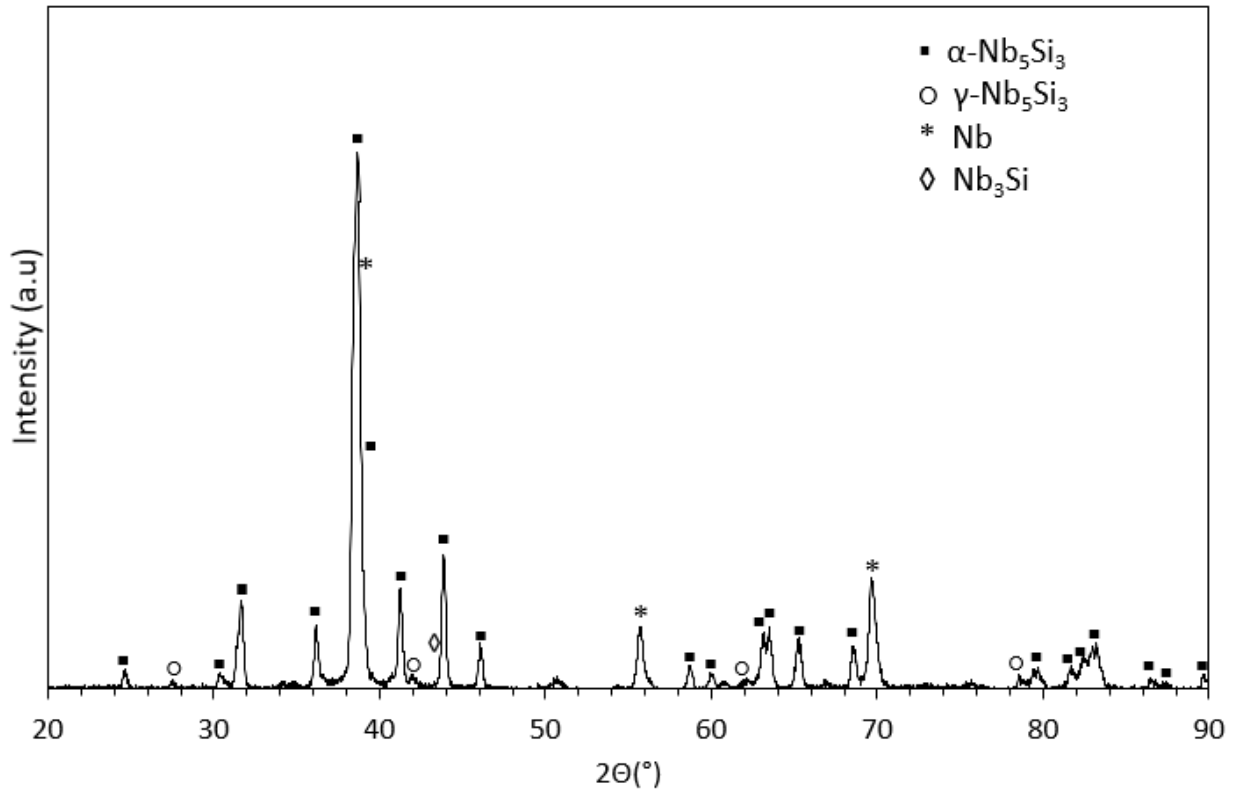


Figure 4.31: XRD pattern of combustion products of the Nb/Si mixture with 23 at% Si.

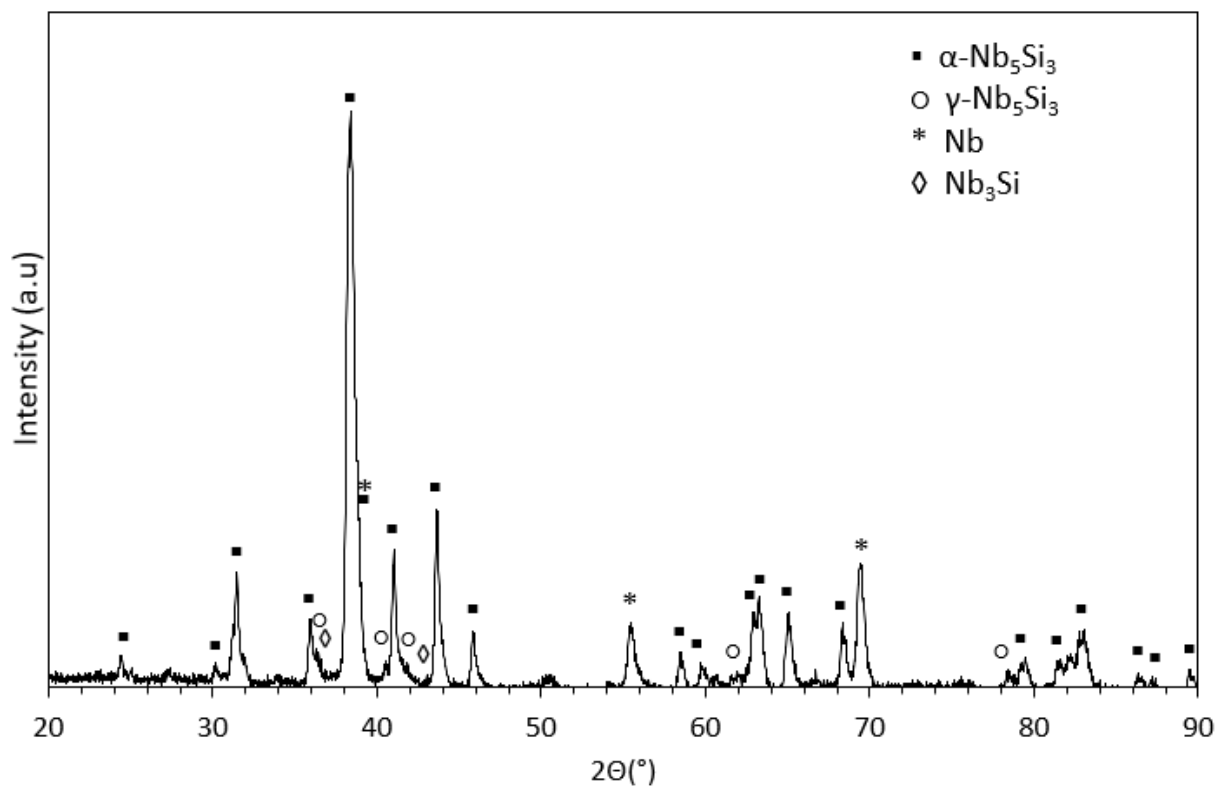


Figure 4.32: XRD pattern of combustion products of the Nb/Si mixture with 24 at% Si.

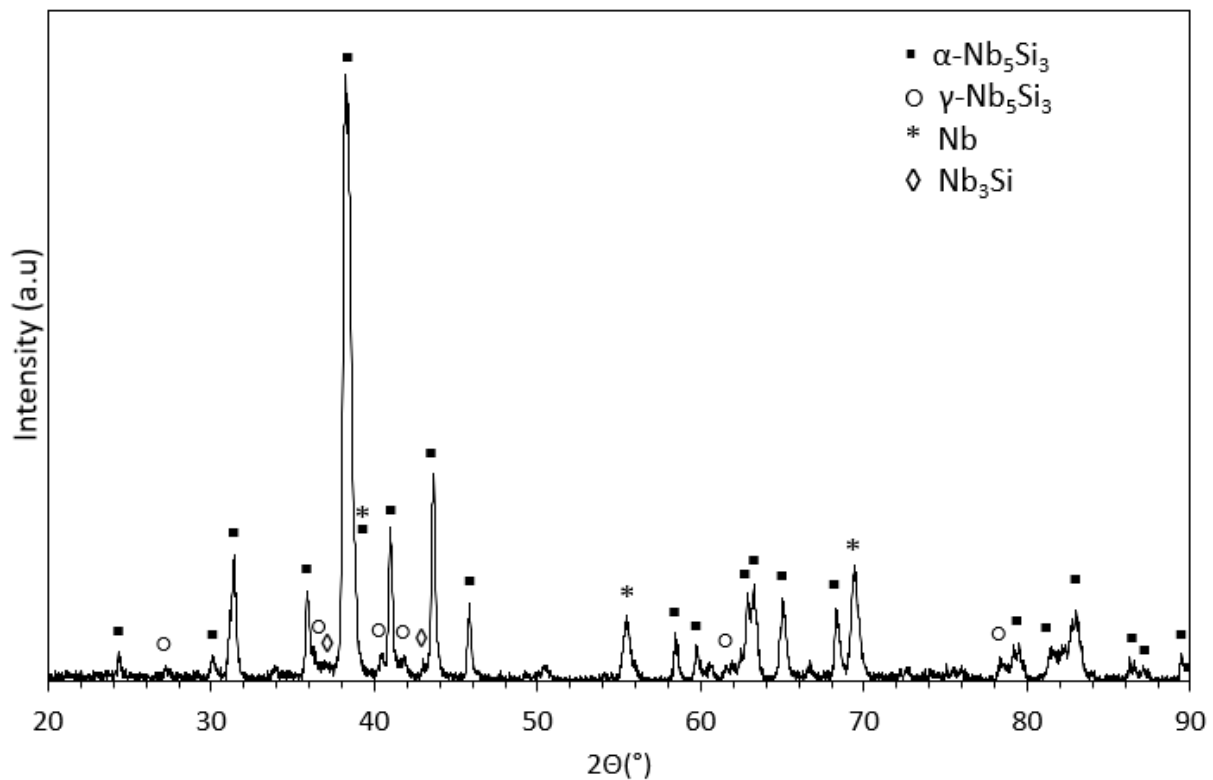


Figure 4.33: XRD pattern of combustion products of the Nb/Si mixture with 25 at% Si.

Table 4.6: XRD peak intensities for the products obtained from Nb/Si mixtures with 23–25 at% Si.

Si Concentration	α -Nb ₅ Si ₃ at 38 °	γ -Nb ₅ Si ₃ at 40 °	Nb at 70 °	γ -to- α Ratio	Nb-to- α Ratio
at%	a.u.	a.u.	a.u.		
23	1966	25	370	0.013 : 1	0.188 : 1
24	1345	53	279	0.039 : 1	0.207 : 1
25	1266	58	228	0.046 : 1	0.180 : 1

4.3 MASHS of Nb₅Si₃/Ti₅Si₃/Nb Composites

Thermodynamic calculations were conducted with Nb, Si and various chemical elements, considered as useful additives to Nb-Si alloys, in order to determine whether the reaction of the added element with Nb or Si is thermodynamically favorable over the reaction between Nb and Si. The calculations generated the values of the adiabatic flame temperatures and the product composition. The calculations were performed using THERMO software at 1 atm pressure. The initial mixture included 5 moles of Nb, 3 moles of Si, and 1 mole of one of the following elements: Hf, Cr, Fe, Ge, Al, Sn, Co, Ni, Y, Ti, B, and Mo. Table 4.7 shows the resulting adiabatic flame temperature and products for each mixture.

The results have shown that most additives remained inert when mixed with Nb and Si. However, three elements (Ti, B, and Mo) reacted with either Nb or Si, decreasing the amount of Nb₅Si₃ and leaving some Si or Nb, respectively, unreacted. It is seen that the adiabatic flame temperatures for all the mixtures with additives were lower than that of the stoichiometric Nb/Si mixture. However, at the used concentrations of additives, the temperatures remained sufficiently high for self-sustained combustion. To eliminate the unreacted Nb or Si, thermodynamic calculations were made with different concentrations of Ti, B, and Mo. Table 4.8 shows the mixture compositions with no unreacted Nb or Si. It should be noted that the composition 4Nb-3Si-Ti had the highest combustion temperature (2348 K). This temperature is higher for the stoichiometric Nb/Si mixture because Ti-Si reaction is more exothermic than Nb-Si reaction. Since the melting point of Ti is 1668 °C, during combustion of this mixture, both Ti and Si will be liquid in the reaction zone, allowing their rapid reaction with no preheating or mechanical activation [71-74]. This could be used to help ignite mixtures with lower Si concentrations.

Table 4.7: The adiabatic flame temperatures and numbers of moles of products for Nb/Si mixtures with additives.

5Nb-3Si	
Temperature (K)	2289
Nb ₅ Si ₃ (Solid)	1.0000
5Nb-3Si-Hf	
Temperature (K)	2043
Nb ₅ Si ₃ (Solid)	1.0000
Hf (Solid)	1.0000
5Nb-3Si-Cr	
Temperature (K)	2041
Nb ₅ Si ₃ (Solid)	1.0000
Cr (Solid)	1.0000
5Nb-3Si-Fe	
Temperature (K)	1975
Nb ₅ Si ₃ (Solid)	1.0000
Fe (Liquid)	1.0000
5Nb-3Si-Ge	
Temperature (K)	1969
Nb ₅ Si ₃ (Solid)	1.0000
Ge (Liquid)	1.0000
5Nb-3Si-Al	
Temperature (K)	2039
Nb ₅ Si ₃ (Solid)	1.0000
Al (Liquid)	1.0000
5Nb-3Si-Sn	
Temperature (K)	2065
Nb ₅ Si ₃ (Solid)	1.0000
Sn (Liquid)	1.0000

5Nb-3Si-Co	
Temperature (K)	1981
Nb ₅ Si ₃ (Solid)	1.0000
Co (Liquid)	1.0000
5Nb-3Si-Ni	
Temperature (K)	2000
Nb ₅ Si ₃ (Solid)	1.0000
Ni (Liquid)	1.0000
5Nb-3Si-Y	
Temperature (K)	2000
Nb ₅ Si ₃ (Solid)	1.0000
Y (Liquid)	1.0000
5Nb-3Si-Ti	
Temperature (K)	2148
Nb ₅ Si ₃ (Solid)	0.8000
Si ₃ Ti ₅ (Solid)	0.2000
Nb (Solid)	1.0000
5Nb-3Si-B	
Temperature (K)	2190
Nb ₅ Si ₃ (Solid)	0.9000
NbB ₂ (Solid)	0.5000
Si (Liquid)	0.3000
5Nb-3Si-Mo	
Temperature (K)	2107
Nb ₅ Si ₃ (Solid)	0.8889
Mo ₃ Si (Solid)	0.3333
Nb (Solid)	0.5556

Table 4.8: The adiabatic flame temperatures and numbers of moles of products for Nb/Si/Ti, Nb/Si/B, and Nb/Si/Mo mixtures that exhibit complete conversion.

4Nb-3Si-Ti	
Temperature (K)	2348
Nb ₅ Si ₃ (Solid)	0.8000
Si ₃ Ti ₅ (Solid)	0.2000
5Nb-2.7Si-B	
Temperature (K)	2294
Nb ₅ Si ₃ (Solid)	0.9000
B ₂ Nb (Solid)	0.5000
4.44Nb-3Si-Mo	
Temperature (K)	2215
Nb ₅ Si ₃ (Solid)	0.8889
Mo ₃ Si (Solid)	0.3333

Thus, thermodynamic calculations show that titanium is a promising additive because Ti reacts with Si and this reaction is more exothermic than Nb-Si reaction. On the other hand, as noted in the Introduction, niobium silicide-based composites include large amounts of Ti. For this reason, MASHS of Nb-Si-Ti composites was studied experimentally.

Prior to the experiments, thermodynamic calculations for combustion of Nb/Ti/Si mixtures (Ti/Si mole ratio: 1; Nb/Si mole ratio: 1–4, i.e. 33.3 to 16.7 at% Si) were conducted at 1 atm using THERMO software. Figure 4.34 shows the adiabatic flame temperature and the product composition at different Nb/Si mole ratios. For all mixtures, the combustion products consist of Nb₅Si₃, Ti₅Si₃, and Nb. With the addition of more Nb, the temperature decreases, and at Nb:Si > 2 it becomes lower than the melting point of Si.

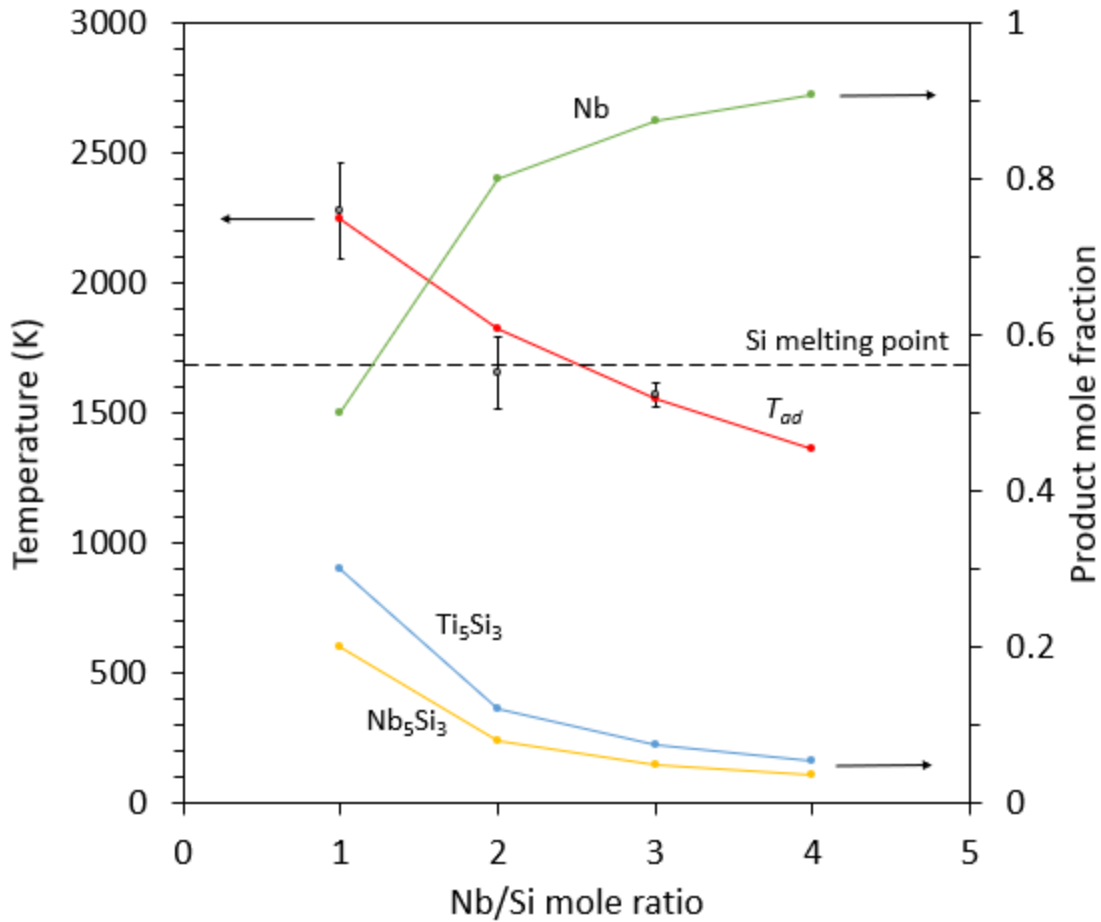


Figure 4.34: Measured maximum temperatures (open circles and error bars), adiabatic flame temperatures (T_{ad}), and mole fractions of the products (filled circles and lines) vs. Nb/Si mole ratio.

The MASHS experiments have been conducted with the same mixture compositions. They have shown that in the mixture with Nb/Si mole ratio of 1, the combustion wave propagated steadily at a velocity of 8.6 ± 0.3 mm/s. Figure 4.35 shows a typical thermal profile. With increasing this ratio to 2, the velocity decreased to 7.1 ± 0.3 mm/s. In the mixture with Nb:Si = 3, unsteady propagation was observed. More specifically, a spinning propagation took place, where hot spots were traveling over the lateral surface of the pellets at an average axial velocity of $2.1 \pm$

0.4 mm/s and a much higher tangential velocity. In the mixture with Nb:Si = 4, the reaction was occurring in the top layer, but it did not propagate down the pellet.

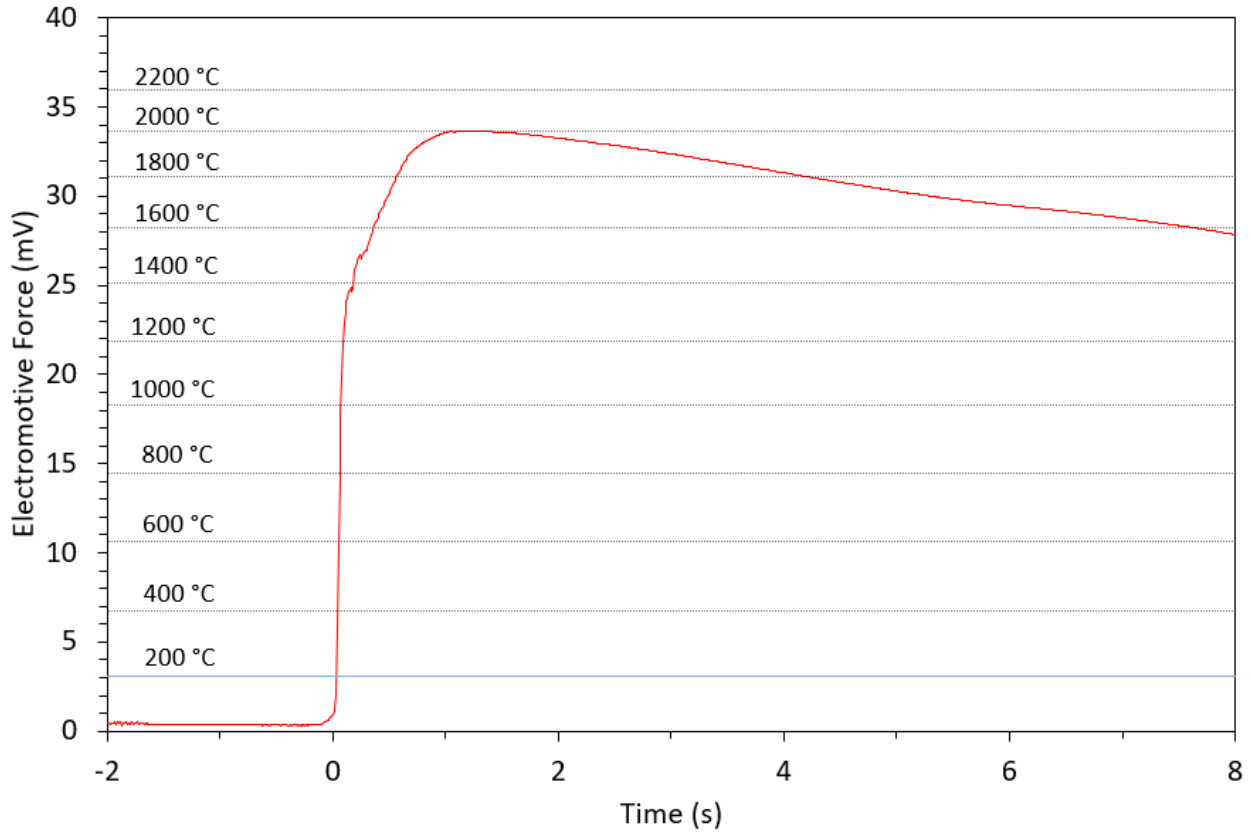


Figure 4.35: Thermal profile during combustion of Nb/Si/Ti mixture (1:1:1 mole ratio).

The average values and standard deviations of the maximum temperatures are shown in Fig. 4.34. Good agreement with the thermodynamic calculations is observed. It should be noted that the formation enthalpy of Nb_5Si_3 in THERMO database is apparently lower than the actual value, which explains the insignificant effect of heat losses on the combustion temperature. It is remarkable that the spin combustion occurred when the temperature in the reaction zone was significantly below the melting point of Si. Apparently, when Si is solid, the rate of heat release is

not sufficiently high for maintaining a steady propagation of the combustion wave, so the transition to spin combustion occurs.

Figure 4.36 shows the XRD patterns of the products obtained from the mixtures with Nb/Si mole ratios of 1, 2, and 3. The observed silicide phases are α -Nb₅Si₃ and Ti₅Si₃. Other peaks, according to the XRD database, may belong to Nb and Ti. However, since Ti is more active than Nb with respect to Si, it is unlikely that there is unreacted Ti in the products. Therefore, these peaks were identified as Nb. It is seen that with increasing the mole fraction of Nb from 1 to 2, the intensities of the silicide phases significantly decrease, while the peaks of Nb become much higher. This trend continues, though to a lesser extent, with further addition of Nb. It can be concluded that the results are in agreement with the thermodynamic calculations. It is worth noting that no peaks of γ -Nb₅Si₃ phase, which has poor mechanical properties, were detected.

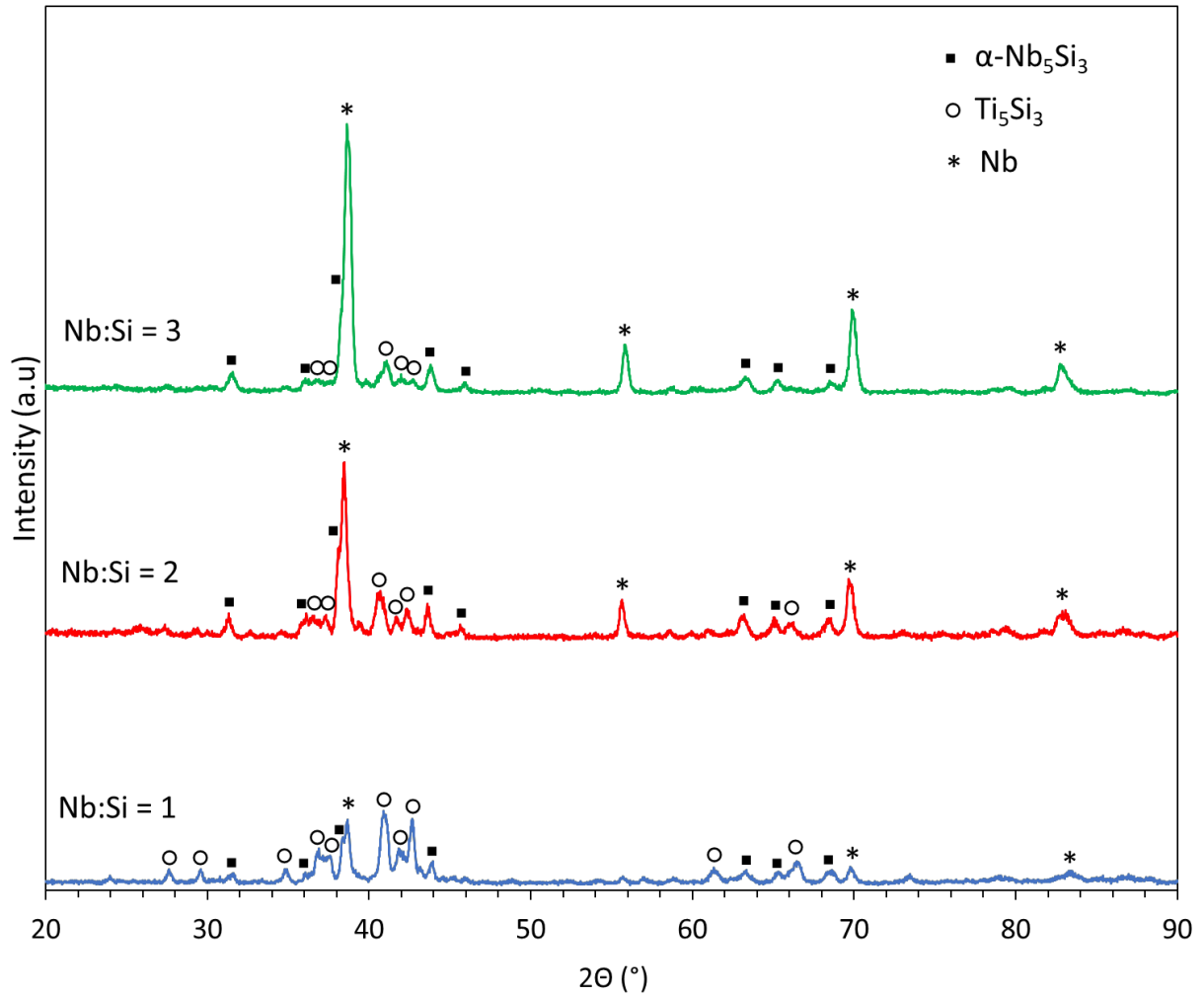


Figure 4.36: XRD patterns of the products obtained from mixtures with Nb/Si mole ratios of 1, 2, and 3.

Figure 4.37 shows SEM images of the products obtained from the mixture with Nb:Si = 2 (steady propagation) and from the mixture with Nb:Si = 3 (spin combustion). It is seen that despite the different combustion modes, the obtained particles are similar to each other.

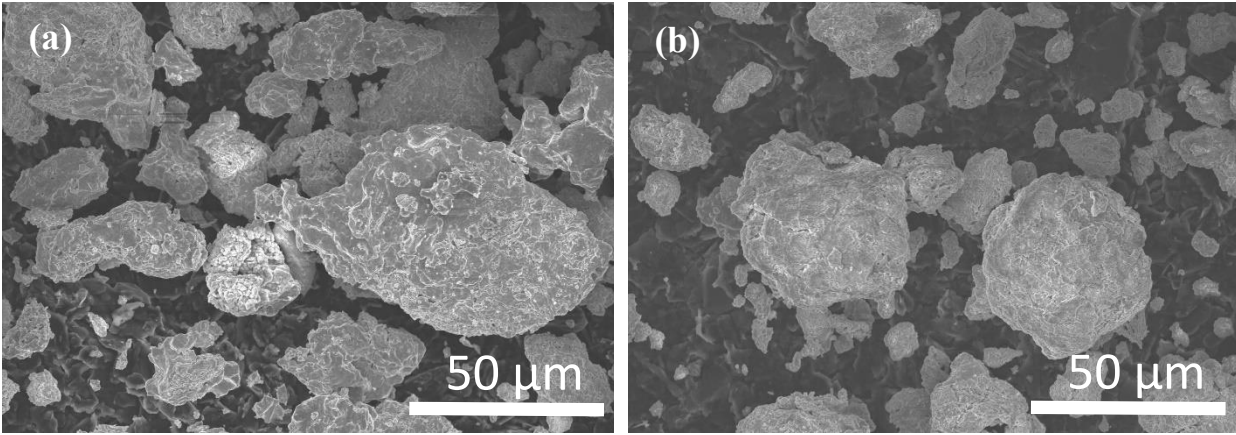


Figure 4.37: SEM images of the products obtained from the mixtures with Nb/Si mole ratios of (a) 2 and (b) 3.

Chapter 5: Conclusions

Thermodynamic calculations revealed the adiabatic flame temperatures and product compositions for combustion of Nb/Si mixtures with mole fractions of excess Nb, with respect to Nb_5Si_3 stoichiometry, from 0 to 1. With increasing this mole fraction from 0 to 0.8 (Nb/Si mole ratio: 1.67 – 3), the adiabatic flame temperature decreases from 2289 K to 1677 K, which is still expected to be sufficiently high for self-sustained combustion.

Mechanical activation in a planetary ball mill at 1000 rpm enabled SHS of Nb_5Si_3 with no preheating. After milling for 2-5 min, SHS products contained NbSi_2 and Nb in addition to the desired Nb_5Si_3 . When the milling time was 10 min or longer, these impurities, as in NbSi_2 and Nb, were not detected, and the product consisted of Nb_5Si_3 (α and γ phases) with traces of Nb_3Si . Particle size analysis and scanning electron microscopy have shown that not only does milling grind coarse particles, but it also creates agglomerates where Nb and Si are uniformly mixed, which improves conditions for effective solid-solid reactions. Prior research on MASHS of Nb_5Si_3 , where a shaker mill at 875 cycles/min was used showed the required milling time was longer by an order of magnitude. Thus, a planetary mill is more effective for MASHS of Nb_5Si_3 than a shaker mill.

Increasing the pellet diameter from 6 to 13 mm decreased the content of $\gamma\text{-Nb}_5\text{Si}_3$ phase, apparently because of a longer cooling time, which promoted transformation of the metastable γ phase to the [thermodynamically stable \$\alpha\text{-Nb}_5\text{Si}_3\$ phase](#). The β phase was not formed because the reaction temperature was lower than the $\alpha\text{-}\beta$ transformation temperature. Chemical oven experiments, with even longer cooling times and higher temperatures, were conducted in an effort to decrease the amount of γ phase, which has poor mechanical properties, and obtain the high-

temperature β - Nb_5Si_3 phase. The amount of γ phase was, indeed, decreased, but the β phase still was not detected. The β -to- α transformation probably occurs quickly upon cooling of the sample.

For the first time, $\text{Nb}_5\text{Si}_3/\text{Nb}$ composites have been obtained by MASHS with no preheating, at a milling time of 10 min. The products obtained by combustion of a mixture with Nb/Si ratio of 2 contained α and γ phases of Nb_5Si_3 as well as Nb and some amount of Nb_3Si . Combustion took place at an Nb/Si mole ratio as high as 3.35, i.e. at 23 at% Si in the mixture. In the range of Nb/Si mole ratios 3 – 3.35 (i.e. at 23 – 25 at% Si), a spinning propagation of the combustion wave was observed, which is explained by a low exothermicity of the initial mixture. The products obtained from these mixtures also consisted of α - Nb_5Si_3 , γ - Nb_5Si_3 , Nb_3Si , and Nb. However, the increase in Nb/Si ratio from 1 to 3.35 dramatically decreased the content of the γ phase, which may be associated with its metastability and the longer duration of the combustion process. This is an attractive result since the γ phase has poor mechanical properties.

The obtained porous products had a compressive strength of approximately 100-200 MPa, which would allow for these materials to be used in some chemical engineering applications. For use in gas turbines, these materials need to be consolidated, for example, using hot pressing or spark plasma sintering. Stronger material could also be fabricated by SHS compaction method.

Thermodynamic calculations were conducted for Nb/Si with additives such as Hf, Cr, Fe, Ge, Al, Sn, Co, Ni, Y, Ti, B, and Mo. The results showed that three of these additives (Ti, B, and Mo) react with Nb or Si. Since Ti-Si reaction is even more exothermic than Nb-Si reaction and niobium silicide-based composites include large amounts of Ti, MASHS of Nb-Si-Ti materials was studied experimentally. The addition of Ti enabled combustion of mixtures with the concentration of Si as low as 20 at%. The obtained composites with 20 – 33 at% Si consisted of α - Nb_5Si_3 , Ti_5Si_3 , and Nb phases, with no presence of γ - Nb_5Si_3 . Decreasing the concentration of Si

from 25 to 20 at% resulted in the transition from a steady propagation of the reaction wave to spin combustion, which, however, did not change the morphology of the products.

References

1. "Natural gas generators make up the largest share of overall US generation capacity", U.S. Energy Information Administration, <https://www.eia.gov/todayinenergy/detail.php?id=34172> (Accessed: Apr. 20, 2020)
2. Perepezko, J.H., "The hotter engine, the better", *Science*, vol. 326, 2009, no. 5956, pp. 1068-1069, DOI: 10.1126/science.1179327
3. Dimiduk D.M. and Perepezko J.H., "Mo-Si-B Alloys: Developing a revolutionary turbine-engine material", *Ultrahigh-Temperature Materials for Jet Engines*, vol. 28, 2003, pp. 639–645, DOI: 10.1557/mrs2003.191
4. Lemberg J.A. and Ritchie R.O., "Mo-Si-B alloys for ultrahigh-temperature structural applications", *Advanced Materials*, vol. 24, 2012, no. 26, pp. 3445–3480, DOI: [10.1002/adma.201200764](https://doi.org/10.1002/adma.201200764)
5. Levashov, E.A., Mukasyan, A.S., Rogachev, A.S., and Shtansky, D.V., "Self-propagating high-temperature synthesis of advanced materials and coatings", *International Materials Reviews*, vol. 64, 2017, no. 4, pp. 203–239, DOI: 10.1080/09506608.2016.1243291
6. Gauthier, V., Bernard, F., Gaffet, E., Josse, C., and Larpin, J.P., "In-situ time resolved X-ray diffraction study of the formation of the nanocrystalline NbAl₃ phase by mechanically activated self-propagating high-temperature synthesis reaction", *Materials Science and Engineering*, vol. 272, 1999, no. 2, pp. 334-341, DOI: [10.1016/S0921-5093\(99\)00488-8](https://doi.org/10.1016/S0921-5093(99)00488-8)
7. Bewlay, B.P., Jackson, M.R., Zhao, J.-C., and Subramanian, P.R., "A review of very-high-temperature Nb-silicide-based composites", *Metallurgical and Materials Transactions A*, vol. 34, 2003, no. 10, pp. 2043–2052, DOI: 10.1007/s11661-003-0269-8

8. Schlesinger, M.E., Okamoto, H., Gokhale, A.B., and Abbaschian, R.J., "The Nb-Si (niobium-silicon) system", *Journal of Phase Equilibria*, vol. 14, 1993, pp. 502–509, DOI: [10.1007/BF02645283](https://doi.org/10.1007/BF02645283)
9. Bewlay, B.P., Jackson M.R., Zhao J.-C., Subramanian P.R., Mendiratta M.G., and Lewandowski J.J., "Ultra-high-temperature Nb-silicide-based composites", *Ultra-high-Temperature Materials for Jet Engines*, vol. 28, 2003, no. 9, pp. 646–653, DOI: [10.1557/mrs2003.192](https://doi.org/10.1557/mrs2003.192)
10. Yonghua, D., "Stability, elastic constants and thermodynamic properties of (α , β , γ)-Nb₅Si₃ phases", *Rare Metal Materials and Engineering*, vol. 44, 2015, no. 1, pp. 18–23, DOI: [10.1016/S1875-5372\(15\)30004-7](https://doi.org/10.1016/S1875-5372(15)30004-7)
11. Perkins, R.A. and Meier, G.H., "The oxidation behavior and protection of niobium", *JOM*, vol. 42, 1990, pp. 17-21, DOI: [10.1007/BF03221046](https://doi.org/10.1007/BF03221046)
12. Togo A. and Tanaka I., "First principles phonon calculations in materials science", *Scripta Materialia*, vol. 108, 2015, pp. 1–5, DOI: [10.1016/j.scriptamat.2015.07.021](https://doi.org/10.1016/j.scriptamat.2015.07.021)
13. Schachner, H., Cerwenka, E., and Nowotny, H., "New silicides of M₅Si₃-type with D_{8h}-structure", *Monatshefte für Chemie - Chemical Monthly*, vol. 85, 1954, pp. 245-254.
14. Alyamovskii, S.I., Gel'd, P.V., and Matveenko, I.I., "Concentration regions of stability of silicides of niobium at 1250°C", *Russian Journal of Inorganic Chemistry.*, vol. 7, 1962, pp. 432-435.
15. Bewlay, B.P., Jackson, M.R., and Gigliotti, M.F.X., "Niobium silicide high temperature *in situ* composites", In: J.H. Westbrook, R.L. Fleischer (Eds.), *Intermetallic Compounds – Principles and Practice, Volume 3*, Wiley, New York, 2002, pp. 541-560, DOI: [10.1002/0470845856.ch26](https://doi.org/10.1002/0470845856.ch26)

16. Kim, J.-H., Tabaru, T., Hirai, H., Kitahara, A., and Hanada S., "Tensile properties of a refractory metal base in situ composite consisting of an Nb solid solution and hexagonal Nb₅Si₃", *Scripta Materialia*, vol. 48, 2003, no. 10, pp. 1439–1444, DOI: [10.1016/S1359-6462\(03\)00084-8](https://doi.org/10.1016/S1359-6462(03)00084-8)
17. Merzhanov, A.G., "The chemistry of self-propagating high-temperature synthesis", *Journal of Materials Chemistry*, vol. 14, 2004, no. 12, pp. 1779–1786, DOI: [10.1039/B401358C](https://doi.org/10.1039/B401358C)
18. Mendiratta, M.G., Lewandowski, J.J., and Dimiduk, D.M., "Strength and ductile-phase toughening in the two-phase Nb/Nb₅Si₃ alloys", *Metallurgical Transactions A*, vol. 22, 1991, no. 1573, DOI: [10.1007/BF02667370](https://doi.org/10.1007/BF02667370)
19. Yeh, C.L. and Chen, W.H., "Preparation of Nb₅Si₃ intermetallic and Nb₅Si₃/Nb composite by self-propagating high-temperature synthesis", *Journal of Alloys and Compounds*, vol. 402, 2005, nos. 1-2, pp. 118–123, DOI: [10.1016/j.jallcom.2005.04.134](https://doi.org/10.1016/j.jallcom.2005.04.134)
20. Kajuch, J., Short, J., and Lewandowski, J.J., "Deformation and fracture behavior of Nb in Nb₅Si₃/Nb laminates and its effect on laminate toughness", *Acta Metallurgica et Materialia*, vol. 43, 1995, no. 5, pp. 1955-1967, DOI: [10.1016/0956-7151\(94\)00391-T](https://doi.org/10.1016/0956-7151(94)00391-T)
21. Carrillo-Heian, E.M., Unuvar, C., Gibeling, J.C., Paulino, G.H., and Munir, Z.A., "Simultaneous synthesis and densification of niobium silicide/niobium composites", *Scripta Materialia*, vol. 45, 2001, no. 4, pp. 405–412, DOI: [10.1016/S1359-6462\(01\)01023-5](https://doi.org/10.1016/S1359-6462(01)01023-5)
22. Gavens, A.J., Van Heerden, D., Weihs, T.P., and Foecke, T., "Fabrication and evaluation of Nb/Nb₅Si₃ microlaminate foils", *Metallurgical and Materials Transactions A*, vol. 30, 1999, pp. 2959-2965, DOI: [10.1007/s11661-999-0133-6](https://doi.org/10.1007/s11661-999-0133-6)

23. Rigney, J.D. and Lewandowski, J.J., "Loading rate and test temperature effects on fracture of in situ niobium silicide-niobium composites", *Metallurgical and Materials Transactions A*, vol. 27, 1996, pp. 3292-3306, DOI: [10.1007/BF02663879](https://doi.org/10.1007/BF02663879)
24. Mendriatta, M.G., Lewandowski, J.J., and Dimiduk, D.M., "Strength and ductile-phase toughening in the two-phase Nb/Nb₅Si₃ alloys", *Metallurgical Transactions A*, vol. 22, 1991, no. 1573, DOI: [10.1007/BF02667370](https://doi.org/10.1007/BF02667370)
25. Bewlay, B.P., Lipsitt, H.A., Jackson, M.R., Reeder, W.J., and Sutliff, J.A., "Solidification processing of high temperature intermetallic eutectic-based alloys", *Materials Science and Engineering: A*, vols. 192-193, 1995, no. 2, pp. 534-543, DOI: [10.1016/0921-5093\(95\)03299-1](https://doi.org/10.1016/0921-5093(95)03299-1)
26. Zelenitsas, K. and Tsakiroopoulos, P., "Study of the role of Ta and Cr additions in the microstructure of Nb-Ti-Si-Al in situ composites" *Intermetallics*, vol. 14, 2006, no. 6, pp. 639-659, DOI: [10.1016/j.intermet.2005.10.005](https://doi.org/10.1016/j.intermet.2005.10.005)
27. Su, L, Lu-Steffes, O., Zhang, H., and Perepezko, J.H., "An ultra-high temperature Mo–Si–B based coating for oxidation protection of Nb_{SS}/Nb₅Si₃ composites", *Applied Surface Science*, vol. 337, 2015, pp. 38-44, DOI: [10.1016/j.apsusc.2015.02.061](https://doi.org/10.1016/j.apsusc.2015.02.061)
28. Hayashi, S., Takagi, S., Yamagata, R., Narita, T., and Ukai, S., "Formation of Exclusive Al₂O₃ Scale on Nb and Nb-Rich Alloys by Two-Step Oxygen–Aluminum Diffusion Process", *Oxidation of Metals*, vol. 78, 2012, pp. 167-178, DOI: [10.1007/s11085-012-9298-2](https://doi.org/10.1007/s11085-012-9298-2)
29. Wang, W., Yuan, B., and Zhou, C., "Formation and oxidation resistance of germanium modified silicide coating on Nb based in situ composites", *Corrosion Science*, vol. 80, 2014, pp. 164-168, DOI: [10.1016/j.corsci.2013.11.029](https://doi.org/10.1016/j.corsci.2013.11.029)

30. Morsi, K., "The diversity of combustion synthesis processing: a review", *Journal of Materials Science*, vol. 47, 2012, pp. 68–92, DOI: 10.1007/s10853-011-5926-5
31. Varma, A., Rogachev, A.S., Mukasyan, A.S., and Hwang, S., "Combustion synthesis of advanced materials: principles and applications", *Advances in Chemical Engineering*, vol. 24, 1998, pp. 79–226, DOI: [10.1016/S0065-2377\(08\)60093-9](https://doi.org/10.1016/S0065-2377(08)60093-9)
32. Crider, J.F., "Self-propagating high temperature synthesis-a soviet method for producing ceramic materials", <http://www.ism.ac.ru/handbook/84crid.htm> (Accessed: May 7, 2020)
33. Merzhanov, A.G. and Borovinskaya, I.P., "Discovery of SHS", *Concise Encyclopedia of Self-Propagating High-Temperature Synthesis*, 2017, pp. 87-89, DOI: [10.1016/B978-0-12-804173-4.00038-7](https://doi.org/10.1016/B978-0-12-804173-4.00038-7)
34. Subrahmanyam, J. and Vijayakumar, M., " Self-propagating high-temperature synthesis", *Journal of Materials Science*, vol. 27, 1992, pp. 6249-6273, DOI: [10.1007/BF00576271](https://doi.org/10.1007/BF00576271)
35. Yeh, C-L., "Combustion Synthesis: Principles and Applications", *Encyclopedia of Materials: Science and Technology*, 2010, pp.1-8, DOI:10.1016/B978-0-12-803581-8.03743-7
36. Yi, H.C. and Moore, J.J., "Review self-propagating high-temperature (combustion) synthesis (SHS) of powder-compacted materials", *Journal of Materials Science*, vol. 25, 1990, pp. 1159-1168, DOI: [10.1007/BF00585421](https://doi.org/10.1007/BF00585421)
37. Merzhanov, A.G., *40 years of SHS: a lucky star of a scientific discovery*, Bentham Books, 2001, DOI: 10.2174/97816080512811120101
38. Merzhanov, A.G. and Sytshev, A.E., "About self-propagating high-temperature synthesis", Institute of Structural Macrokinetics and Materials Science, Russian Academy of Sciences, <http://www.ism.ac.ru/handbook/shsf.htm> (Accessed: May 7, 2020)

39. Mossino, P., "Some aspects in self-propagating high-temperature synthesis", *Ceramics International*, vol. 30, 2004, pp. 311-332, DOI: [10.1016/S0272-8842\(03\)00119-6](https://doi.org/10.1016/S0272-8842(03)00119-6)
40. Merzhanov, A.G., "Self-propagating high-temperature synthesis: twenty years of search and findings", In: Z.A. Munir and J.B. Holt (Eds.), *Combustion and Plasma Synthesis of High-Temperature Materials*, VCH, New York, 1990, pp. 1-53.
41. Merzhanov, A.G. and Borovinskaya, I.P., "Historical retrospective of SHS: An autoreview", *International Journal of Self-Propagating High-Temperature Synthesis*, vol. 17, 2008, no. 242, DOI: [10.3103/S1061386208040079](https://doi.org/10.3103/S1061386208040079)
42. Zenin, A.A., Merzhanov, A.G., and Nersisyan, G.A., "Structure of heat wave in some processes of self-propagating high-temperature synthesis", *Doklady Akademii Nauk SSSR*, vol. 250, 1980, no. 4, pp. 880-884.
43. Zenin, A.A., Merzhanov, A.G., and Nersisyan, G.A., "Thermal wave structure in SHS processes (by the example of boride synthesis) ", *Combustion, Explosion and Shock Waves*, vol. 17, no. 1, 1981, pp. 63-71, DOI: [10.1007/BF00772787](https://doi.org/10.1007/BF00772787)
44. Zeldovich, Y.B. and Frank-Kamenetskii, D.A., "A theory of thermal propagation of flame", *Acta Physicochimica URSS*, vol. 9, 1938, pp. 341-350.
45. Novozhilov, B.V., "The theory of surface spin combustion", *Pure and Applied Chemistry*, vol. 65, 1993, no. 2, pp. 309-316.
46. Bayliss, A., Matkowsky, B.J., "Interaction of counterpropagating hot spots in solid fuel combustion", *Physica D: Nonlinear Phenomena*, vol. 128, 1999, no. 1, pp. 18-40. DOI: [10.1016/S0167-2789\(98\)00296-6](https://doi.org/10.1016/S0167-2789(98)00296-6)

47. Bayliss, A., Matkowsky, B.J., and Aldushin, A.P., "Dynamics of hot spots in solid fuel combustion", *Physica D: Nonlinear Phenomena*, vol. 166, 2002, nos. 1-2, pp.104-130. DOI: 10.1016/S0167-2789(02)00387-1
48. Ivleva, T.P. and Merzhanov, A.G., "Structure and variability of spinning reaction waves in three-dimensional excitable media", *Physical Review E*, vol. 64, 2001, DOI: 10.1103/PhysRevE.64.036218
49. Ivleva, T.P. and Merzhanov, A.G., "Three-dimensional modes of unsteady solid-flame combustion", *Chaos*, vol. 13, 2003, no. 80, DOI: [10.1063/1.1540772](https://doi.org/10.1063/1.1540772)
50. Alam, M.S., and Shafirovich, E., "Mechanically activated combustion synthesis of molybdenum silicides and borosilicides for ultrahigh-temperature structural applications", *Proceedings of the Combustion Institute*, vol. 35, 2015, no. 2, pp. 2275–2281, DOI: 10.1016/j.proci.2014.05.019
51. Filonenko, A.K., In: A.G. Merzhanov (Ed.), *Combustion Processes in Chemical Technology and Metallurgy*, Chernogolovka, 1975, pp. 258-273
52. Esparza, A.A., and Shafirovich, E., "Mechanically activated combustion synthesis of molybdenum borosilicides for ultrahigh-temperature structural applications", *Journal of Alloys and Compounds*, vol. 670, 2016, pp. 297–305, DOI: 10.1016/j.jallcom.2016.02.029
53. Sarkisyan, A.R., Dolukhanyan, S.K., and Borovinskaya, I.P., "Investigation of processes of the combustion of hafnium, niobium, and tantalum with silicon", *Combustion, Explosions, and Shock Waves*, vol. 15, 1979, no. 1, pp. 95–97, DOI: 10.1007/BF00785339
54. Yeh, C.L. and Chen, W.H., "A comparative study on combustion synthesis of Nb–Si compounds", *Journal of Alloys and Compounds*, vol. 425, 2006, nos. 1-2, pp. 216–222 DOI: 10.1016/j.jallcom.2006.01.083

55. Gedevanishvili, S. and Munir, Z.A., "Field-activated combustion synthesis in the Nb-Si system", *Materials Science and Engineering: A*, vol. 211, 1996, nos. 1-2, pp. 1–9 DOI: 10.1016/0921-5093(95)10162-4
56. Delgado, A., Cordova, S., Lopez, I., Nemir, D., and Shafirovich, E., "Mechanically activated combustion synthesis and shockwave consolidation of magnesium silicide", *Journal of Alloys and Compounds*, vol. 658, 2016, pp. 422–429, DOI: 10.1016/j.jallcom.2015.10.231
57. Cordova, S., and Shafirovich, E., " Toward a better conversion in magnesiothermic SHS of zirconium diboride", *Journal of Materials Science*, vol. 53, 2018, no. 19, pp. 13600-13616, DOI: 10.1007/s10853-018-2460-8
58. Maglia, F., Milanese, C., and Anselmi-Tamburini, U., "Combustion synthesis of mechanically activated powders in the Nb–Si system", *Journal of Materials Research*, vol. 17, 2002, no. 8, pp. 1992–1999, DOI: 10.1557/JMR.2002.0295
59. Song, B., Feng, P., Wang, J., Ge, Y., Wu, G., Wang, X., and Akhtar, F., "Oxidation properties of self-propagating high temperature synthesized niobium disilicide", *Corrosion Science*, vol. 85, 2014, pp. 311–317, DOI: 10.1016/j.corsci.2014.04.029
60. Terekhova, O.G., Shkoda, O.A, Maksimov, Yu.M., and Chalykh, L.D., "Mechanical activation of silicon and niobium and its influence on SHS", *International Journal of Self-Propagating High-Temperature Synthesis*, vol. 8, 1999, pp. 299–306.
61. Shkoda, O.A., Terekhova, O.G., Itin, V.I., Chalykh, L.D., and Maksimov, Yu.M., "Effect of mechanoactivation on phase and structural transformations during SHS of niobium silicides", *International Journal of Self-Propagating High-Temperature Synthesis*, vol. 11, 2002, pp. 201–207.

62. Shkoda, O.A. and Terekhova, O.G., "Combustion of Nb–Si powder blends: Interrupted mechanical activation", *International Journal of Self-Propagating High-Temperature Synthesis*, vol. 20, 2011, no. 4, pp. 224–228, DOI: 10.3103/S1061386211040121
63. Shkoda, O.A. and Terekhova, O.G., "SHS in the Nb–Si system: Influence of mechanical alloying", *International Journal of Self-Propagating High-Temperature Synthesis*, vol. 25, no. 1, 2016, pp. 14–16, DOI: 10.3103/S106138621601012X
64. Shkoda, O.A. and Terekhova, O.G., "SHS in the Nb–Si system: separate mechanical alloying", *International Journal of Self-Propagating High-Temperature Synthesis*, vol. 25, no. 3, 2016, pp. 200–201, DOI: 10.3103/S1061386216030109
65. Takacs, L. and Sepelak, V., "Quantitative comparison of the efficiency of mechanochemical reactors", *Journal of Materials Science*, vol. 39, 2004, pp. 5487-5489, DOI: [10.1023/B:JMSC.0000039271.90810.5b](https://doi.org/10.1023/B:JMSC.0000039271.90810.5b)
66. Voloskova, E.V., Poluboyarov, V.A., Berdnikova, L.K., and Gusev, K.P., "Mechanochemical synthesis of calcium orthosilicate from high-calcium fly ash", *Solid Fuel Chemistry*, vol. 49, 2015, pp. 183-187, DOI: [10.3103/S0361521915030118](https://doi.org/10.3103/S0361521915030118)
67. Kwoon, Y.-S., Gerasimov, K.B., and Yoon, S.-K., "Ball temperatures during mechanical alloying in planetary mills", *Journal of Alloys and Compounds*, vol. 346, 2002, nos. 1-2, pp. 276-281, DOI: [10.1016/S0925-8388\(02\)00512-1](https://doi.org/10.1016/S0925-8388(02)00512-1)
68. Khoa, H.X., Bae, S., Bae, S., Kim, B.-W., and Kim, J.S., "Planetary ball mill process in aspect of milling energy", *Korean Powder Metallurgy Institute*, vol. 21, 2014, no. 2, pp. 155-164, DOI: 10.4150/KPMI.2014.21.2.155

69. Kematick, R.J. and Myers, C.E., "Thermodynamics of the phase formation of the titanium silicides", *Chemistry of Materials*, vol. 8, 1996, no. 1, pp. 287–291, DOI: 10.1021/cm950386q
70. Meschel, S.V. and Kleppa, O.J., "Standard enthalpies of formation of some 4d transition metal silicides by high temperature direct synthesis calorimetry", *Journal of Alloys and Compounds*, vol. 274, 1998, nos. 1–2, pp. 193–200, DOI: 10.1016/S0925-8388(98)00504-0
71. Azatyan, T.S., Mal' tsev, V.M., Merzhanov, A.G., Seleznev, VA, "Some principles of combustion of titanium-silicon mixtures", *Combustion, Explosion, and Shock Waves*, vol. 15, 1979, no. 1, pp. 43–49, DOI: 10.1007/BF00785326
72. Rogachev, R.S., Shugaev, V.A, Khomenko, I., Varma, A., and Kachelmyer, C.R., "On the mechanism of structure formation during combustion synthesis of titanium silicides", *Combustion Science and Technology*, vol. 109, 1995, nos. 1–6, pp. 53–70. DOI: 10.1080/00102209508951895
73. Anselmi-Tamburini, U., Maglia, F., Spinolo, G., Doppiu, S., Monagheddu, M., and Cocco, G., "Self-propagating reactions in the Ti–Si System: A SHS-MASHS comparative study", *Journal of Materials Synthesis and Processing*, vol. 8, 2000, nos. 5–6, pp. 377–383, DOI: 10.1023/A:1011315016232
74. Yeh, C.H. and Chen, W.H., "Formation of titanium silicides Ti_5Si_3 and $TiSi_2$ by self-propagating combustion synthesis", *Journal of Alloys and Compounds*, vol. 432, 2007, no. 1–2, pp. 90–95, DOI: 10.1016/j.jallcom.2006.05.131
75. Shiryayev, A., "Thermodynamics of SHS processes: an advanced approach", *International Journal of Self-Propagating High-Temperature Synthesis*, vol. 4, 1995, no. 4, pp. 351–362.

76. ASTM E9-19, "Standard test methods of compression testing of metallic materials at room temperature", ASTM Int., West Conshohocken, PA, 2019.
77. Sarkisyan, A.R., Dolukhanyan, S.K., and Borovinskaya, I.P., "Self-Propagating high-temperature synthesis of transition metal silicides", *Soviet Powder Metallurgy and Metal Ceramics*, vol. 17, 1978, pp. 424-427, DOI: 10.1007/BF00795793
78. Shao, G., "Thermodynamic assessment of the Nb-Si-Al system", *Intermetallics*, vol. 12, 2004, no. 6, pp. 655-664, DOI: 10.1016/j.intermet.2004.03.011
79. Gorelkin, O.S., Dubrovin, A.S., Kolenikova, O.D., and Chirkov, N.A., "Measurement of the heat of formation of intermetallic compounds by the sintering method in an isothermal calorimeter", *Russian Journal of Physical Chemistry A*, vol. 46, 1972, pp. 431-432
80. Fujiwara, H., Ueda, Y., Awasthi, A., Krishnamurthy, N., and Garg, S.P., "Determination of standard free energy of formation of niobium silicides by EMF measurements", *Journal of the Electrochemical Society*, vol. 150, 2003, no. 8, DOI: 10.1149/1.1591757
81. Bertolino, N., Anselmi-Tamburini, U., Maglia, F., Spinolo, G., and Munir, Z.A., "Combustion synthesis of Zr-Si intermetallic compounds", *Journal of Alloys and Compounds*, vol. 288, 1999, nos. 1-2, pp. 238-248, DOI: 10.1016/S0925-8388(99)00077-8
82. Delgado, A. and Shafirovich, E., "Towards a better combustion of lunar regolith with magnesium", *Combustion and Flame*, vol. 160, 2013, no. 9, pp. 1876-1882, DOI: 10.1016/j.combustflame.2013.03.021

Vita

Born and raised in El Paso, Texas, Reina Treviño graduated from Transmountain Early College High School. She attended the University of Texas at El Paso from Fall of 2012, after graduating with her associate's degree from El Paso Community College. She obtained her bachelor's degree in Mechanical Engineering in Fall 2016 and began graduate school right after.

During her undergraduate studies, Reina worked in the W.M. Keck Center for 3D Innovation on projects relating to studies in additive manufacturing. She interned with Lockheed Martin Space for three years, before halting internships to focus on her research. In September 2017, Reina started her PhD studies in the MIRO Center for Space Exploration and Technology Research with Dr. Evgeny Shafirovich as her advisor.

Reina coauthored two peer-reviewed journal articles: one in the *Journal of Alloys and Compounds*, "Mechanically activated SHS of Nb₅Si₃ and Nb₅Si₃/Nb composites" (published) and another in the *International Journal of Self-Propagating High-Temperature Synthesis*, "Mechanically Activated SHS of Nb-Ti-Si Compounds" (in press). She has presented her results at several conferences, including the 2018 Southwest Emerging Technology Symposium, the 2019 Annual Meeting of The Minerals, Metals & Materials Society (TMS 2019), and Materials Science & Technology (MS&T19). Plans were made for presentation at the 2020 Spring Technical Meeting held by the Central States Section of The Combustion Institute, however the event was cancelled due to COVID-19 pandemic. There are also plans to present the latest work at TMS 2021.

Email: trevinoreina@gmail.com

This dissertation was typed by Reina Treviño.